A new type of mechanical walking machine

By

Anthony James Ingram

A dissertation submitted to the Faculty of Engineering
in partial fulfilment of the requirements for the degree

Doctor Ingeneriae

in

Mechanical Engineering
in the
Faculty of Engineering and the Built Environment

at the

UNIVERSITY OF JOHANNESBURG

Supervisor: Prof. A.L. Nel

November 2006

Abstract

This thesis introduces a new type of walking machine that appears promising due to its relative simplicity and efficiency. After an introduction to a selection of previous walking machines, the new machine's history, advantages, operation and a method for solving its kinematics are given. Early attempts to optimize the mechanism to a range of criteria are described and their shortfalls exposed. A second attempt to optimize the leg geometry by genetic algorithm is detailed and the results of this search discussed. A mechanics model of a hypothetical machine is developed from first principles and the implications of the analysis described. Stability limits and tractive abilities of the machine are explored. A method for determining the loads on the links that constitute the leg and the vehicle chassis is given. A series of prototypes has been constructed and discussions of these machines are given. The most recent prototype is used in a pair of experiments to validate the kinematic and kinetic models. The experimental method, a statistical analysis of results and a discussion are provided for each. The thesis concludes by considering what work remains to be done before a practical cargo carrying transport walking machine can be designed.

Opsomming

Hierdie proefskrif beskryf 'n nuwe tipe stapmasjien wat relatief eenvoudig en effektief is. Na 'n inleiding tot 'n verskeidenheid vorige stapmasjiene, word die geskiedenis van die nuwe masjien, voordele, operasie en 'n metode om die meganisme kinematies te analiseer gegee. Vroeë pogings om die meganisme te optimaliseer in terme van 'n reeks kriteria word beskryf en die nadele van die meganisme aangewys. 'n Tweede poging om die geometrie van die been te optimaliseer deur middel van genetiese algoritmes word beskryf en die resultate van die evolusionêr word bespreek. 'n Meganika model van 'n hipotetiese masjien word van eerste beginsels ontwikkel en die implikasies van die analise word gegee. Stabiliteitsbeperkings en die trekvermoë van die masjien word ontwikkel. 'n Metode om die kragte in die beensegmente en voertuig se onderstel te bereken word gegee. 'n Reeks prototipes is gebou en besonderhede van die masjiene word gegee. Die nuutste prototipe is gebruik om enkele eksperimente uit te voer om die kinetiese en kinematiese modelle te valideer. Die eksperimentele metode en statistiese analise van resultate word vir albei modelle bespreek. Die proefskrif sluit met gedagtes oor die werk wat nog gedoen moet word voordat 'n praktiese vervoerstapmasjien finaal ontwerp en vervaardig kan word.

Acknowledgements

Many people provided various forms of assistance which enabled this research to be completed. These include:

Professor Andre Nel, my thesis supervisor, whose comments and inputs have been extremely helpful.

Gillian Eagle, my partner, for financial, emotional and academic support.

Claire Ingram, my daughter, who drilled all the 3mm holes in the Perspex prototype, a very useful but tedious job, especially when you're eighteen and broken fingernails are a concern!

Theo Jansen, the inventor of the mechanism discussed, for inventing the mechanism and for not patenting it, thereby making this work possible.

My bridge partners, Nicholas Chetwin, Michael Haddad, Alan Welcich and Kerron Johnson, who have followed this project from the start and been enthusiastic and supportive for the past 6 years.

Ken O'Halloran, my electronics adviser, for the time he spent discussing instrumentation issues.

Gideon Ferriera, a fellow student, for helping with soldering.

This thesis is dedicated to James Valentine Ingram, my father, who would have loved the machines and been very proud of his son.

Table of Contents

List of Figures

Chapter 1 Introduction

1.1 Previous Work

This thesis continues research started in a previous dissertation [1]. That research was concerned with a new type of mechanism that lent itself well to use as a leg mechanism for a mechanical walking machine. The previous dissertation concerned itself primarily with qualitatively and mathematically describing the new mechanism. It described a method of solving both the kinematics of the various links in the linkage and also provided a method of investigating the forces within the mechanism as it moves.

This thesis extends this prior work by exploring the possible linkage configurations in the new class, defining criteria for good legs, and finding particular geometries that will make good walking machines. Although it is perhaps worthwhile to describe this new class of mechanisms for their own sake – there are some configurations with interesting properties – this thesis is primarily interested in application of the mechanism to walking machines.

There has been much research into walking as a means of locomotion. Many designs of machine using a variety of means of obtaining foot motion have been developed over the years. If a new class of mechanism is worth considering, it needs to be located in the context of the other solutions attempted. The advantages of a new method must be demonstrated not only in relation to alternative designs for walking machines, but also in relation to other forms of overland locomotion, especially wheels and tracks.

Prior to any assessment, the criteria against which options will be rated need to be established. It is also necessary to obtain sufficient information about the various options, to enable the ratings to be determined. Although this thesis does consider criteria for assessing means of locomotion, the majority of the effort is directed toward understanding how the new class of mechanism could be used and what its performance may be.

Although the new class has been previously broadly described in [29] and [31], no formal analysis has been previously published. Insufficient information about the performance of this mechanism is currently available to allow it to be compared to other means of locomotion. This thesis therefore serves as a first attempt to create a validated model of a walking machine with Jansen legs. Application of this model will generate sufficient data for such a machine to be compared to existing solutions.

For a reasonable comparison to be made, it will also be necessary to create an internal assessment mechanism, to allow the “best” of the new class of machines to be selected. Competing designs, being older, are likely to have evolved to be the best representatives of their class. If they are unique prototypes, then they presumably represent the “best” designs that their respective designers could come up with. So in addition to understanding how the new class may work, it is also a requirement that optimization be performed to ensure that the design that will be used for comparison is the “best” it could be. “Best” is placed in quotations, as the number of options is very large, and there is no way of knowing whether a better design may be encountered at some future date.

In addition to theoretical work, this thesis covers a technique that is used to find the linkage that will give the “best” performance. Although this synthetic evolution technique is only used to optimise linkage proportions in this work, it is quite general, and in principle could be extended to enable optimization of other aspects of the proposed designs.

1.2 Research Goals

The primary goal of this thesis is to create a suitable theoretical framework to justify the design choices that will need to be made in the design a new type of walking machine.

There are two further secondary aims. The first of these is to validate the mathematical model developed in previous work [1]. The second is to use this design opportunity to develop methods to automate complex parameter related designs. These methods, once developed, could be later extended to optimize other aspects of the design.

1.3 Thesis layout

Chapter 2 provides a broad overview of walking as a means of transportation. A brief history of older ideas is presented. A selection of more recent solutions is considered and various fundamental issues that need to be addresses are introduced. A brief review of mechanical design of current walkers and proposed walkers extracts the salient commonality, which is the uniformity of linkage used to achieve foot motion. The chapter goes on to assess walking as an alternative to wheels and tracks and describes niches where walking machines may be particularly well suited to operate. Finally the chapter lists some criteria which can be used to assess various walking machines.

Chapter 3 starts by introducing Theo Jansen, his “strandbeeste”, the mechanism that powers them and a critique of his implementation of the mechanism. An assessment of the mechanism against the criteria presented in the previous chapter indicates how promising this mechanism could be with another implementation. The chapter ends with discussions of

the previously developed models as well as extensions that were implemented to facilitate work described later.

The fourth chapter opens with a discussion of optimization problems in general, with a brief review of alternative optimization methods. This leads to consideration of what parameters may need to be considered when optimising a linkage for a leg for a walking machine. The possibility of using mechanism synthesis techniques is considered, but dismissed. The chapter closes with a description of some early attempts to find suitable linkage using an exhaustive search. The limitations of this approach are exposed in the closing section of the chapter.

Chapter 5 is concerned with the use of a genetic algorithm to find solutions. The broad principles of these algorithms are discussed and the particular implementation used here is described in detail. The chapter ends with an assessment of the effectiveness of the algorithm and a description of the best mechanism found.

Chapter 6 gives the development from first principles of a theoretical model to describe the mechanics of walking under a variety of circumstances. A general layout for a theoretical machine is given, based on prototypes built. The mathematical formulae produced by the model are analysed and their implications explained. The findings of the model on topics such as stability and traction are also discussed. The off-road performance and the loads that the chassis may experience are considered. The final section discusses the power requirements for operating a walker with Jansen legs.

Chapter 7 covers the various prototype walking machines that have been constructed pursuant to this research. Three such machines have been built and each of these is described in its own section in this chapter. The final section describes prototypes that may be constructed in the future.

Chapter 8 describes two experiments that were conducted to verify the model developed. The experimental method used, the results obtained and a discussion is provided for each of the experiments. The experiments conducted were generally successful and the model is considered validated.

The last chapter, chapter 9 concludes the thesis by drawing together the results of the research conducted, assessing the progress made and making suggestions for further work that will be required before a practical walker with Jansen legs can be constructed.

Chapter 2 Walking machines

2.1 Early walking machines

History records many attempts to create machines that use legs in place of wheels. The following table lists early walking machines that have been identified during research.

Year	***Maker***	***Country***	***Description***	***Ref.***
200 AD	Zhuge Liang	China	Wooden ox, a transport vehicle used for military supply. Some think it refers to the wheelbarrow.	[2], [3]
1663	Robert Hooke	UK	Cart with legs instead of wheels.	[4]
1770	Richard Edgeworth	UK	A wooden horse with eight legs, capable of leaping over high walls. In spite of forty years work and hundreds of models, he was never able to make the idea work.	[5]
1893	L.A. Rygg	U.S.A.	Mechanical horse, patented in the U.S.A. in 1893, but no prototype was ever built.	[6]
1945	Wallace	U.S.A.	Hopping tank. A patent applied for, but no record of construction.	[6]
1968	General Electric	U.S.A.	Walking truck. Capable of up to 5 mph and could climb over large obstacles, see Figure 3.	[7]
1976	Frank & McGhee	U.S.A.	“Phony Pony”. First computer controlled walking machine.	[6], [7]

Although it seems that the earliest walking machines were manufactured in the 1960’s, in fact small toys, automata, have been manufactured in Europe since the 18th century, including bipedal walkers that became the inspiration of modern passive dynamic bipeds, such as the Cornell Biped (Figure 6).

2.2 More recent walking machines

Subsequent to this early period, research into walking machines has been extremely active. Machines have been constructed on many scales, from some the size of insects, to some the size of small trucks. There are many sites on the internet which have extensive lists of walking machines – see [8], [9], [10], [11] or [12]. The number and creativity of different methods of copying that which all animals do so easily is staggering. Many possible walking mechanisms, from enormous two footed drag line excavators, to twelve legged steam powered experimental prototypes [8] have been attempted.

It is instructive to consider this diversity of designs, as it will aid the process of creating a new type of machine, which is the subject of this thesis. The following figures, Figure 1 to Figure 14 below, shows a selection of the wide variety of walking machines that have been designed and constructed in the years subsequent to 1960.

The following sections describe the possible options in more detail, with a view to selecting some of the possible configurations for further exploration.

Figure 1. MECANT.

Helsinki University of Technology, Automation Technology Laboratory [13]. A hexapod with pantograph legs.

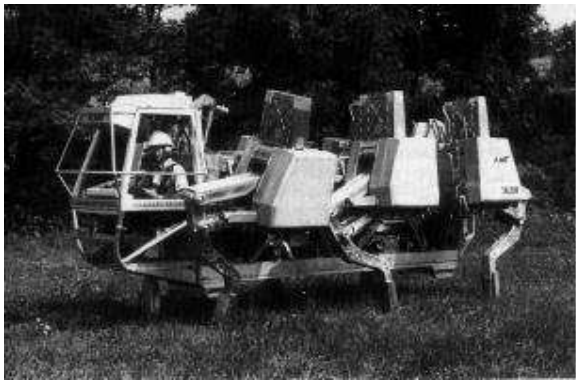

Figure 2. Adaptive Suspension Vehicle.

Defense Advanced Research Projects Agency, US DOD. [14]. Another hexapod with pantograph legs.

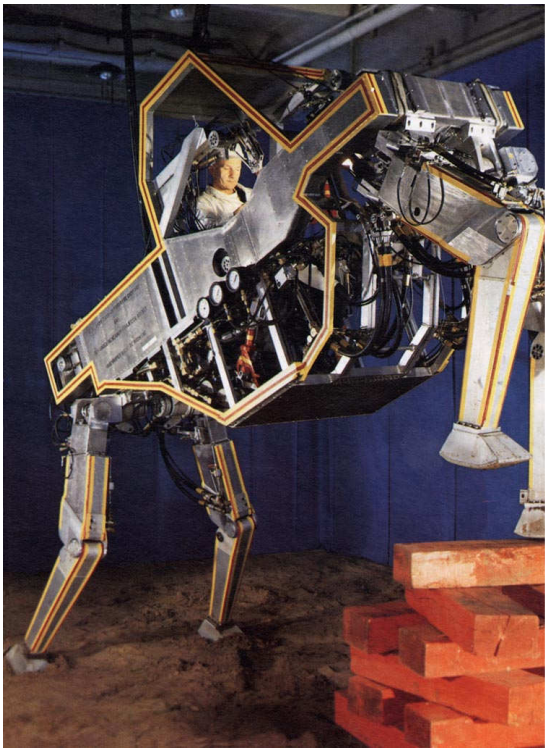

Figure 3. The walking truck.

General Electric. [6] Capable of up to 5 mph and could climb over large obstacles. A quadruped with hips and pantograph legs.

Figure 4. Plustech.

Plustech Oy, Finland. A division of John Deere.[15]. Designed by the same group that designed Figure 1. MECANT. Clearly attempting to resemble a grasshopper or locust.

Figure 5. Baasilisc.

Universidad Nacional Autonoma De Mexico. [16]. A tripod that drags itself along. A limited form of walking.

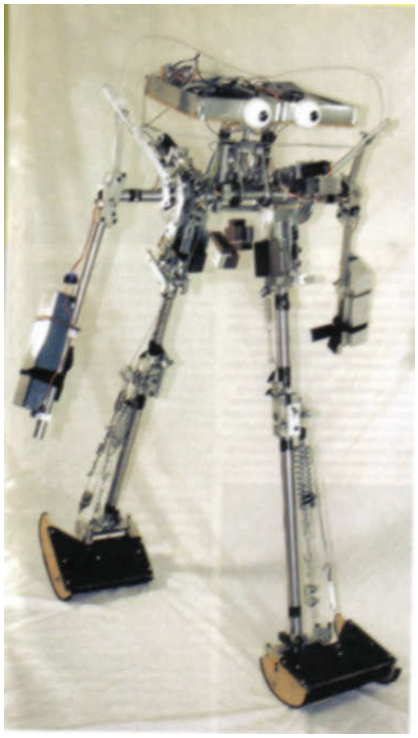

Figure 6. The Cornell Biped

This energy efficient biped robot walks passively, with motors driving its ankles [17].

Figure 7. Honda Human Robot.

Honda Motor Co., Ltd. Tokyo, Japan. [18]. Anthropoid robot, not autonomous. Electrically powered with legs based on human anatomy.

Figure 8. Centaurob I.

Cooperation of C-LAB; HNI, Paderborn University; LKL, Paderborn University , Germany. [19]. A biped with large interlocking feet, to increase static balance abilities.

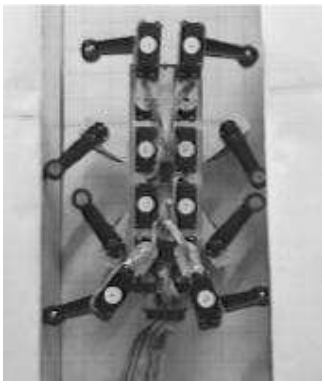

Figure 9. Pipe Climbing Robot.

Corporate Research and Development, Intelligent Systems, Siemens AG [20]. An octopod with revolute jointed legs, each joint being powered.

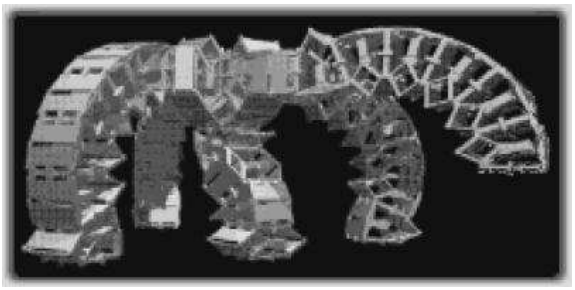

Figure 10. Polypod.

Stanford University, CS Robotics Lab, Palo Alto [21]. This design only project envisages modular legs based on multiple five bar chains. This particular version is a pentapod, though other configurations are possible.

Figure 11. The STIC Insect.

Mechatronics Research Group, University of Southern Queensland, National Centre for Engineering in Agriculture, Australia. [22]. A pneumatically powered quadruped.

Figure 12. Dante II.

Carnegie Mellon University, Field Robotics Center. [23]. A quadruped with pantograph legs and ankles. This robot entered an active volcano, Mt Spurr in Alaska in 1994.

Figure 13. Spring Walker bipedal exoskeleton.

Applied Motion, Inc. [24]. A biped that uses a spring to bounce the vehicle along. Sophisticated control system a necessity!

Figure 14. Walking Beam.

Martin Marietta Automation and Robotics Group [25] An heptapod that has four feet on the ground at all times. Foot movement achieved by a sliding beam with fast acting jacks.

2.3 Number of legs

A convenient way of classifying walking machines is to group them according to the number of legs they have. Animals too are classified on this basis, being considered bipeds (humans and birds), quadrupeds (mammals and reptiles), hexapods (insects), octopods (arachnids) or polypods (caterpillars, centipedes and millipedes).

The number of legs has a major impact on the physics of the problem of walking. It is well known that to maintain a structure's position in a three dimensional space requires three points of support. If a machine has fewer than three legs, it is said to be dynamically balancing. In other words, the walker must have some mechanism to vary the position of its centre of gravity in relation to its foot position, to prevent it falling over. Machines with three or more legs continuously in contact with the ground are said to be statically balanced – that is they may maintain their centre of gravity at any constant position, providing the vertical projection of this centroid is within the polygon constructed by connecting the foot points on the support plane. This polygon is known as the "support polygon" and would be triangular for a tripod or some form of quadrilateral for a quadruped.

2.3.1 Bipeds

The Honda robot (Figure 7) and the Centaurob (Figure 8) are examples of this configuration. Bipeds are usually anthropomorphic – that this they attempt to mimic the human mode of locomotion. In most gaits that humans use to move, the foot of one leg is always on the ground. The other leg is lifted, and in the process of moving to a suitable position for the next footfall. So walking in humans equates to the balancing of a weight on a single column which is unconstrained in any dimension except its height. To maintain stability, the walking human or machine must ensure that their centre of gravity lies vertically above their footprint. As the legs and feet are usually arranged to lie side by side, the walker must move their centroid laterally by the size of the transverse pitch between the feet. This is the approach taken by humans and other natural bipeds, and also by the Honda robot.

Another approach, as typified by the Centaurob, is to make the feet so large that their footprint is large enough to enclose a fixed centroid. Hence the annular shape of the feet on this machine. This is also the method used by walking drag lines. Some reduced lateral movement of the centroid may be required even with large feet.

Both of these approaches to maintaining stability have limitations. Active balancing requires a system to move the body, and sensors to detect position or imminent falling over and some type of response system to make corrections, in short, a control system. This control system makes any dynamically balanced walker complicated to design and implement.

In large footed bipedal walkers, the size of the feet may limit where the machine can place them. Such a machine would also be relatively unstable, as the centroid location must be kept within a small range of positions, to ensure that it is always within the footprint. Any small changes in centroid position may make the walker topple over. This type of walker is only capable of walking on very flat surfaces, as any inclination or wobble in the foot can shift the centroid outside the footprint.

Most recently much attention has been given to passive, dynamic walkers. In this type of machine, as typified by the Cornell biped (Figure 6), the legs are not powered, and the biped is dynamically balanced. The main advantages of this configuration are low power consumption, humanoid appearance and negligible foot impact forces [17]. Although this robot has knees, it would be incapable of negotiating everyday obstacles such as stairs.

2.3.2 Quadrupeds

Quadrupeds may also be dynamically or statically balanced. The balancing condition depends on the duty cycle of the leg mechanism. If each individual leg can be moved fast enough, the quadruped may maintain three legs supporting the body at all times, as shown in the walking truck (Figure 3). This type of gait will be statically balanced and a balance control system can be dispensed with. The disadvantage is that the leg mechanism must have fast action, in order to move the foot to the new foot placement position in 25% of the step time. This may be difficult to implement.

Quadrupeds may also have gaits where only two legs support the body. These gaits all require balance control to ensure stability.

2.3.3 Hexapods

Six legs are the minimum required to ensure static balancing with leg mechanisms with a symmetrical duty cycle, that is, where the return part of the cycle is the same duration as the walking part. Three legs can be in the walking phase of their cycle, while the additional three legs are moving along their return trajectory. This configuration has the twin advantages that it requires no balance control system, and the leg mechanism's movement can be more easily achieved due to the relative similarity between walking and return phases.

The triangular shape of the support polygon for each tripod means that a rigid legged walker will be completely fixed in space once the legs are in contact with the ground. There would be no rocking, and the orientation of the walker body can be determined completely from knowledge of the terrain, which may vary from planar. Rough terrain can be tolerated with a symmetric gait. Hexapods are a common and popular configuration amongst research groups, as the elimination of balance control simplifies the design of the machine significantly.

The main problem with hexapodal walkers is the complexity of the additional legs. In electrically controlled and individually actuated legs, this overhead may be considerable.

2.3.4 Octopods

Walkers with eight legs may maintain four legs on the ground at all times, and have four legs in the return stroke. The support polygon is a quadrilateral, with an area approximately twice that of the triangular support polygon of the hexapod with the same leg-base and track. This makes the vehicle much more capable of tolerating uneven walking surfaces, as the centroid position projection has a much greater locus of stable positions.

However, if the legs are non-compliant, the potential for a rocking condition can occur. This would occur on an uneven surface, where three legs find purchase, but rigidity of leg and frame prevents the fourth from reaching the surface. If the centroid changes position, due perhaps to leg movement, the walker body may shift weight onto the free leg, causing it to move groundward, simultaneously lifting the leg which was on the ground before. The body would experience a rapid rocking motion, and perhaps some impact as the foot hits the ground. This could be dubbed the “restaurant table” effect.

2.3.5 More than eight legs

Although walking machines have been designed with more than eight legs, these machines are rare. The extra complication of the extra legs does not usually create sufficient stability benefits to make the complication worthwhile.

The overall layout of the walking machine will be determined by the number of legs it has, and how it uses them to travel. However, there is more than this required to make a practical walker, as described in the following section.

2.4 Mechanical design of walking machines

Although the superstructures of walking machines can be innovative, generally it is the legs that are of most interest. In spite of the wide variety of walker types, the mechanical principles that the legs use are remarkably limited. The vast majority of walking machines have leg mechanisms that are effectively pantographs. In natural walkers too, if muscle/ligament assemblies are considered as extensible links, the pantograph is also the dominant mechanism.

2.4.1 Pantographs

The reason that pantographs are so ubiquitous is their simplicity and versatility. They are a form of four bar linkage, which in the usual configuration, where point O is fixed, have the interesting property that whatever the kinematic motion experienced by the point A in Figure 15 below, it is mimicked by point E, in an amplified form. The amplification or scaling factor depends on the proportions of the links.

The pantograph is a two degree of freedom mechanism – to completely define its position requires knowledge of two parameters. In this case, the x and y coordinates of the driving point A are required to be known, before the position of the foot, E, can be determined.

Although this property of pantographs is used to create a suitable foot trajectory, there are other modes of operating the pantograph. In Figure 15 the motion of point E is determined by

moving point A horizontally and point O vertically. This leg mechanism is evidently effective as it was used to propel the successful Adaptive Suspension Vehicle (Figure 2). This mode of operation suffers from requiring two actuators per leg. This limitation is common to most pantograph based leg mechanisms.

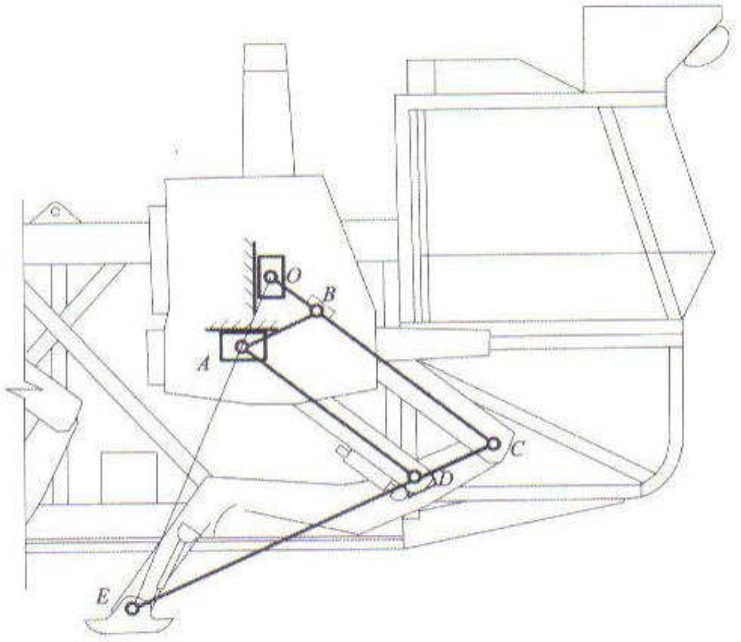

Figure 15. Schematic showing pantograph legs of the adaptive suspension vehicle. [26]

A further limitation of this design is that some leg kinematic control system must be implemented to determine the trajectory of the foot point. This control system usually incorporates ground sensing, and must have kinematic control to maintain the vehicle body position in relation to the ground.

Another attempt to use a pantograph leg in a simpler walker is that shown in Figure 16 below. In this design the follower point of the pantograph is attached to a four bar chain at Point B. The four bar linkage comprises the links A_oA, AB, BB_o with the link A_oB_o being fixed. The link BB_o is common to both the four bar mechanism and the pantograph.

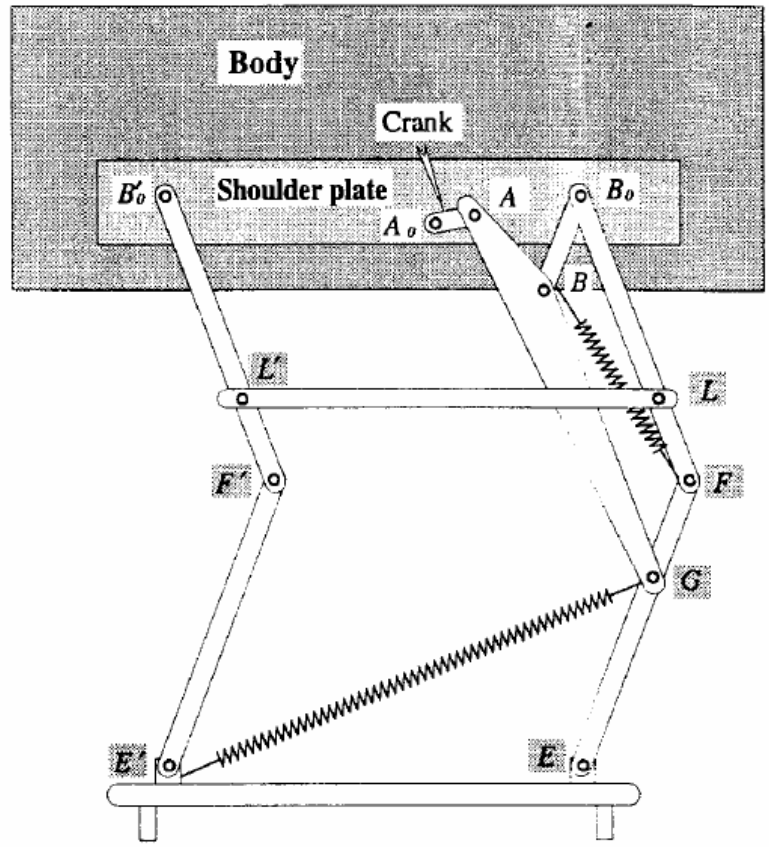

Figure 16. Pantograph coupled to a four bar chain. [27]

The major advantage of this layout is that the leg can now be powered by a single rotary actuator per leg – the two degree of freedom pantograph is effectively reduced to a single degree of freedom mechanism, as the coupler point trajectory fully defines a two dimensional curve. Another advantage is that the foot point trajectory is determined by the four bar chain's coupler point motion. The motion of this point can be synthesized to completely define a suitable foot point trajectory. The need for foot trajectory control and ground sensing functions is removed.

Other discussions on different pantograph configurations can be found in [1] and [28].

2.5 Drives & power supply

Most of the walking machines described in previous sections are laboratory prototypes. Many of them are electrically powered, and have tethers or connecting cables through which power and sometimes control information can be supplied.

Some prototypes are more independent power-wise, for example the Adaptive Suspension Vehicle (Figure 2) or the Walking truck (Figure 3). Although the limbs are operated by pneumatic or hydraulic actuators, the pneumatic compressors or hydraulic pumps are driven by internal combustion engines. Some electric vehicles may carry their power source in the form of batteries. The range of possible motive power sources for walking machines is limited by similar factors to those that limit motor vehicle power sources, primarily energy density. The weight of fuel or stored energy in battery form and the weight of the structure and drive systems needs to be minimized, as transporting the weight of the vehicle is the main consumer of power.

One of the most notable disadvantages of most walking machine prototypes is their energy inefficiency. Due to a combination of high weight, numerous actuators, conversion losses, sensor and control system power, these machines are much less efficient than wheeled vehicles and especially biological walkers. Though the efficiency of animals is a remote target, it may be possible to design a walking machine with energy consumption per distance travelled similar to that obtained for wheeled off-road vehicles.

2.6 Advantages over wheels or tracks

Walking vehicles have many advantages over wheeled or tracked vehicles. These may be listed as follows:

2.6.1 Contact with the ground at discrete points

The rims of wheels have continuous contact with the ground over which they travel. Walking machines place their feet, and once placed, frictional forces prevent further movement of the foot and movement is confined within the linkage system of the leg. The dynamics of the vehicle body is determined by the leg kinematics alone, whereas in wheeled vehicles, the body position is continuously affected by the contour of the road surface. Vehicle suspension mitigates this effect on modern vehicles, but it is entirely eliminated in walking machines.

2.6.2 Elimination of roads

Although heavy usage would lead to tracks forming, as found when animals move along the same path regularly, walking machines do not require roads or other prepared surface to walk on. With light traffic, a legged vehicle should leave only a series of discrete footprints.

2.6.3 Minimal contact area with ground

In walking machines, the total ground area touched is the area of each footprint times the number of footprints per distance travelled. This is considerably less than the area moved over by a wheeled or tracked vehicle, which is the width of tyre or track times the distance travelled. For example, in an area of land where land mines have been randomly deployed, the continuous track of a wheeled vehicle increases the chance of a land mine being triggered, whereas a walker touches a much smaller area of the land over which it travels, and there would be reduced risk of triggering mines.

2.6.4 Reduced ground pressure

As a walking machine may carry a foot of practically any size, the average ground pressure it exerts can be made extremely small. In wheeled vehicles, the diameter of the wheels places a physical limit on the length of footprint. Although tyres can be made wide, the maximum contact patch size is limited, and ground pressure cannot easily be reduced below a certain value. Tracked vehicles can have a large contact area, and hence are preferred where low ground pressure is advantageous, for example vehicles that operate in snow or swamps. A walking machine could be competitive with a tracked vehicle in these conditions, although this still depends on the reduced body weight that could result from improved design of walkers.

2.6.5 Vehicle height

If a walking machine has a mammalian type body plan, with the legs attached underneath its body, then the body is carried higher off the ground than the body of a conventional wheeled or tracked vehicles would be. This body position may be advantageous where the vehicle is intended as a moveable vantage point, for example in game viewing applications. Greater vehicle height would also enhance wading abilities.

2.6.6 Increased traction

Wheeled vehicles are subject to slip, especially when applying high tractive effort on loose, slippery or wet surfaces. A suitable walking machine, with sharp feet to increase ground pressure, and hence penetration, could apply more tractive effort than a wheeled vehicle. It may not be able to compete with a tracked vehicle however. Other types of feet that firmly attach to the walking surface could also be employed to allow increased traction. See section 2.6.8 below.

2.6.7 Amphibious potential

With a suitable leg arrangement carrying a set of floats or pontoons, a walking machine could be made an effective amphibious vehicle. If the area of float can be made large enough, then vertical displacement of the weight carrying floats can be less than the foot lift of the returning leg. This means the vehicle could walk on the surface of water, as returning floats would be lifted clear of the water surface, and placed forward of the current float. Preliminary calculations on the current Perspex walker (see section 7.5 below) show that this mode of locomotion may be possible. Such a vehicle could also walk on land, with extremely low ground pressure.

2.6.8 Climbing abilities

With the addition of suitable foot attachment devices, such as electro-magnets for steel surfaces, or suction devices for smooth surfaces, such as glass, it should be possible to make a walking machine travel vertically or even upside down. The foot attachment mechanism would need to have grip control, releasing grip to allow the leg to be lifted on the return stroke and acquiring it when the leg is on its duty cycle.

The Siemens pipe climbing robot (Figure 9) is an example of this type of robot, although it seems to attach itself by exerting pressure on the pipe walls, much like a rock climber does when “chimneying”. The walking beam (Figure 14) had an intended role as an inspection platform for doing non-destructive testing on aircraft exteriors and used vacuum pads to attach itself to the aircraft surface. Wheeled machines have never successfully been used as climbers.

2.7 Disadvantages with respect to wheels or tracks

The fact that vehicles that use wheels or tracks are the only types of vehicles currently being constructed in any significant numbers, and given that many attempts have been made to create walking machines, there must be severe disadvantages to using walking machines for transportation. These include:

2.7.1 Complication

Wheels are extremely simple, in the simplest form, a circular plate with a central hole. The wheel is widely considered one of human kind's greatest inventions. It is probably the simplest device that can be used for land transportation. It requires no ground sensing, and with suitable vehicle design, no balance control. Steering is easily achieved. With suspension and drive to all wheels, wheeled vehicles can have good off road abilities, but their primarily realm is tarred roads in the modern world.

Tracks are somewhat more complex than wheels, being equivalent to a set of wheels that carry their own small section of roadway with them. Indeed it is only in the last 100 years that tracked vehicles have been used, and even today they are limited to specialist uses such as earth moving, military and arctic conditions.

Walking vehicles are generally orders of magnitude more complex. There are many joints, kinematic links, sensors, software, multiple actuators, difficult manoeuvrability issues and stability issues that all make most current walking machines extremely complex. Though dreamers have often dreamt of such machines, it is only in the last 40 years that any progress has been made in achieving the dream.

2.7.2 Inefficiency

As mentioned in section 2.5 above, walking machines are not fuel-efficient, especially considering the slow speeds at which they travel. Wheels running on a good road surface are the most efficient way to travel on land. It is no surprise that ultra-efficient solar challenge race cars all use wheels.

Tracks are considerably less efficient than wheels. This is primarily due to the energy required to move the track itself. The large number of revolute joints connecting the track sections, with their associated friction, means that simply turning a track absorbs considerable power.

Although it is hard to accumulate data or find a means of comparing tracks to legs in terms of transport efficiency, a brief consideration would indicate that walking machines could be made to be similar in efficiency to tracked vehicles.

2.7.3 Cost

The cost of construction will generally be related to its complexity. Given the complexity of most current walkers it is not surprising that none has entered production, as presumably they could not be sold at a reasonable price.

However, tracked vehicles are also extremely costly in relation to wheeled ones. Even specialist wheeled vehicles command a premium price. If a sufficiently simple, hence cheap, walking machine could be constructed, and located in specific marketing and operational niches, it may be possible to sell these at a competitive price.

2.7.4 Novelty

The unfamiliarity of the public with walking machines, and their gangly unlikely looking appearance may create some resistance to their adoption. It is also possible that these same features may make them popular. However in accordance with the law of “maximum cussedness”, what can go wrong will. This factor is therefore considered a disadvantage, though with clever marketing it could be turned into an advantage. The current South African produced TV commercial concerning Theo Jansen and his “strandbeeste” may be a portent of popularity to come.

2.8 Practical applications

The final design of this new walking machine is intended for transport service across rough terrain. It should be large enough to carry a significant payload, of some tons. It should be capable of operating without roads, and should be self-sufficient with respect to motive power. The envisaged operating environment would be somewhat flat land, such as open bush country, or light forest. It should be capable of ascending and descending slopes of up to 40°, and should be sufficiently manoeuvrable to avoid large obstacles. It should be able to move at reasonable walking speeds, up to 50 kilometres per hour and have a useable range of several hundred kilometres before refuelling. It should be robust, simple and easy to maintain. Complex parts that cannot be repaired in the field should be minimized.

The practical applications of such a vehicle could include:

1. forestry applications,
2. land mine clearing,
3. game viewing,
4. off-road use in areas where roads are undesirable e.g. in game parks,
5. transportation across snow or ice,
6. travel in swampy areas, and
7. travel on beaches or sandy areas.

2.9 Design Criteria

Applying the principle of parsimony (also known as the “KIS” (Keep It Simple) principle or Occam’s razor) makes the criteria for an envisaged walking machine much clearer. This principle is not mentioned facetiously, but as a conscious reminder that complexity is what has kept most walking machines confined to laboratories. The KIS philosophy will need to be applied continuously during design and development of such a machine. In this light, the criteria which the prospective walking machine should meet are:

1. Static balance, so that no balance control system is required.
2. Active propulsion, as powered legs will extend the navigable terrain immensely.
3. Minimal power consumption.
4. Minimum number of prime movers, to simplify implementation and maintenance of the machine. If a single prime mover can be used, the control system for the prime mover can be greatly simplified.

5. The prime mover should preferably require rotary rather than linear motion, as rotary prime movers are varied, simple and can be easily portable, particularly internal combustion engines and electric motors. Hydraulic or pneumatic linear actuators require more sophisticated systems and still require a rotary prime mover to be portable.
6. Deterministic foot trajectory, to eliminate the need for ground sensing, impact control and leg kinematic control systems.
7. A slow return mechanism to reduce mechanism dynamic loads in the leg's return stroke.
8. A stiff mechanism, to ensure that body movement is controlled by leg position.
9. Variable foot size to enable management of the machine/environment interface area.
10. Hinged legs, or legs with knees, so the walking vehicle body can be maintained in the same horizontal plane, minimizing changes in potential energy.
11. A scalable design to allow testing and validation on reduced scale prototypes that may later be applied to the full sized vehicle.
12. The final design should be for a large walking machine, as outlined in section 2.8 above.

It may be feasible to construct such a walking machine if a suitable linkage could be found. With hindsight, a four bar chain coupled to a pantograph as shown in Figure 16 could have been used. In 2000, a brief article in New Scientist magazine [29] supplied the idea for a new type of linkage. Although interest was largely intuitive, and initially sceptical, it was sufficient to warrant further study. The article concerned a new type of leg mechanism, used by an eccentric Dutch kinetic sculptor to make large plastic machines that were blown by the wind across beaches near the North Sea. Theo Jansen and his "strandbeeste" are the subject of the next chapter.

Chapter 3 Twelve bar linkage

3.1 Theo Jansen's "strandbeeste"

The idea for a new type of linkage came from an article in New Scientist magazine [29], concerning the work of Theo Jansen, a Dutch physicist / artist creating a series of kinetic sculptures, collectively named "strandbeeste", see Figure 17. He has constructed a wide variety of machines, all based on a similar principle. More of his creations can be seen at his web site [30] and in his book [31].

Figure 17. One of Theo Jansens's "strandbeeste"

Examination of this mechanism shows that it could provide legs that meet the design criteria listed in section 2.9 above. The "strandbeeste" are large enough that they could be used for transportation. They operate successfully on beaches and so have demonstrable off-road performance. However they are primarily intended as kinetic sculptures, and would not be practical as transportation vehicles in their present forms.

The primary problems with Jansen's "strandbeeste" are the method of construction, and the layout of the machines. They are constructed from plastic tube, said to be electrical conduit. The joining methods are not clear, but the main components appear to be lashed together with twine. It is doubtful whether this type of construction would be suitable for a working transport vehicle.

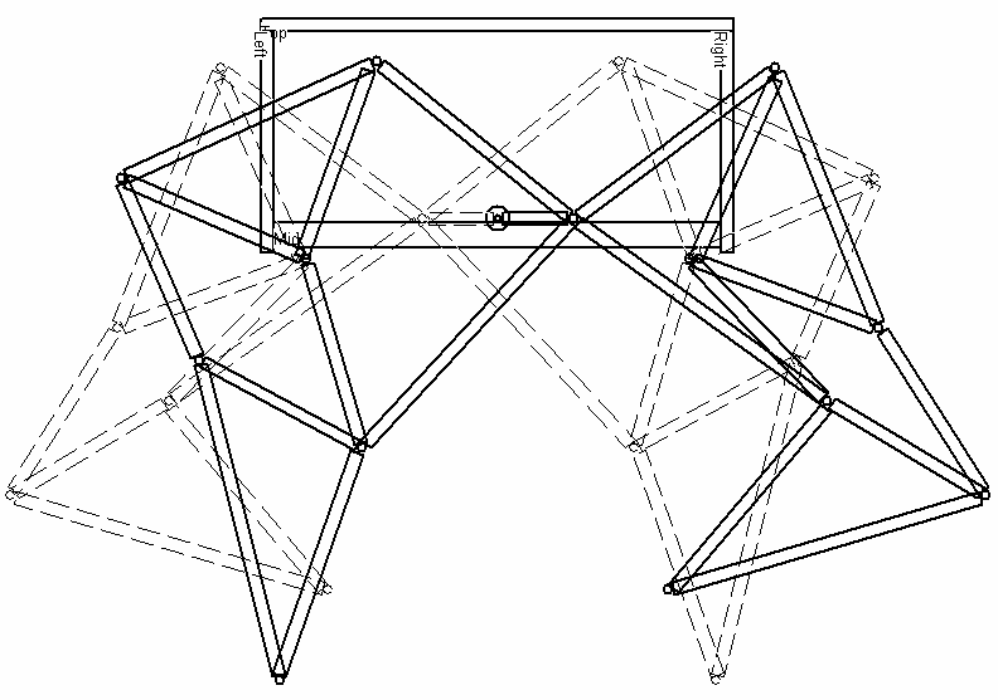

Figure 18. Sketch of Jansen's single crank layout.

The second problem is that all legs are driven from a single central crankshaft, as shown in Figure 18. The rear mounted legs effectively turn in reverse relative to the front legs. However, the horizontal velocity of the foot is asymmetrical i.e. it moves faster at the beginning of the cycle than it does at the end, or vice versa. This can be seen in Figure 19, which shows the velocity of the foot, for a mechanism with the same proportions that Jansen uses.

The front legs experience the profile as shown by moving from left to right between the two purple vertical lines, which indicate the footfall and foot lift positions. The rear mounted legs will experience velocity changes in the opposite direction, that is, the velocity changes would be as indicated by moving from the right vertical line, towards the left.

The feet therefore experience longitudinal movements in relation to each other as the machine walks, and they cannot remain firmly planted on the ground. At least one foot must move to accommodate the pull exerted by the mechanism.

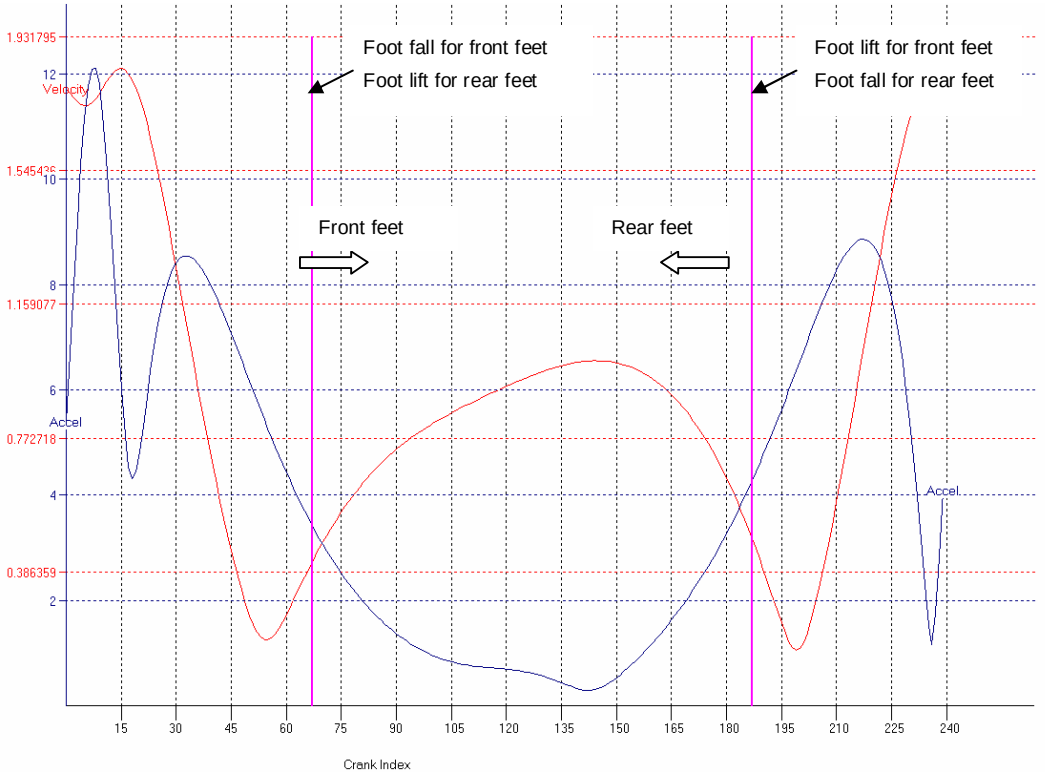

Figure 19. Velocity at the foot point for Jansen's linkage proportions.

This effect can also be seen clearly in the animation provided in the file "Animation of Single Crank Walker.gif" on the accompanying CD ROM in the "*Animations\Animation of Jansens Single crank walker*" directory.

It is no surprise that many of Jansen's "strandbeeste" actually use wheels as feet – the wheels are there to allow for this movement. Technically this gait should not be considered a walk, it more closely resembles ice skating or a skiing gait.

3.2 Advantages of the Jansen twelve bar mechanism

The Jansen mechanism is worth pursuing as a valid alternative mechanism for use as a leg for a walking machine, if considered in relation to the criteria previously listed in section 2.9. Although it is the only leg design assessed in this way, the only other design contender worth considering, the four bar chain driven pantograph from section 2.4.1, has already been discussed in the literature [27], whereas the Jansen linkage has not. In addition the Jansen linkage assesses so positively in relation to the design criteria that it should at least be considered further before rejection as a possible mechanism to use.

Table 1. Assessment of Jansen mechanism's suitability for use in walking machines

No	Criterion	Comment in relation use of Jansen legs
1	Static balance.	The static balance is not affected by the leg design itself, and a six or eight legged walker could be designed with this leg type. Quadrupeds cannot be achieved, as the best duty cycle found was 67% (see section 4.4).
2	Active propulsion.	It would be simple to power all legs on a walker with this leg mechanism.
3	Minimal power consumption.	As the Jansen mechanism is a linkage with stiff links, and single actuation, it will not require much energy to turn. The main obstacle would be friction, and this can be minimized with suitable detail design.
4	Minimum number of prime movers.	If a two crankshaft machine is built, then the problems encountered with the walking of "strandbeeste" can be avoided. The drive crankshafts would have to be driven together, with gear trains, chains or belts and their relative phase maintained.
5	Rotary prime mover.	Power to the Jansen leg is provided by a crank, which is easily driven directly from a motor, via a gearbox to ensure correct speed.
6	Deterministic foot trajectory.	The Jansen mechanism has a single degree of freedom. The foot position is found from knowledge of link dimensions and crank position.
7	A slow return mechanism.	As will be seen, the Jansen mechanism can be made to a have a gentle foot return trajectory.
8	A stiff mechanism.	As the mechanism is a single degree-of-freedom system, the stiffness depends on the crankshaft's ability to hold its position. Links themselves can be made extremely stiff.
9	Variable foot size.	The coupling point at the end of the leg could easily be made to accommodate feet of different designs.
10	Hinged legs.	The leg joint is hinged.
11	Scalable design	This is perhaps one of the largest advantages of this mechanism. As the linkage is planar, it can be scaled up or down and the trajectories will also change by the scale factor. Any kinematic work can be done at any scale, enabling use of scale models for testing. It also means that the upper size limit of such a walker is limited by structural considerations.

Jansen has not patented his mechanism, neither has he published any technical papers on the matter [32]. He has alluded to a trigonometric solution and to the fact that he used an “evolution program” to develop mechanism proportions, but the details of his design have not been published [29].

Before the researcher could explore the possibility of designing a walking machine based on the Jansen mechanism, a mathematical model had to be developed. This model would need to provide data on motion of the feet, in addition to other kinematic and kinetic information. This was done in previous work [1]. The following section provides a brief overview of this model, along with enhancements that became necessary to support the author’s own version of an “evolution program” to find useful configurations of the mechanism.

3.3 Analytic model

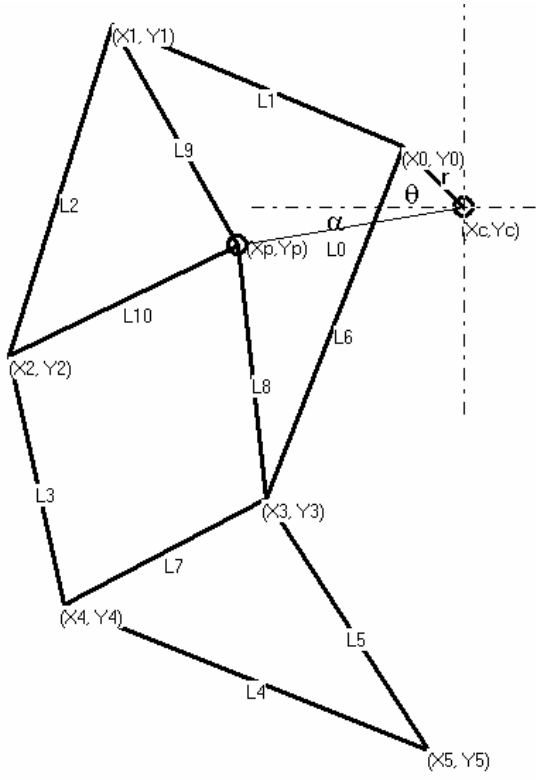

Figure 20. Twelve bar Jansen linkage

Considering the sketch of the linkage shown in Figure 20, it is possible to derive the motion of the foot point, (x_5, y_5), as a function of the crank angle θ. This requires knowledge of the lengths of the links, which can be represented as a vector

$$L = [l_0, l_1, l_2, l_3, l_4, l_5, l_6, l_7, l_8, l_9, l_{10}] \qquad \text{Equation3.3.1}$$

where l_0 represents the distance between the crank shaft and the fixed pivot, and the other subscripts represent lengths of the links as named in Figure 20.

The crank radius is taken as a constant, r, rotating about the crank centre point (x_c, y_c). The fixed pin position is given by (x_p, y_p), and is inclined by angle α to the horizontal. The fixed pin coordinates (x_p, y_p) are given by:

$$x_p = x_c + (l_0 \times \sin(\alpha)) \qquad \text{Equation (3.3.2)}$$

$$y_p = y_c + (l_0 \times \cos(\alpha)) \qquad \text{Equation (3.3.3)}$$

The positions of the various nodes of the linkage can be represented as a vector of points

$$N = [(x_0, y_0), (x_1, y_1), (x_2, y_2), (x_3, y_3), (x_4, y_4), (x_5, y_5)] \qquad \text{Equation (3.3.4)}$$

Considering Node 0, we can write the following equations.

$$x_0 = x_c + r \times \sin(\theta)$$ Equation (3.3.5)

$$y_0 = y_c + r \times \cos(\theta)$$ Equation (3.3.6)

The position of Node 1 is determined by the intersection of the arcs made by Link 1 around (x_0, y_0) and the arc of Link 9 around point (x_p, y_p). These are all known quantities, so it should be possible to compute the position of node 1.

$$(x_1 - x_0)^2 + (y_1 - y_0)^2 = (l_1)^2$$ Equation (3.3.7)

$$(x_1 - x_p)^2 + (y_1 - y_p)^2 = (l_9)^2$$ Equation (3.3.8)

Simplifying equation (3.3.7) above yields

$$x_1 = x_0 \pm \sqrt{(l_1)^2 - (y_1 - y_0)^2}$$ Equation (3.3.9)

Similarly, equation (3.3.8) can be re-arranged thus

$$x_1 = x_p \pm \sqrt{(l_9)^2 - (y_1 - y_p)^2}$$ Equation (3.3.10)

Equating equations (3.3.9) and (3.3.10) gives

$$x_0 \pm \sqrt{(l_1)^2 - (y_1 - y_0)^2} = x_p \pm \sqrt{(l_9)^2 - (y_1 - y_p)^2}$$ Equation (3.3.11)

Unfortunately equation (3.3.11) cannot be easily solved for y_1, due to the presence of square roots on both sides of the equation. There will always be terms in $\sqrt{(y_1 - y_{o,p})^2}$ which cannot be eliminated, making an algebraic solution difficult, as detailed in previous work [1]. The actual method of solution derives from coordinate geometry, specifically the intersection points of two intersecting circles, shown in Figure 21.

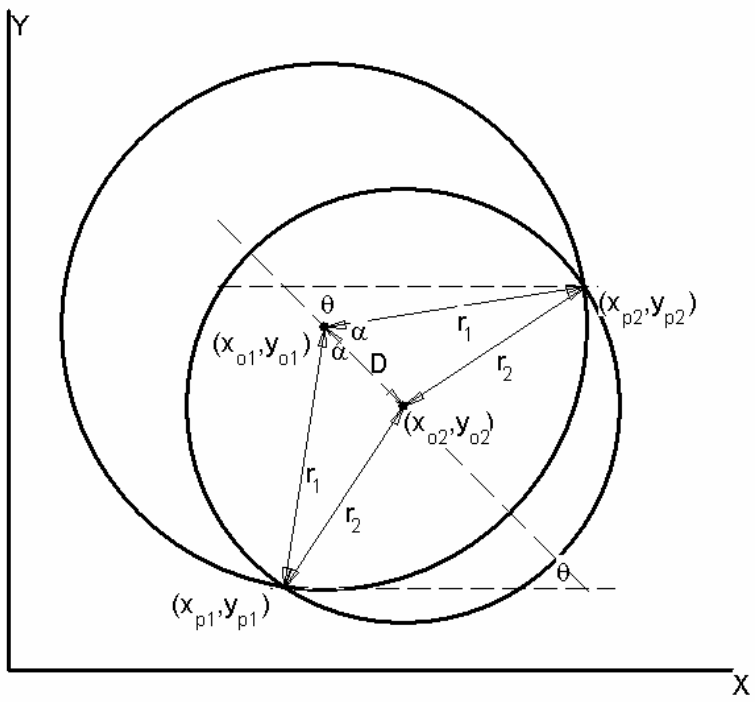

Figure 21. Intersection of two circles

The following equations for the intersection points (x_{p1}, y_{p1}) and (x_{p2}, y_{p2}) are standard in the field of coordinate geometry [33].

$$x_{p1} = x_{O1} + r_1 \cos(\theta + \alpha) \qquad \text{Equation (3.3.12)}$$

$$y_{p1} = y_{O1} + r_1 \sin(\theta + \alpha) \qquad \text{Equation (3.3.13)}$$

$$x_{p2} = x_{O1} + r_1 \cos(\theta - \alpha) \qquad \text{Equation (3.3.14)}$$

$$y_{p2} = y_{O1} + r_1 \sin(\theta - \alpha) \qquad \text{Equation (3.3.15)}$$

where

$$\theta = \tan^{-1}\left(\frac{(y_{O2} - y_{O1})}{(x_{O2} - x_{O1})}\right) \qquad \text{Equation (3.3.16)}$$

$$\alpha = \cos^{-1}\left(\frac{(D^2 + r_1^{\,2} - r_2^{\,2})}{(2 \times D \times r_1)}\right) \qquad \text{Equation (3.3.17)}$$

$$D = \sqrt{(x_{O2} - x_{O1})^2 + (y_{O2} - y_{O1})^2} \qquad \text{Equation (3.3.18)}$$

Although equations (3.3.12) to (3.3.15) will yield the positions of both intersection points, only one point is relevant at each node. The solution software contains additional information to ensure that the correct intersection possibility is used. In addition, the software checks for conditions which may make finding the intersection points impossible, such as non overlapping circles etc.

3.4 Computer model

The solution to solving this mechanism uses repeated application of the simple method outlined. Each node is considered as the intersection of two circular arcs, and by moving sequentially from node 0 to node 5, the positions of all nodes can be found. This method is shown graphically in the flow chart, Figure 22.

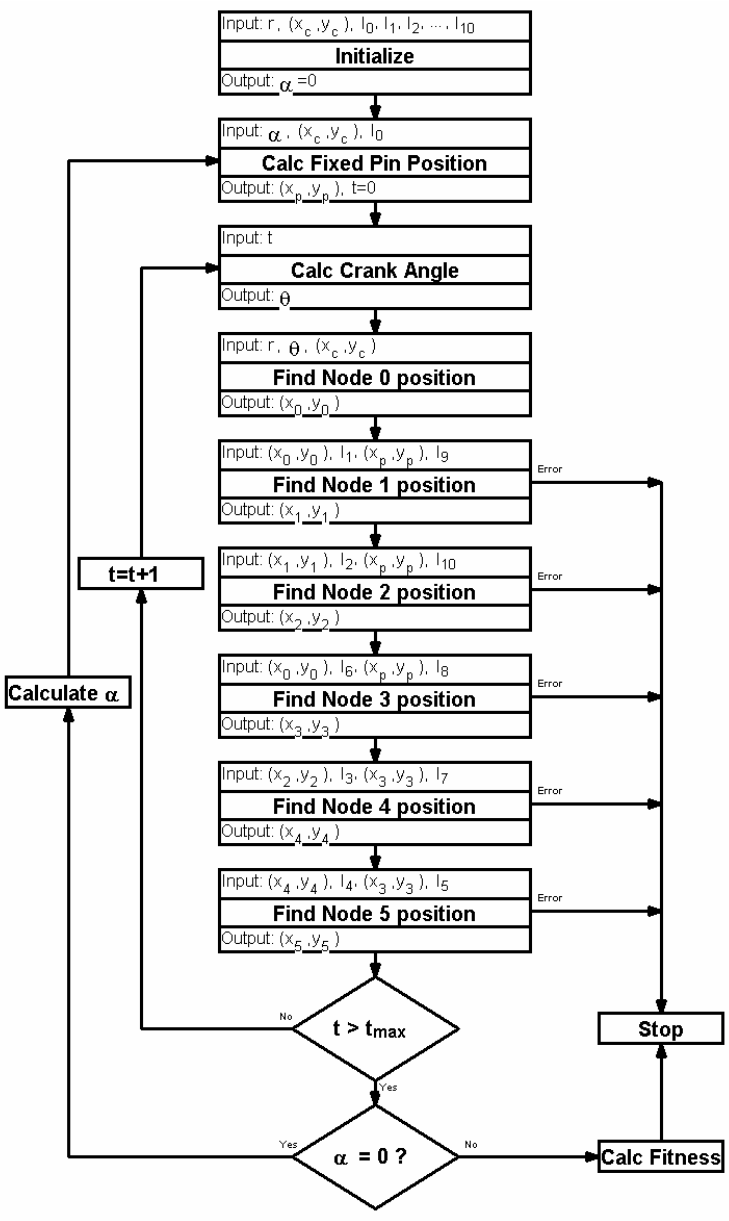

Figure 22. Flowchart of solution of twelve bar linkage

The inner loop of the algorithm detailed in Figure 22 shows that a single revolution of the crank is broken up into a number of time slices, which are equivalent to angular positions, given that the drive shaft is assumed to be rotating at a constant angular velocity. In the software implementation, the maximum number of time slices permitted is 256, but there is no theoretical upper limit on how finely the time may be sliced. So t ranges from 0 to 255, although t_{max}= 239 is usually used, as this equates to 240 time slices with an angular position change between each of 1.5°.

3.4.1 Calculation of mechanism orientation angle, α

Figure 22 further shows that the orientation angle α is calculated after the mechanism has been solved once for a complete revolution. This is achieved by scanning through the foot positions and comparing the velocities of two points which correspond to crank positions 180° apart. When points with the most similar veloc ities are found, these two points are taken as the points when the foot will touch the ground, and 180° later, when the foot will leave the ground, i.e. the points that delimit the walking cycle. This algorithm has an implicit assumption that the duty cycle of the leg is 50%, as 180° of the 360° of a full revolution are spent with the foot grounded.

The slope of a straight line that connects the two points found is taken as the correct orientation angle for the mechanism. Rotating the entire mechanism through this angle will result in the connecting line being horizontal, and so the walking part of the foot trajectory is also kept more-or-less horizontal. This makes evaluation of usefulness for walking much easier.

The reason velocities are compared is that minimising the speed difference between the feet arriving on the ground and those feet leaving the ground will limit the amount of slip or scuffing that may occur as the vehicle's weight is shifted from one set of legs to another.

Once the mechanism's orientation has been adjusted, the positions of all nodes are recalculated for all crank angles. These new node positions are used as the basis for evaluating the foot trajectory amongst other things.

3.4.2 Fitness calculation

The last action in the algorithm of Figure 22 is calculation of fitness. The fitness is simply a numerical score, a higher score indicating a fitter or better mechanism. This scoring is to enable the performance of different leg configurations to be compared. Various different methods of fitness calculation may be implemented, to allow mechanisms to be selected for different purposes. Exactly how this fitness is calculated is crucial to the selection of appropriate legs, and is discussed in more detail in section 4.2.1 in the following chapter.

Having established a method of solving the kinematic model of the Jansen mechanism, this model will be used to generate legs that could be used in a successful walking machine. The process of creating and selecting good leg configurations is discussed more fully in the next chapter.

Chapter 4 Optimization of link geometry

4.1 Optimization problems

The class of Jansen twelve bar linkages contains an infinite number of possible geometries. The linkage is represented by eleven different parameters - the vector of link lengths $L = [l_0, l_1, l_2, l_3, l_4, l_5, l_6, l_7, l_8, l_9, l_{10}]$ as shown in Equation 3.3.1 previously. As the lengths of all links can vary across the range of real numbers, there is no end to the number of configurations that can be defined. However, many, if not most, of these theoretical assemblies either cannot be assembled at all, or if they can, they do not provide trajectories of interest to a walking machine leg designer. How to find the “best” design or even a selection of “good” designs? What constitutes the relative merits of various layouts?

In both nature and in human development of tools, a process of continued improvement over time has led to “optimal” designs for many creatures. Many human artefacts – knives, pottery and cars to name but three – have also been continuously improved, resulting in current “good” designs. Both in nature and in early human inventions, these were evolutionary processes, progressing by trial and error, with chance playing a major role in forming design variations.

The same is true of pre-Renaissance human affairs – progress was made, but in an uneven, haphazard fashion. Since the development of scientific principles during the Renaissance, especially in mathematics, the search for improvement in designs has become more formalised and systematic. The development of the calculus, which finds points of inflection in mathematical curves, has allowed much improved designs to be developed. This is a familiar problem to engineers, and there is an extensive body of research on finding the best solutions to problems. The area of research is known as “optimization” and has been studied formally at least since the time of Pareto in the 18th Century, although an argument can be made that seeking best performance is a fundamental property of nature.

In more recent times techniques such as linear programming have been used to solve linear optimization problems. Most engineering problems are complex and require mathematical models that are neither linear nor differentiable, and thus lie outside the scope of classical mathematical optimization techniques. Coello [34] and Andersson [35] give general reviews of the different methods of optimization that have been used to improve engineering solutions.

As was seen in Chapter 3, the mathematical model for the Jansen twelve bar mechanism is both non-linear and not analytically differentiable. How then to find the best geometry for such a linkage for a walking machine? Perhaps the question needs to be re-phrased, and the problem approached from a functional point of view. What are the properties of the linkage that need to be optimized?

Several parameters have been identified and are discussed in the following section.

4.2 Optimization parameters

The following general parameters have been isolated as being significant in discriminating between good and bad leg mechanisms. The items discussed in the following sections are not prioritized, but methods for evaluating each parameter are given where possible.

4.2.1 Foot point trajectories for walking

From previous work [1] and the work of others [27], [36] and [37], the path that the foot of a walking machine follows is of crucial importance to the machine's correct functioning. There is a relationship between the trajectory provided by the mechanism and the overall design and format of the walking machine. The general consensus of the papers reviewed, concurring with both Jansen's ideas and the author's own, is that the foot should follow a somewhat triangular path, as shown in Figure 23 and Figure 24.

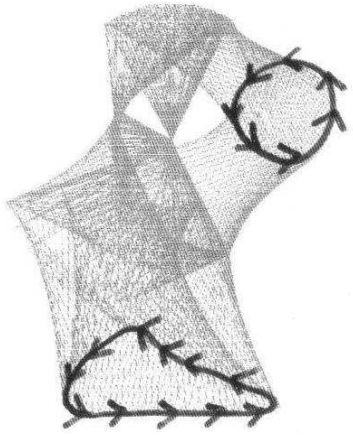

Figure 23. Theo Jansen's diagram, showing his mechanism's foot trajectory [31].

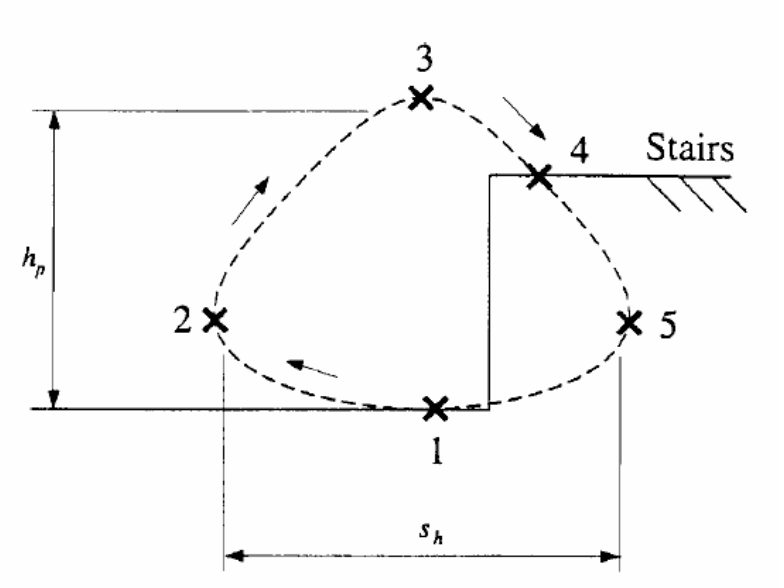

Figure 24. Foot trajectory used by Shieh et al [27].

Figure 24 shows the trajectory the foot would follow for a machine walking from the left side of the page toward the right side, up a single stair.

The diagram starts with the foot at the midpoint of its stride, at point 1. The foot leaves the ground at point 2, and travels on its return stroke through points 3 and 4 to point 5, where the foot is again taking the vehicle's weight. This sketch shows the additional point, point 4, which would be where the foot may strike a step in a staircase – Shieh's robot was intended to be able to climb stairs.

The foot trajectory shown in Figure 24 above is not necessarily the optimum trajectory shape. The problem with this specific trajectory is the curve between points 2 and 5, the walking portion of the cycle. The vehicle body, being connected to the foot by a rigid leg, would experience a motion inverse to this foot curve. Vehicle occupants would feel the vehicle rising and falling. A better foot trajectory would have this portion of the curve as near to a horizontal straight line as possible, keeping the body horizontal on a horizontal walking surface. Note that flatter lower portion in Jansen's trajectory in Figure 23

The flatness of the walking curve can be determined by obtaining a straight line fit to the trajectory points using a least squares linear regression. The correlation coefficient of the regression is taken as a measure of the flatness. In later work the actual sum of variances was used to quantify flatness.

4.2.2 Duty Cycle

The duty cycle of a leg mechanism is the proportion of the total cycle time that the leg is touching the ground, making it capable of bearing weight. Mathematically this can be expressed as

$$DC = \frac{T_l}{T_t} \qquad \text{Equation (4.2.1)}$$

where

DC = Duty Cycle

T_l = loaded time

T_t = total leg cycle time

Initial investigations into the properties of the Jansen mechanism were to see if mechanisms with 75% duty could be found, see section 4.4. Such a mechanism would allow the design of a statically balanced quadruped machine layout, as discussed in section 2.3.2. Unfortunately, no such mechanism was found, using a simple exhaustive search algorithm. Later searches all implicitly accept mechanisms with a 50% duty cycle.

4.2.3 Mechanism size

Clearly, the smaller the mechanism is for a given performance, the better. Smaller mechanism will be lighter, have stiffer links and have lower inertial loads. The size of the mechanism can be represented by the sum of the length of the links.

$$L_l = \sum_{i=1}^{10} l_i \qquad \text{Equation (4.2.2)}$$

where

L_l = Total link length

L_i = Length of link i

4.2.4 Mechanism Compactness

The trajectories of the farthest nodes will determine how much space a particular mechanism will need to operate within. Some arrangements will require a larger space than others, which will in turn affect the detail design of any walking machine based on this leg proportion. The area required to operate in is taken as being limited by the leftmost point of node 4's trajectory, the top most point of node 1, the right most extent is given by node 0, and the lowest point is node 5. Compactness can be expressed as an area, given by

$$A = \frac{\left(x_{4(\min)} + x_{0(\max)}\right)}{2} \times \frac{\left(y_{1(\min)} + y_{5(\max)}\right)}{2} \qquad \text{Equation (4.2.3)}$$

where

$x_{4(min)}$ = Minimum x value of node 4's trajectory

$x_{0(max)}$ = Maximum x value of node 0's trajectory

$y_{1(min)}$ = Minimum y value of node 1's trajectory

$y_{5(max)}$ = Maximum y value of node 5's trajectory

4.2.5 Stride length

The longer the stride of a mechanism, the faster it will be able to move the machine for a given motor speed. This parameter corresponds to S_h in Figure 24. For a Jansen walker, this length, which we will call S_l, would be given by:

$$S_l = \left(x_{5(fl)} - x_{5(ff)}\right) \qquad \text{Equation (4.2.4)}$$

where

S_l = Stride length

$x_{5(fl)}$ = Node 5's trajectory x value, at foot lift, at the end of the stride

$x_{5(ff)}$ = Node 5's trajectory x value, at foot fall, at the start of the stride

4.2.6 Average speed

Maximum average foot speed corresponds to maximum stride length, in that longer strides will have higher average foot speeds. However, considering foot speed eliminates an implicit assumption about the timing of foot/ground contact events. This parameter is measured by averaging all the instantaneous velocity values.

$$V_{ave} = \frac{\sum_{i=ff}^{fl} (x_{i+1} - x_i)}{N_w \times t} \qquad \text{Equation (4.2.5)}$$

where

V_{ave}	=	Average foot speed
ff	=	Crank index at foot fall
fl	=	Crank index at foot lift
x_i, x_{i+1}	=	Foot *x* position at instant *i, i+1*
N_w	=	Number of time slices during the walking cycle = fl - ff
t	=	Time for one crank revolution

4.2.7 Speed fluctuation

Speed fluctuation determines how “smooth” the vehicle feels when walking. The hope is to avoid major mechanism speed changes as the pairs of legs change. This phenomenon cannot be avoided entirely, due to the fundamental simple harmonic nature of rotating mechanisms, but it may be minimized. The speed fluctuation is quantified by considering the distribution of foot speeds as a Gaussian distribution, and taking the fluctuation parameter as 1 standard deviation. Mathematically this parameter, which we can call V_f, can be expressed as:

$$V_f = \frac{\sum_{i=ff}^{fl} (V_i - V_{ave})^2}{N_w} \qquad \text{Equation (4.2.6)}$$

where

V_f	=	Foot speed fluctuation factor
ff, fl	=	Crank index at foot fall and lift, as before
V_i	=	Foot *velocity* at instant *i*
V_{ave}	=	Average foot speed, from Equation (4.2.5)

4.2.8 Foot lift

During the return part of the walking cycle, the foot point should be raised off the ground. This is the height h_p in Figure 24. The higher the foot is lifted, the more capable it will be of avoiding surface irregularities between footfalls. Conversely, the higher the foot is lifted, the more energy is expended overcoming gravity, and the foot's travel path is longer, requiring faster foot motion. The required degree of lift required will depend on the intended duty of the walker. Rough terrain vehicles will need to lift their feet higher and pay a corresponding energy cost.

$$h_p = y_{5(\max)} - y_{5(\min)} \qquad \text{Equation (4.2.7)}$$

where

h_p = Foot lift

$y_{5(max)}$ = Maximum y value during node 5's entire trajectory

$y_{5(min)}$ = Minimum y value during node 5's entire trajectory

4.2.9 Body lift

As mentioned in section 4.2.1, the amount of vertical movement the vehicle body experiences is a function of the curvature of the foot point trajectory when the foot is in ground contact. Minimization of body lift will make the vehicle smoother to travel in, and will also influence power consumption. This parameter can be measured by considering the vertical component of the foot node's trajectory:

$$L_b = y_{5(w\max)} - y_{5(w\min)} \qquad \text{Equation (4.2.8)}$$

where

L_b = Body lift

$y_{5(wmax)}$ = Maximum y value during node 5's walking trajectory

$y_{5(wmin)}$ = Minimum y value during node 5's walking trajectory

4.2.10 Body carriage height

The overall height at which the body will be carried will depend on the lengths of the two vertically adjoining links that carry it. Different purpose may have different requirements. If the walker was intended as a moveable vantage point, then the body would be carried high, on long legs. A small stable walker may require short legs to make it more difficult to overturn. The carriage height is taken as the vertical distance between the foot node and the fixed pin position.

$$H_b = y_{ref} - y_{5(i)} \qquad \text{Equation (4.2.9)}$$

where

H_b = Body carriage

Y_{ref} = The *y* position of some reference point on the vehicle body

$y_{5(i)}$ = The *y* value of node 5's walking trajectory, at instant *i*

4.2.11 Approach and departure angles

In common with wheeled off-road vehicles, a walking machine would be limited in the change of angle of terrain that it could walk over. If it encounters a slope steeper than a certain angle, then its foot would not be able to find purchase, and the machine would be stopped. In the Jansen mechanism, the limiting factor would be the position of node 4, the "knee" of the mechanism. This would act as the leading edge of the machine, and would be the first to touch an approaching steep slope. In a wheeled vehicle this limit is a function of the geometric positions of wheels and the body. In walking machines, especially those with Jansen mechanism legs, this limit would vary with foot and knee position.

Similarly, when walking down a sloped surface onto a horizontal surface, the rear portion of the vehicle may become caught on the ground behind the machine. The rear legs would be unable to find foot positions and the machine may stop. If the front legs had traction, the machine may able to drag the rear section until the legs can reach the surface.

4.2.12 Steering ability

An interesting but not obvious property of the Jansen mechanism is that the stride length and foot trajectory can be easily changed by moving the fixed pin position. This effect is suggested as a simple means of steering a walking machine. Different mechanism have different responses to fixed pin position changes, so those with “better” response are preferred, all other factors being equal.

4.2.13 Power consumption

Although power consumption primarily depends on vehicle weight, factors such as transmission angle (especially when considering friction) and link geometry can have a substantial influence on the energy required to walk the machine. It is a stated design criterion that this parameter be minimized (see section 2.9).

4.2.14 Structural considerations

The load carrying ability of the leg will determine the success of the walking machine. The Jansen mechanism has superior intrinsic structural properties to a pantograph, due to the fact that walking loads are transmitted along at least two paths in the Jansen leg, whereas in a pantograph, loads are carried by a single set of links. However, differing Jansen linkages will adopt different shapes during their cycle, which may influence their ability to carry load, or to move smoothly when loaded. This parameter is difficult to quantify, though the kinetic model developed in [1] could be enhanced to quantify it.

4.2.15 Reversability

Although the Jansen mechanism can rotate in either direction, one direction will be favoured, as this may lead to lower loads or apply loads in a preferred direction. All mechanism found work best when walking such that the lower link attaching to the crank, link 6, is loaded in tension. Reversing the direction would load this link in compression, which necessitates a heavier link, to resist buckling. Mechanisms that can rotate in either direction with minimum impact on link loading will be better suited to a practical walking machine.

4.3 Mechanism synthesis

The classical solution to finding the best mechanism would be to synthesize a suitable one. Synthesis, in mechanism jargon, is the reverse of kinematics. It is the process of finding a linkage configuration that will give the motion defined. Much work has been done on the synthesis of mechanisms – see [38], [39] and [40].

Generally mechanism synthesis can be considered function generation, path generation or synthesis to create mechanisms that pass through specific defined points. Synthesis methods are generally mathematically complex and only solve a limited set of trajectory points.

The main limitation of synthesis techniques in this context is that they require exact definition of the mechanism output motion. In the case of a Jansen mechanism for a walking machine, this information is not known, or of any particular interest. What is of interest is the general form or shape of the foot trajectory curve and a variety of other parameters that are best assessed relatively. Thus mechanism synthesis techniques were not considered further in this research.

4.4 Exhaustive search

The initial approach taken to finding good mechanisms was by exhaustive search. The approach was to consider the links in the mechanism pair wise. The paired links were then considering as two sides of a triangle, with another known parameter making the third side. In this manner, L1 and L9 were associated with L0, L6 and L8 also with L0, L2 and L10 with L9 and so on, creating 5 sets of triangular relations. The lengths of the variable sides were varied as a proportion of the known length.

Using this scheme, effectively eleven nested loops, a program was developed to compute link dimensions for a large number of configurations, and calculate the foot point trajectory for each using the algorithm shown in Figure 22 above. Different mechanism were previously rated using a fitness score calculated on the basis of a selection of parameters listed in section 4.2.

The exhaustive search was used with two different fitness assessment calculators. The first searches assessed each leg on the basis of the following factors:

1. The total length of links
2. The duty cycle of the leg
3. The flatness of both the walking and return portions of the trajectory
4. The maximum stride length

The final fitness factor was calculated as a weighted average, thus:

$$F = \frac{(W_l \times LL) + (W_d \times DC) + (W_w \times FW) + (W_r \times FR) + (W_s \times SL)}{(W_l + W_d + W_w + W_r + W_s)} \qquad \text{Equation (4.4.1)}$$

where

F	= fitness
W_l, W_d, W_w, W_r, W_s	= weighting factors
LL	= total link length
DC	= duty cycle
FW	= flatness of walking portion of cycle
FR	= flatness of return portion of cycle
SL	= stride length

In most tests the weighting factor W_d was given most precedence, thus attempting to find mechanisms with high duty factors. In these tests, the stride of the cycle was taken as extending from the left-most position to the right-most. The highest duty cycle found was 67%. This mechanism was not considered suitable for a practical walking machine as the foot trajectory provided was quite curved during ground contact and the foot lift on return was so small that the returning feet may interfere with uneven ground.

At this point the best mechanism that had been found was the one used by Jansen. These dimensions had been determined by scaling from the small sketch that had appeared in the *New Scientist* article [29]. Accordingly, these dimensions were used for the first prototype built, the drinking straw walker, see section 7.2.

Subsequently, the exhaustive search routine was run with another fitness assessment method. In this method, the following factors were considered:

1. The total length of links
2. Maximum stride length
3. Mean velocity of the foot point
4. Standard deviation of the foot point velocity distribution
5. The foot lift height

The final fitness factor was again calculated as a weighted average of the above values. These tests were attempting to find a fast walker. Hence the weights for stride length and mean velocity were increased. The resulting best mechanism configuration was used for the steel walker, see section 7.3.

The software used to generate these searches is provided and described on the accompanying CD ROM in the "*Software\BG Walker*" directory.

4.5 Lessons learnt

The main problem encountered with the exhaustive search implemented was its granularity. It calculated a large series of discrete mechanism possibilities. It proved impossible to determine if any relationship between good solutions existed. An attempt to do this failed, as no easily understandable representation of the eleven dimensional solution space could be found. The process resembled looking for a needle in a haystack rather than a systematic attempt to find good solutions.

Another problem that was emphasized by later practical experience was that the incorrect criteria were being used to assess mechanism fitness. The kinetic analysis of the Jansen mechanism, developed subsequent to these searches, showed the importance of minimizing body lift. The mechanisms selected from the first two exhaustive searches had not considered this factor, and thus led to designs of walking machines that failed to walk.

It was clear that the exhaustive searches conducted were limited in finding suitable legs. Further work would be needed on both the search mechanism and the search criteria if a leg as good as, or better than, Jansen's could be found. The idea of evolving solutions had been used by Jansen in his search for good dimensions. The author too had prior experience with cellular automata and life simulation software. Given that constructing a walker is an attempt to emulate animals, it seemed likely and appropriate that a process that had designed all animals would also be capable of designing a synthetic walker. Thus it was decided to investigate genetic algorithms as a possibly improved way of finding good legs. These algorithms are the subject of the next chapter.

Chapter 5 Foot trajectory optimization by genetic algorithm

5.1 Genetic algorithms

As an alternative to deterministic optimization techniques, a new class of methods, based on natural evolution, has been developed. These software techniques attempt to mimic the natural selection process, as first described by Charles Darwin in *"The origin of species"* [41].

In nature, individual animals compete against other members of their species in a given environment. Those who are best able to make use of resources in their environment, said to be well adapted, will have sufficient means to give birth to and maintain offspring. These children will inherit properties and abilities from their parents, but will in general have a slightly different set of abilities than either parent. If the abilities of the children are still adapted enough to the environment, they in turn will bear children. If some offspring have variations that make them maladapted, then they will have fewer or no children. The result of this ongoing process is that new variations that are better adapted to an environment (or at least no worse adapted) and changes that match changes in the environment will come to predominate in a species of animal. All this presupposes some method of transmitting information about abilities from parents to children.

Evolutionary biology is much more complicated than this. In fact it is doubtful if the full extent and mechanisms of natural evolution are yet known and many aspects will remain mysterious for many years to come. And so it is with computing based on evolutionary principles. The field itself is evolving, and many attempts have been made to borrow the fundamental process of nature to solve specific engineering problems.

Although early work was started in the 1950's and 60's, Holland's 1975 book [42] was hugely influential and started the modern theory of optimization based on evolutionary principles. In subsequent years many authors have contributed to the field including Goldberg in 1989 [43], Michalewicz in 1992 [44], Mitchell in 1996 [45] and Bäck, also in 1996 [46].

These genetic programming techniques have not escaped the notice of mechanism designers, not least Theo Jansen, with his "evolution programs", but have also been used by Kanarachos [47] and Cabrera [48]. These techniques are also used in solving general engineering design problems, as discussed in Coello [34] and Renner and Ekart [49].

These researchers have shown that this method has many advantages over other optimization methods, specifically genetic algorithms are:

1. simple to implement,
2. robust,
3. capable of finding multiple solutions, and
4. not restricted to finding local maxima.

These various authors have described a wide diversity of ways of implementing computer software that uses the principles of competition, selection and breeding to search for good solutions to a variety of problems. However this is not to say that there are no core principles of all evolutionary software. These principles are detailed in the following sections.

5.2 How genetic algorithms work

Figure 25 depicts a flowchart of a simple genetic algorithm. Although simplified, this high level flowchart highlights some of the features of genetic algorithms (GAs).

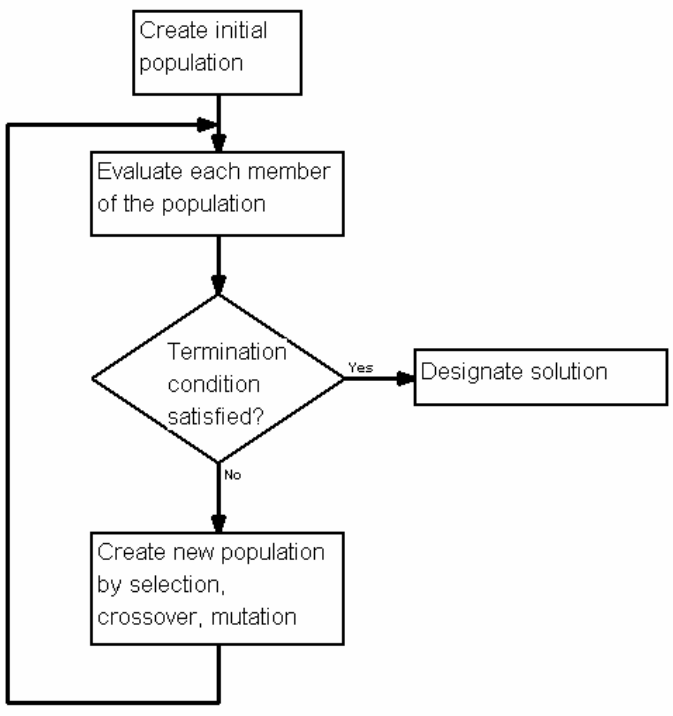

Figure 25. Flowchart of a genetic algorithm.

The first activity box in the flowchart emphasizes that GAs operate on populations of solutions. This presupposes an initial population, which can be drawn either from existing known solutions or may be randomly generated.

The fact that a group of solutions is operated on together gives the GA parallelism. A number of different paths can be taken to maximise fitness, which is how the GA ensures that it can cover the Pareto front of acceptable solutions.

The second step in the algorithm is that each generation of solutions is rated. In nature, the testing of individuals is done by the environment. In simulated evolution, a fitness score is calculated. The fitness score will be higher for “better” individuals, that is, GAs are inherently maximising processes.

In nature, some aspects of the environment are more important than others, and animals that cope better with these factors are better adapted. These aspects are said to exert “evolutionary pressure”, that is, they have a tendency to push the evolutionary process in a particular direction. Similarly, in GAs, the specific details of how the fitness function is calculated creates a tendency for solutions to become fitter in some specific areas more than in others.

The third step in the flowchart is a termination decision. In nature, evolution is an ongoing process that will continue ad infinitum. In a computer environment, this infinite loop cannot be tolerated, so a termination condition is applied. This is usually the maximum number of generations allowed, though if an end point is known beforehand, termination could be by a solution’s proximity to the desired point.

If the termination condition is met, the algorithm terminates, presenting a range of solutions found. The solutions that the GA will designate usually contain the fittest individuals ever encountered. The final generation will not necessarily contain all these solutions, though it is likely that the average fitness of the final generation will be higher than the average fitness of any previous generation. The solutions found are also not necessarily the fittest individuals possible – each run of the GA will be influenced by both the initial population make-up, chance and the parameters that control crossover and mutation. Given the size and multiple dimensions of the search space, there may be many disconnected hypervolumes of the search space where good solutions may be found. In other words, a GA is not guaranteed to find global maxima, although it is does not become entirely attracted to local maxima either. This ability to jump between local maxima is controlled by mutation in the GA, and the pursuit of multiple maxima is allowed by the population that is maintained.

If the termination condition is not met, then the algorithm continues by creating a new population, which can in turn be evaluated. This is done by taking a selection from the last generation to start as the basis of the new generation. The selection is done on the basis of fitness – the fitter (those with a higher numerical fitness score) individuals are preferentially selected.

If the new generation were evaluated at this point, it is likely that the average fitness would be higher than the previous generation's, but the maximum fitness could not have increased, as there are no new individuals. Some transformation must be performed on individuals in the new generation to allow some to be better than their parents.

This next stage of creating the new population is called "crossover". This stage is analogous to sex in natural creatures. It involves an exchange of information between creatures or solutions. This is the engine that drives variability between individuals. In nature, the information is transferred by the production of gametes with a single strand of each parent's chromosomes. Joining two gametes from different individuals forms the first cell of the new child, who therefore contains a portion of genetic material from both parents.

In GAs, crossover presupposes that there is some representation of the solution that can be easily transformed. The solution itself will require further work or calculation before a fitness score can be arrived at. Hence the GA requires a coding / decoding module to handle changes from fitness calculation representation to GA representation, and back again. This is made easier by representing numeric parameters of the solution as a string of binary digits. All this binary data is then concatenated to form a single longer string. The crossover transfer is achieved by splitting the binary strings of both parents, and swapping them, as shown in Figure 26.

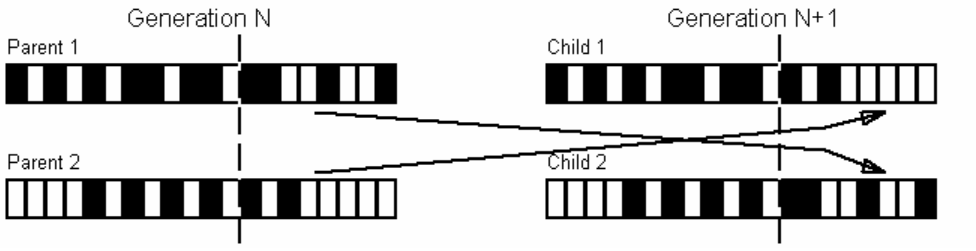

Figure 26. Crossover of binary strings.

This type of crossover is known as “single point crossover”, as the binary strings are split at a single point only, indicated by the dashed line. The binary strings that the children end up with are different from either parent. Once these binary strings are translated back to solution parameters, and the solutions are evaluated, they are likely to have different fitness scores from their parents. They will not necessarily be better, but some may, and these improved individuals will be retained by the next selection process.

Single point crossover will tend to carry parameters together as groups, directly affecting only the value of the single parameter which has been cut. If digitized versions for co-dependent parameters are placed near to each other in the binary string that represents the solution, then successful co-dependent groups of information will be kept together. The groups of values that the children inherit will have the same values as their parents had, but they will have new combinations of these groups of parameters. Although we need the children to differ from their parents, they must not be so different that accumulations of successful subsets of information are lost.

The crossover process is controlled by two parameters - how frequently crossovers occur, and where in the binary string the cut is placed. If crossover occurs too frequently, then none of the solutions from prior generations are retained, and the process becomes too random. If the crossover rate is too low, then the GA becomes slow in finding new improved variations. The cut position is usually randomly assigned, as it does not have a major influence on the operation of the GA.

The final stage in transforming the new population is mutation. In this stage, random changes are made to the binary strings, in effect a random binary digit’s value is switched, from 0 to 1 or vice versa. This mutation is based on mutations found in nature, which affect the DNA molecules in chromosomes and can result from copying errors when gametes are produced or radiation damage or attack by some viruses. In GAs, the mutation is a random change in the binary string, which can allow a new direction for the search to take, potentially a jump to another hypervolume of the search space.

Mutation is affected by a mutation rate. If too much mutation occurs, then the GA again has a tendency to chaos, and finding good solutions becomes more random. If the mutation rate is too low, then the GA will tend to confine itself to a single hypervolume in the search space, and much of the search space will be left un-searched.

Once the new population is completely defined, it is re-evaluated, and the process continues until the termination criterion is met.

Although these are the common principles by which GAs operate, the specific details of how various aspects of the algorithm are achieved in practical implementations of GAs vary widely. One of the obvious points of difference between GAs is how the fitness of solutions is assessed. Clearly, as each problem has its best solution, so each GA has to represent this numerically. Various selection, recombination and mutation methods have also been applied. As this thesis is not primarily concerned with GAs, further discussion of these varieties of GAs are confined to those pertinent to the actual problem at hand. The implementation of a GA specifically to find Jansen linkages for legs for a walking machine is described in detail below.

5.3 Implementation

The GA implemented attempts to solve the problem of finding a Jansen twelve bar mechanism that will make a suitable leg for a walking machine. The type of solution required is a particular mechanism geometry that will give desired values for various properties as mentioned in section 4.2. To assess these properties, the kinematics and kinetics of the leg must be solved. The methods for doing this are detailed in section 3.4, but the vector of link lengths is required. The other major parameter not known is *r*, the radius of the driving crank for the Jansen mechanism.

Due to the scalability properties of the mechanism, the crank radius need not be considered as a variable property of each solution, if the search is for kinematically good legs. The problem can be simplified by eliminating this variable. If other factors, such as calculated stiffness or body height, need to be considered in the design, then a second round of size optimization of the mechanism may need to be performed. For the purposes of this GA, *r* is taken as a fixed value of 100mm.

That this GA will search only for kinematically "good" legs is implied by the above. Specifically, legs that can provide a constant body ride height are the primary target, as the kinetic analysis in [1] has shown that legs with this property will have minimal overall power consumption, as they do not need to cyclically lift and lower the walker body. The only criterion from those listed in section 4.2 that will be explicitly used is the foot point trajectory, though this will cover subsidiary criteria such as stride length, foot lift and body lift.

The software implementation was executed with Inprise Corp.'s Delphi object oriented Pascal compiler. The application ("*GA_Leg.exe*") uses an object oriented design, with objects

representing individual solutions, generations and the algorithm as a whole. The mechanism solving modules are inherited from the previous exhaustive search software. The program incorporates facilities to vary the GA parameters i.e. crossover and mutation rates, number of generations, population size, initial population source and selection and crossover methods. It can also monitor GA performance, maintain a list of best ever mechanisms and provide graphics both of the leg in motion and also a magnified and parameterized view of the foot trajectory. Software execution is fast, being able to execute a GA run of 500 generations with 200 solutions per generation, a total of 100 000 mechanisms to evaluate, in around 2 minutes on a Pentium 4 3 GHz PC. The software is available on the CD ROM in the "*Software\GA Leg*" directory.

5.3.1 Binary string representation

Each solution is represented by an array of eleven link lengths. Link lengths are allowed to vary from 0 to 1023 mm, given the crank radius of 100 mm. Initially the binary string used to represent each length was 12 bits wide, which can represent 2^{12} = 4096 discrete values. This gives an effective resolution of 1024 / 4096 = 0.25mm. In later trials the number of bits was changed to 10 bits per link, with 1024 points of resolution, making length differences of 1mm significant.

The binary representations of the link lengths were then concatenated to form a total string length of 11 x 12 = 132 bits, later 11 x 10 = 110 bits, per solution. This means that the search space comprises $2^{110} \approx 10^{33}$ possible mechanisms. If it took 1 millisecond to evaluate each mechanism, it would take 4×10^{22} years to do a complete exhaustive search of this space. The rationale for the change in bit length was that the extra 2^{22} possible linkages were not that different to warrant the additional search time they would add.

The bit strings were concatenated in an order that sensibly mapped onto the physical layout of the linkage. This was to ensure grouping of related genetic information, as mentioned prior. The pin to crank length l_0 was stored first, followed by the other link lengths, in the order shown in Figure 27.

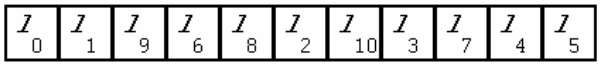

Figure 27. Binary string concatenation order.

5.3.2 Fitness calculation

The “correct” shape of the foot trajectory was the main attribute needed in the leg mechanism. Previous searches had not considered this aspect of the mechanism explicitly, so new methods of assessing suitability of trajectories needed to be developed. These methods evolved as it became clearer how the GA responded to changes in the fitness calculation method and also to the types of trajectories being found by the GA. It became clear that the way the fitness function was defined mathematically would indeed apply significant selection pressure, and the mechanisms found would definitely provide foot trajectories that resembled the curve defined by the fitness scoring method. Defining the curve required was the fundamental problem.

The following sections use graphics, created by the GA software, showing foot point trajectories. These show a counter-clockwise trajectory, the walker moving from right to left, with the indices of the time slices shown every 10th index. Each cycle, corresponding to one revolution of the driving crankshaft, comprises 120 indices or time slices. The red line is used for determining flatness of the walking cycle.

5.3.2.1 Straight line portion

Initially only the straightness of the walking part of the foot trajectory was assessed. This was done by calculating the squares of the deviations of each trajectory point from the straight line connecting terminal points, which were found while computing the mechanism orientation angle, see section 3.4.1. The higher the total deviation, the less like the straight line the actual curve would be.

To convert the fitness score to an increasing score, the total deviation was subtracted from a constant value. This could also have been achieved by inverting the total deviation, but this would introduce a non-linearity, while subtraction from a constant would give a linear response. Subtraction also acts as a penalty function, as curves with deviation greater than the constant would have negative fitness.

This fitness criterion was implemented and solutions were found that certainly provided flat walking trajectories, but it was clear that the assessment mechanism was not tight enough. Many of the mechanism found, though flat walking, would not be useable in a real walking machine, as evident in the foot trajectory shown in Figure 28.

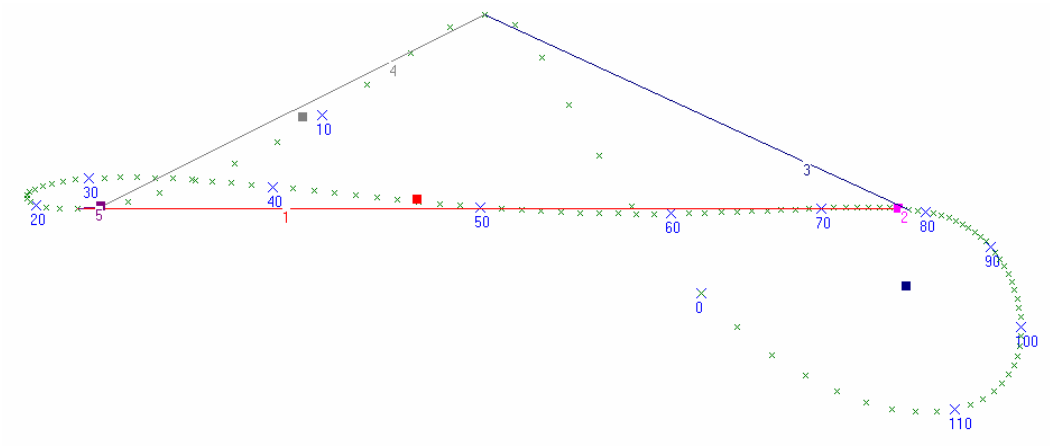

Figure 28. Foot trajectory that walks flat, but is unuseable.

5.3.2.2 Triangular trajectory

From experience with the straight line fitness factor, it became clear that a more complete definition of the shape of the entire foot trajectory curve would be required, to create selection pressure for a practical curve. To this end, the fitness calculation function was extended to consider the trajectory as triangular. The base of the triangle would be the walking portion of the trajectory, comprising 50% of the trajectory points. The other two legs of the triangle would be the upward, right-most part of the path and the left-most downward part.

This new actual fitness score was defined as a sum of factors. The first factor was the flatness, as calculated previously. The second factor was the equality of the lengths of the two upper arms of the triangle, equal lengths being preferred. Finally, a factor proportional to the area of the triangle was added to the sum.

This new fitness calculation method was more successful in finding mechanism that gave practical foot trajectories. Although it was also clear that the shape of many of the curves found, as exemplified by Figure 29 below, was not yet perfect. The mechanism shown will drag its foot on the ground at the end of its walking cycle, near index 100 on the figure.

Figure 29. Triangular foot trajectory, with dragging foot.

5.3.2.3 Pentagonal trajectory

The final version of the fitness calculation mechanism considered the foot trajectory as an irregular pentagon, shown in Figure 30 below. The hope was to select mechanisms that would have positive approach and retreat angles, and the machine was therefore unlikely to drag its feet at the beginning and end of the walking cycle.

The foot trajectory is represented by the pentagon shown in solid lines. Line 1 (PQ) is the walking portion of the trajectory, line 2 (QR) is where the foot is lifted, returning along lines 3 (RS), 4 (ST) and ending at line 5 (TP), where the foot is returning to the ground. By regularising the pentagon, as shown by the dotted lines, it is simple to calculate the pentagon's area, as the sum of A_r, the area of the lower rectangle and A_t, the area of the upper triangle.

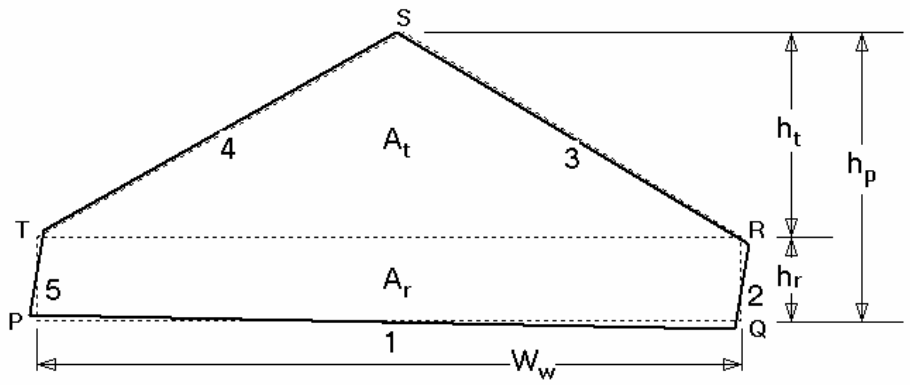

Figure 30. Foot trajectory considered as a pentagon.

Fitting a pentagon to the data point array provided by the mechanism solver was achieved in a step-wise fashion. First the walking portion of the cycle (PQ - line 1) was found, using the method used to compute the mechanism orientation angle, see section 3.4.1. The index of the highest point in the trajectory, point S, had been recorded when the data array was generated. To locate point T, the data was scanned from point S, until a point was found with the same horizontal coordinate or further to the left of point P, and this point taken as T. Similarly, point R is found by scanning backwards from point S, until a point directly above or to the right of Q is found. The ability to find a useable pentagon in the data points was a significant selection pressure, as those mechanisms whose data could not be fitted were scored with a ten point fitness score reduction, while those who could be fitted had a 10 point increase in fitness score.

If a suitable pentagon could be fitted, then the fitness score could be calculated as a weighted average in a similar fashion to the method used in section 4.4.

Mathematically:

$$F = 10 + (W_f \times F_f) + (W_t \times F_t) + (W_b \times F_b) + (W_r \times F_r) + (W_a \times F_a) + (W_s \times F_s)$$

Equation (5.3.1)

where

F	=	fitness
10	=	the 10 point bonus for fitting an assessment pentagon
W_f, W_t, W_b, W_r, W_a, W_s	=	weighting factors
F_f	=	flatness factor
F_t	=	triangle side length factor
F_b	=	bottom rectangle height factor
F_r	=	aspect ratio factor
F_a	=	area factor
F_s	=	mechanism size factor

The evaluation methods for these various factors are described in more detail in the section that follows. It is possible to evaluate what the maximum value of each factor could be. It will also be useful to know what a "good' value would be. These are both specified in the following sections.

The final actual numerical value of the fitness score will depend on the values of the weighting factors used.

Flatness factor, F_f

The flatness factor is effectively a root mean square (RMS) measure of the deviation of the walking part of the trajectory from the straight line, line 1. This is the same fitness factor applied in the straight line and triangular fitness assessment methods previously.

$$F_f = K_1 - \frac{\sqrt{\sum_{i=i_P}^{i=i_Q} \delta_i}}{N}$$

Equation (5.3.2)

where

$\delta_i = (y_{1i} - y_i)^2$

K_1 = a constant = 20

N = number of indices in the walking cycle = (i_Q- i_P)

i_P = index at point P, start of the walk cycle

i_Q = index at point Q, end of the walk cycle

y_{1i} = y position on line 1 for the trajectory's x position, at index i

y_i = actual y position of trajectory, at index i

If the total deviation is zero i.e. every point of the trajectory sits exactly on the line, then $F_{f\,max} = K_1 = 20$

A "good" value would have an RMS deviation of < 1mm, say 0.5. So $F_{f\,good} = 19.5$.

Triangle side length factor, F_t

This factor is computed from knowledge of the side lengths of the triangular upper portion of the pentagon.

$$F_t = K_2 - \left(\frac{K_3 \times |L_3 - L_4|}{(L_3 + L_4)} \right) \qquad \text{Equation (5.3.3)}$$

where

K_2 = a constant = 10

K_3 = a constant = 10

L_3 = length of line segment 3, RS in Figure 30

L_4 = length of line segment 4, ST in Figure 30

If $L_3 = L_4$ then $F_{t\,max} = K_2 = 10$.

A "good" value would have a length difference of less than 1mm. So $F_{t\,good} = 9$.

Bottom rectangle height factor, F_b

$$F_b = K_2 - \left(\frac{K_3 \times |L_2 - L_5|}{(L_2 + L_5)} \right) \qquad \text{Equation (5.3.4)}$$

where

K_2, K_3 = constants, as before

L_2 = length of line segment 2, QR in Figure 30

L_5 = length of line segment 5, TP in Figure 30

If $L_2 = L_5$ then $F_{b\,max} = K_2 = 10$. Using the same logic as for $F_{t\,good}$ above, $F_{b\,good} = 9$.

Aspect ratio factor, F_r

This factor is implemented as a penalty function, based on the aspect ratio (*AR*), and the triangle height to rectangle height ratio (*TRHR*). If a condition is met, then a positive fitness score is added to the cumulative score, but if the condition is not met, then a value is subtracted from the score. This encourages good solutions to have the desired aspect ratio. The foot lift height must be at least 10% of the stride length, and at least 15% of the foot lift

will be during vertical lifting and lowering periods. A high aspect ratio (greater than 0.5) is not desirable, as it means very fast movement on the return stroke.

$$AR = \frac{h_p}{W_w} \qquad \text{Equation (5.3.5)}$$

$$TRHR = \frac{h_r}{h_t} \qquad \text{Equation (5.3.6)}$$

If (AR > 0.1) and (AR < 0.5) and (TRHR > 0.15) *then* $F_r = 5 + (10 \times AR)$

Else $F_r = -5$

Where

h_p, W_w, h_r and h_t are as shown in Figure 30

If the two conditions are met and AR = 0.5, then $F_{r\,max}$ = 10.
A good AR is about 0.3. So for AR = 0.3, then $F_{r\,good}$ = 8.

Area factor, F_a

This is intended to maximise the stride length and lift height of the trajectory with a single factor, by considering the area inside the pentagon. It is implemented as a dual scaled factor, with a fitness increase scaled on a smaller factor for small areas, and larger scale factor used for areas above the threshold area. The intention with this scoring scheme is to keep the area below the threshold area, K_4. The value used for the area is not the actual area of the pentagon, but an effective area (*EA*). This was done to encourage mechanisms with significant foot lift before the leg moves on its return path proper.

This effective area was calculated as:

$$EA = (4 \times A_r) + A_t \qquad \text{Equation (5.3.7)}$$

If (EA < K_4) *then* $F_a = \frac{EA}{K_4}$ Equation (5.3.8)

else $F_a = \frac{EA}{K_5}$ Equation (5.3.9)

where

$$A_r = h_r \times W_w \qquad \text{Equation (5.3.10)}$$

$$A_t = \frac{h_t \times W_w}{2} \qquad \text{Equation (5.3.11)}$$

W_w, h_r and h_t are as shown in Figure 30

K_4 = threshold area, a constant = 45 000

K_5 = a constant = 360 000

If EA = K_4, then $F_{a\ max}$ = 1.

A useful *EA* is greater than about 30 000. So $F_{a\ good}$ = (30 000 / 45 000) = 0.667.

Mechanism size factor, F_s

This factor is intended to promote linkages of a certain size, in this case linkages with a total link length of 4000mm. The concept of total linkage length was also used previously in exhaustive searches. However, the specific factor applied here is structured to encourage mechanism that are as near to this value as possible. Linkages larger than the desired total length are penalised by this factor. This factor was specifically introduced to eliminate large but un-useable configurations that gave good looking foot trajectories.

$$F_s = 1 - \frac{L_l}{K_7}$$ Equation (5.3.12)

where

$$L_l = \sum_{i=1}^{10} l_i$$

l_i = length of link number *i*

K_7 = a constant = 4 000

If L_l = 0, then $F_{s\ max}$ = 1.

This factor will have a small value. A reasonable mechanism total length is about 3 600, so $F_{s\ good}$ = 1 - (3600 /4000) = 0.1.

Weighting factors

The weighting factors are made available for changes by the software user. This enables the effects of sub-factors alone to be determined. It also allows tuning of the weighting factors to give the type of foot trajectory required.

After the fitness of solutions has been evaluated, this information is used to guide creation of the next generation of solutions, by preferentially selecting high scoring solutions from the current generation.

5.3.3 Selection methods

The two main selection mechanisms found in GAs are roulette wheel selection and tournament selection. The GA implemented here implements both of these selection methods.

In roulette wheel selection, each solution is apportioned a segment of a virtual wheel in proportion to its fitness contribution to the fitness of the entire generation. The wheel size is determined by summing the fitness of all members of the generation. Solutions with zero fitness function value are assigned a segment of zero width i.e. the starting value of their number range equals the ending value. These solutions cannot be selected into the next generation. Solutions with fitness scores greater than zero are assigned a numeric range within the range of the wheel size, the range being proportionate to their contribution to the wheel size. Fitter solutions occupy a larger part of the wheel, and so are more likely to be selected.

To do the actual selection, a random number is generated for each slot in the new generation of solutions. The random number is normalized within the range zero to the total fitness of current generation. The value of the normalized random number is then compared to the number ranges of eligible solutions. The solution whose range encloses the random number is copied into the new generation.

In tournament selection, the places in the new generation are filled by holding a tournament for each place, where two solutions from the previous generation compete, and the winning, fitter solution is given the slot. In this implementation, the competitors are chosen by two different means. In tournament selection method 1, the two competitors are both selected randomly from the previous generation. In tournament selection method 2, the incumbent solution in the corresponding slot in the previous generation competes with a randomly selected solution. One of the competitors from the tournament must be selected in either case, to ensure that the new generation has a full complement of solutions.

The salient difference between roulette wheel and tournament selection is that tournaments do not necessarily exclude solutions with zero fitness. If both solutions nominated to compete have zero fitness, then one of them will still need to be included in the new generation, as all slots must be filled. To allow for this scenario, all solutions have a tie-breaking fitness value, to enable a distinction to be made on some basis when overall fitness is zero. This is taken as the flatness factor, F_f. This factor was chosen as it is unlikely ever to be the same for any

two solutions, and this flatness is the primary desirable property being sought for by the GA search.

Theoretically, tournament selection is a superior method, for the following two reasons. Firstly, it is faster than roulette wheel selection, computationally speaking, as fewer calculations and list scans are required before a decision can be made. The second reason concerns variability, corresponding to a gene pool in nature. The exclusion of all zero rated solutions by roulette wheel selection means that, if the fitness assessment mechanism is highly constrained and often yields zero fitness, then solutions that may contain genetic information that could be combined later to give optimal solutions are eliminated prematurely. In GAs, as in nature, a reduction in variability may lead to “thoroughbred frailness”, many solutions that share many common genes and tend to specialize, as opposed to “hybrid vigour”, where solutions with disparate genetics all give reasonable performances. The latter is preferred to the former.

In early runs of the GA, where fitness was assessed by the straight line or triangular fitness calculation, then the roulette wheel selection method was used. For GA runs using pentagonal trajectory fitness calculation, either of the tournament selection methods was used.

5.3.4 Crossover operators

The crossover mechanism used in this GA implementation is single point crossover. This mechanism was selected on the basis of simplicity.

Crossover frequency is controlled by a crossover probability, a floating point number between 0 and 1. For each member of the new generation, a random number is generated, also between 0 and 1. If the random number is less than the crossover probability, then that solution is marked for crossover. If greater, then that individual is bypassed. In this way, a list of crossover candidates is created. This candidate list is then processed, two candidates at a time. This implies the candidate list must have an even number of items. If the crossover probability method of providing items has left the list with an odd number of candidates, then an extra candidate is selected randomly, to make the list count even.

Each crossover event is achieved by establishing the crossover point, by generating a random number within the range of the solution’s bit length i.e. 1 - 110 in this implementation. The bit strings are then crossed over, at the position defined by the random number, as described in section 5.2.

Note that the crossover probability is equivalent to a rate of crossover i.e. the same fractional number will denote both a probability value and the portion of the population who have crossed over bit strings. A crossover probability of 0.6 will mean 60% of the new generation will have experienced crossover.

A variation on this standard technique was also implemented. This was to include a crossover probability modifier (*CPM*), based on the relative fitness of the individual solution being considered for crossover.

This factor was calculated as follows:

$$CPM = 1 + \frac{\left(F_i - \overline{F}\right)}{\overline{F}} \qquad \text{Equation (5.3.13)}$$

where

CPM = crossover probability modifier

F_i = fitness score of the individual being considered

$\overline{F}$ = mean fitness of generation, computed when the generation was created at selection time.

Equation (5.3.13) would mean *CPM* > 1 for fitter than average individuals, and *CPM* < 1 for below average ones. The crossover probability was then multiplied by this factor, thereby increasing the probability for fit individuals, and decreasing it for unfit ones. This modifier was envisaged to encourage crossover for fit individuals, and discourage it for those individuals with less than average fitness, a kind of GA eugenics. As the factor varies around a mean value of one, and the crossover probability is checked for each individual, the factor has no net effect on the number of individuals who experience crossover in a particular generation i.e. the crossover rate is unaffected. It will simply make it more likely that fitter individuals will be in the crossover candidates list than unfit ones.

This modifier was included on the basis of reasoning about crossover in GAs being analogous to sex in nature. In nature, fitter individuals certainly breed more frequently than less fit ones do. And fitter individuals also tend to breed with similarly fitter individuals. It was these two features of sex in nature that the *CPM* was intended to emulate. This modification was not encountered in the GA literature search.

The crossover probability was kept at around 0.6. This is as recommended by Michalewicz [44], and appears to be a good compromise value between allowing good variation with effective heritability. The *CPM* crossover probability modifier was generally applied to the crossover process.

5.3.5 Mutation operators

Mutation in the GA is controlled by a mutation probability, again a real number between 0 and 1. As with crossover probability and rate, mutation probability is equivalent to a mutation rate.

For each bit of the bit string representing the combined bit strings of all the solutions in a generation, a random number is generated. If the number is less than the mutation probability, then the bit is mutated i.e. switched to 1 if it is currently set to 0, or vice versa. This process requires some manipulation as the solution's index in the generation list and the index of the affected bit in the solution's bit string need to be resolved from the progress in the processing loop.

With this algorithm, mutation requires (110 times the population size) passes through a loop, a random number being generated in each pass. For a population of 200, which was commonly used, this means generating 22 000 random numbers. The processing of mutations therefore consumed a considerable portion of the calculation time for each generation of the GA.

Note that this algorithm does not preclude solutions from experiencing multiple mutations, but some may have none at all. If the mutation operator was implemented on a per solution basis, these aspects of mutation may be suppressed. However, the mutation operator could be made much faster, but it is considered that the more accurate representation of natural mutation is worth the extra computational overhead.

The usual value of the mutation rate was small, about 0.03. This was also recommended by Michalewicz [44]. Higher mutation rates were attempted, and these did indeed show evidence of chaos in the results. Later runs stuck to this low value.

5.3.6 Other GA parameters

There are three other main factors that affect the GA. These are the population size, the maximum number of generations allowed (the termination criterion for this GA) and the source of the initial population.

The population size influences the parallelism of the GA, and larger populations make a wider variety of solutions possible. However, the computer time spent on processing large populations, especially mutation, makes very large populations computationally expensive. Although this parameter could be varied for each run, population size was in the range 100 – 1000 individuals per generation, 200 being thought a good compromise. The population size was constant across all generations.

The maximum number of generations has a similar impact on running the GA that population size had i.e. more generations take longer to compute, but may provide better solutions. In this study, the maximum number of generations that a population was allowed to evolve for was also in the range 100 – 1000, with runs of 500 generations being the most common.

The last major parameter is the source of the initial population. There are three sources - random, standard and saved. If a random initial population is required, then records are selected at random from the large database of previously solved linkages. If a standard or saved initial population is used, then records are loaded from a specific file, in the first case, from a standard file of 500 solutions and in the second from the saved interesting / best ever solutions. There are only 80 or so of these, so a smaller population size is currently required when using this option.

5.4 Results

The GA was run many times with various parameters, both to assess performance of the GA and to get a feel for the impact of the various parameters on the process. Although a series of formal experiments could have been run, to record performance and variations in it, this was not done. The primary objective of this thesis is to design walking machines, not to discuss genetic algorithms in detail. Although there is perhaps scope for further work in this direction, this has been deferred, in the interests of pursuing walking.

The conclusion of all runs of the GA and exhaustive searches has been the accumulation of records of some 3.6 million (3 598 666) different twelve bar linkages, all of which can be assembled and solved for a full crank rotation. With a probable success rate of 1%, this means at least 350 million configurations have been tested. The distinctness of these solutions has been checked with commercial SQL database software. These records of linkages found are available on the CD ROM in the "*Software\Leg Catalogue*" directory.

This collection of linkages has been accumulated for three main reasons. Firstly, it serves as feedstock for the current and future GA software, particularly when creating initial populations. Secondly, this catalogue of existing known working linkages can be initially assessed if new selection criteria are created. Lastly, the catalogue of linkages may be of some use to other designers who may wish to find linkages in this class, with other properties.

Of these 3.6 million linkages, only seven are currently considered practical for use in walking machines. There is however a list of approximately 200 configurations that have been considered manually and retained separately. Given the 10^{33} options, this seems slim pickings indeed! There is a definite conviction that the ultimate leg configuration exists in the space, but will forever remain elusive.

The problem with the optimization techniques applied in this thesis, and with all other methods [34], is that it is extremely difficult to encapsulate all knowledge, wisdom and their corresponding factors into software. The trained, observant human observer is by far the best optimization tool available to any optimization process. Like quality, solutions to problems may be impossible to define, but instantly recognised when encountered.

The usefulness of this GA software has been in creating and presenting a wide range of new mechanisms that may be considered. However, the best candidates found have had to be assessed by the author, the decision maker, as even in reasonably well developed current state, the GA software does not have sufficient information to discriminate the finer points of leg suitability.

With respect to finding solutions with high fitness scores, it is worth reconsidering Equation (5.3.1) above, substituting the maximum values permissible for the various fitness factors, to obtain the maximum possible fitness score. This score depends on the weighting factors used, so these have been taken from the software settings and are also shown in the table. The table also lists "good" values for all factors, and a weighted "good" score is calculated.

Description	**Weight factor**	**Max. value**	**Max. weighted**	**"Good" value**	**"Good" weighted**
bonus for pentagon fit	1	10	10	10	10
flatness factor	4	20	80	19.5	78
triangle side length factor	1	10	10	9	9
bottom rectangle height factor	1	10	10	9	9
aspect ratio factor	1	10	10	8	8
area factor	3	1	3	0.667	2
mechanism size factor	1	1	1	0.1	0.1
Maximum			**124**		**116.1**

The highest scoring solution found by this GA implementation achieved a score of 120.19, the second best got 118.74 and the consolidated results of the various searches includes seven solutions with scores over 116. By comparison, the previous best walker leg mechanism used, the Jansen mechanism, scored 108.8. If this value is taken for the value for a good walker, then the GA found 24 mechanisms with scores higher than this.

In this light, the GA software implemented here can be considered a success, in that it created a range of potential solutions that are better than the best solution previously available. This assessment is done in the context of the evaluation criteria set by this model. Jansen almost certainly had different criteria in his model, which led him to choose his leg mechanism proportions for his “strandbeeste”. It would be interesting to know how well the best legs found with this GA would rate when rated with Jansen’s fitness determination algorithm.

The best foot trajectory found by this GA, with a fitness score of 120.19 is shown in Figure 31. As with other legs that have identified as useable by previous searches, in section 4.4 above, this leg design was used as the basis for a new walking machine prototype, detailed in section 7.4.

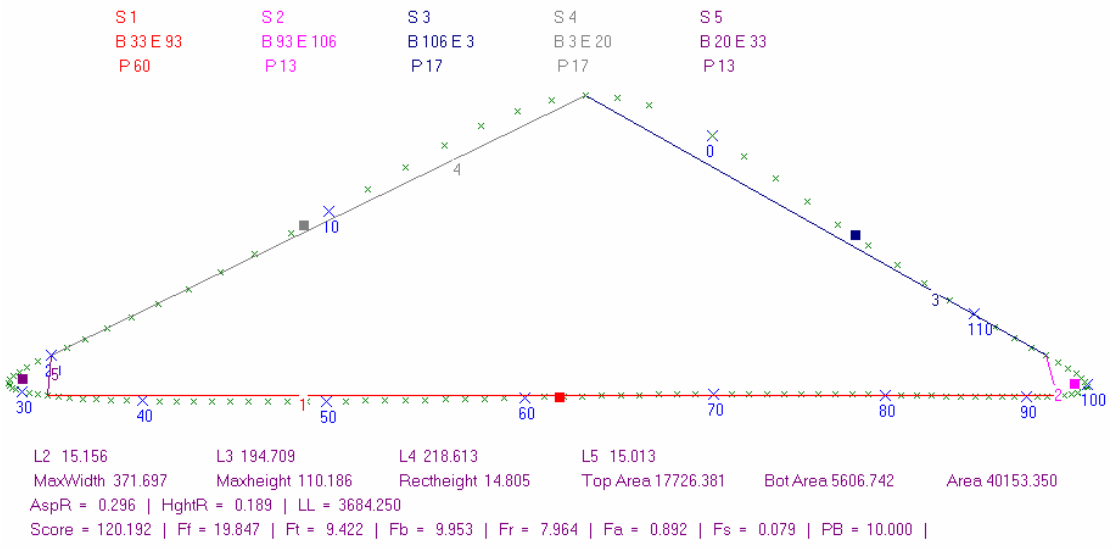

Figure 31. The best foot trajectory found.

Before considering prototypes, the design requirements stemming from another important aspect, the dynamics of walking, need to be discussed. They will have a significant impact on the detail design of any successful walker. This topic is discussed at more length in the next section.

Chapter 6 Mechanics of walking with Jansen legs

The mechanics of walking is the physics of walking, that is, the resolution of forces encountered by the machine as it walks. Once these forces have been quantified, the principle of superposition can be used to assess the total force experienced at salient parts of the walking machine. Of obvious interest are the loads applied to the crankshafts and to the vehicle's frame at the fixed pin. Knowledge of the magnitude, direction and rate of variation of these forces will be invaluable in the design of a practical walking machine.

Another extremely important aspect that must be dealt with is the question of stability. The design requirements outline a vehicle with definite off-road abilities. The stability of the vehicle and its ability to make way in adverse conditions will depend on the forces the vehicle needs to apply to its environment, particularly the surface on which it walks. It's ability to stay on it's feet, climb hills, descend slopes and walk over uneven ground all need to be established, before design criteria can be considered met.

Although previous authors (amongst them [50] and [51]) have done work on the dynamics of walking machines, the leg design used in the new class of machine makes the analyses of others not very pertinent to this specific problem. For this reason simple analyses of the various operating conditions likely to be encountered are built from first principles, in later sections. But before any analysis can be done, it is necessary to resolve the layout of the vehicle.

To resolve forces, information about the overall geometry of the machine is necessary, to know where load paths are and what the lever arms are, to allow bending moments or torques to be calculated. This is discussed in the next section.

6.1 Layout of machine

From previous discussions in section 2.3, the first decision is how many legs to use. The design criteria (section 2.9) require static balance and symmetrical leg duty cycle, so there are only two possible choices – six legs or eight legs.

The minimum, six legs, has the advantage of simplicity, as the least number of legs need to be manufactured, and friction and other losses would be minimized. There are number of ways of arranging these legs. Many current hexapod walkers, including the adaptive suspension vehicle (Figure 2) and the Plustech (Figure 4), arrange three legs down the length of each side of the body, as insect legs are arranged. This was also the layout used in the first prototype constructed, see section 7.2. The disadvantage of this layout is that it makes the walker long, which will adversely affect manoeuvrability as it does in wheeled vehicles. Three crankshafts are required for a walker with Jansen legs.

Another way to distribute the legs is to place three at the front of the vehicle, and three at the rear. This leg layout is used in MECANT (Figure 1) and in the second prototype constructed - see section 7.3. This layout allows a shorter vehicle, and if Jansen legs are used, there need only be two crankshafts. So given the need for the simplest layout, this layout is preferred.

The simplest possible layout, with a single driving crankshaft, as used by Jansen himself, is not considered practical, for the reasons discussed in section 3.1.

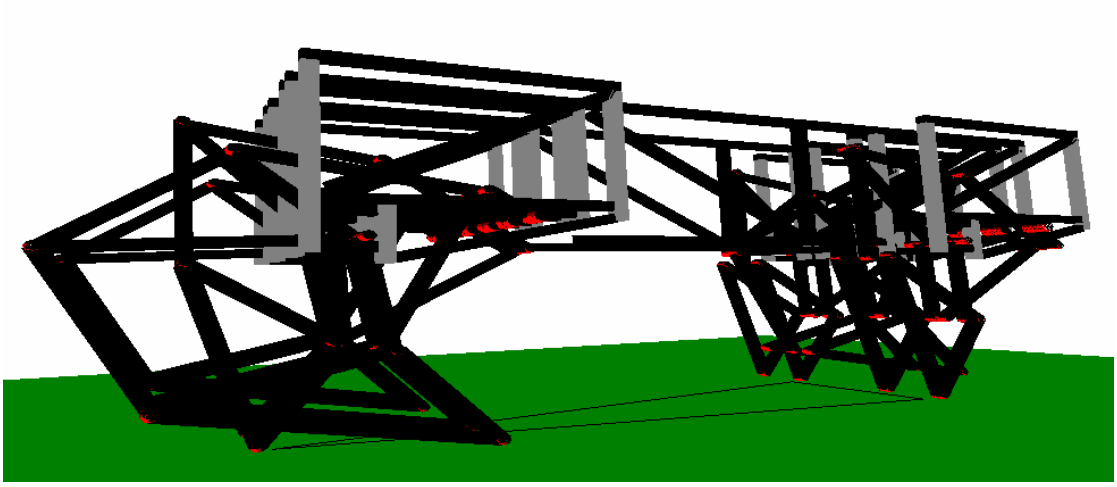

Figure 32. Three dimensional sketch of a hexapod with Jansen legs.

Figure 32 shows a three dimensional sketch of a hexapod walking machine with Jansen legs and two crankshafts. It also shows the support polygon for the machine – the triangle drawn on the green walking surface.

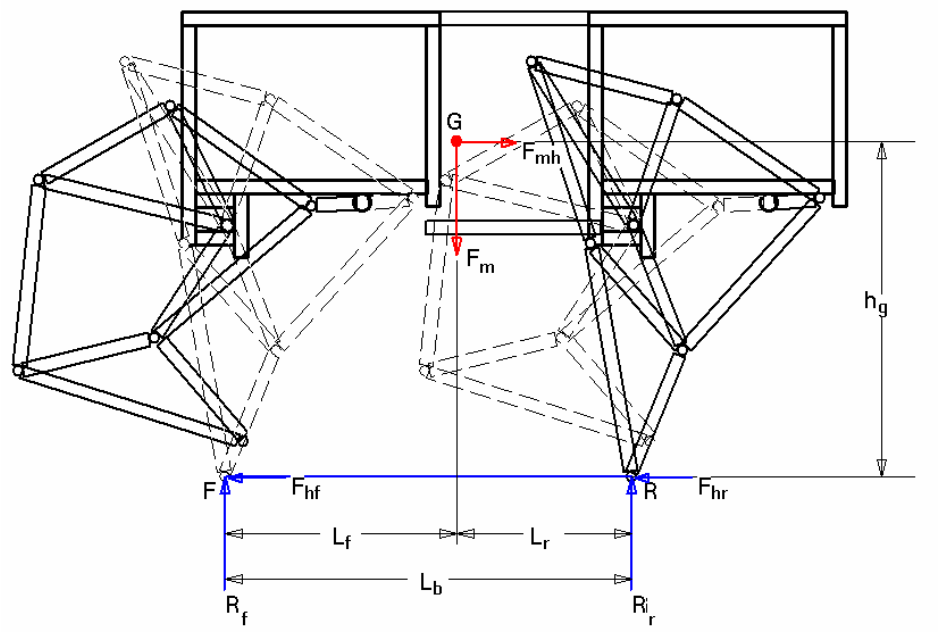

Figure 33. Free body diagram of walking machine with Jansen legs.

Figure 33 shows a two dimensional side view of the same walker as in Figure 32. The blue horizontal line at the bottom represents the side view of the support polygon. The red circle, marked *G*, indicates the centre of gravity of the machine. The two reaction forces R_f and R_r (also in blue) indicate the reaction forces of the ground on the legs, and F_m (in red) is the force due to mass of the walker. This diagram will be used later as a free body diagram (FBD) for evaluating these forces in various circumstances.

Consider now the octopod walker with Jansen legs, shown in Figure 34. This has a similar general layout to the hexapod, except that now each crankshaft drives four legs abreast, not three as in the hexapod. It is no surprise that this octopod resembles the hexapod, as it is in fact a sketch of the third prototype constructed, discussed further in section 7.4. The details of the link design has changed, with ternary links having changed from being simple triangles to “Y” shaped parts. Aside from this detail, if one considered a side view of this machine, for use as a FBD in a statics problem, this diagram would be nearly identical to Figure 33 above, with the triangular ternary links replaced by “Y” shaped ones. In Figure 34 the support polygon for the machine, now a trapezoidal shape, is indicated by the red plane. In a FBD, this would still be represented by the blue line in Figure 33 above.

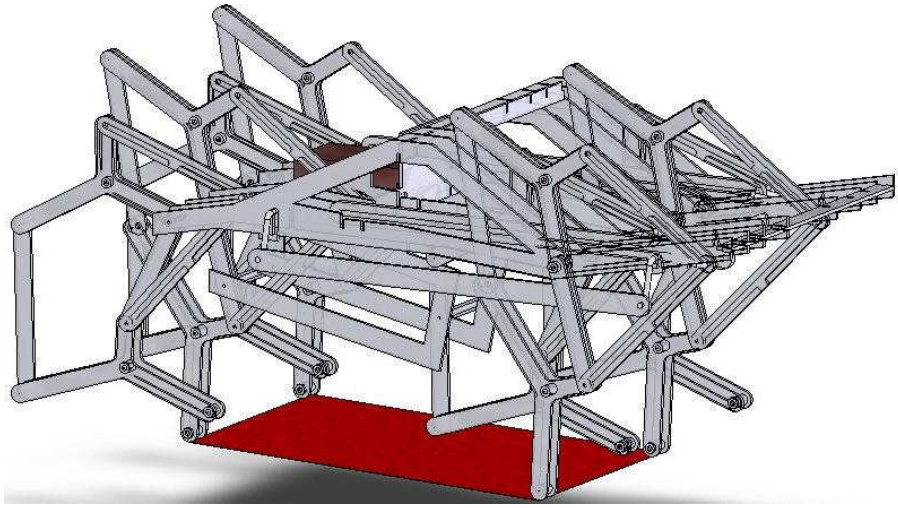

Figure 34.Three dimensional sketch of an octopod with Jansen legs.

Given the fact that the same FBD can be used for either this octopod or the hexapod, the definition of the layout of the machine can be deemed sufficient for the purpose of a simple statics analysis, as covered in the next few sections. The decision about whether six or eight legs will be used is deferred.

6.2 Walking on a level surface

Walking on a level surface is the simplest case to be encountered. Both vertical and horizontal loads on the machine need to be considered. The longitudinal section in Figure 33 indicates both vertical and horizontal loads. Vertical stability must be ensured in this plane, by considering the weight of the vehicle and the reaction forces exerted by the ground.

The analysis that follows concerns a simple walking machine where the feet are held in position by gravity and friction. For a walker with special foot attachments to provide adequate active grip, the discussions concerning over-turning and friction clearly do not apply. The rest of the analysis should still be valid, and could be used to determine the amount of grip these active feet would need to apply in various circumstances.

The walking machine will generally not move longitudinally at a constant velocity, if the crankshaft speed is kept constant. The leg kinematics will tend to slow the body down at the beginning and end of each leg's walking cycle. Forward velocity is highest near the midpoint of the walking legs foot trajectory. In reality, the instantaneous forward velocity of an actual vehicle would depend on the ratio of the vehicle inertia (i.e. mass) to the total moment of inertia of all rotating parts. To simplify the resolution of forces, this varying horizontal acceleration could be ignored, as it is much smaller than *g.*

Lateral FBD's can also be drawn, and the machine must also be stable in this plane. There is assumed to be no lateral horizontal load applied to the machine i.e. it is walking in a lab, with no side winds present. The walking machine, including the legs, must have adequate lateral stiffness to carry its own weight and incidental lateral forces, especially if walking on transverse slopes. This will need to be assured by detail design of the leg mechanisms.

In the following FBD's, the walker's mass is shown lumped at the position G. In a walking machine with Jansen legs, the instantaneous positions of the various links in the legs will influence the exact position of the centre of gravity, depending on the mass of the links. For large walkers with stiff and therefore heavy links, this variation in centroid position may have a significant effect. However, for the purpose of this simplified analysis, it is assumed that the centre of gravity will remain fixed in relation to the walker body. Where exactly this position is will clearly depend on the detail design of an actual walker. Some constraints that limit where it may be positioned will emerge in the following analysis.

The leg-base, L_b, is the longitudinal pitch between the crankshaft centres or between the fixed pin positions, analogous to wheelbase from automotive jargon. The leg-base will depend on the geometry of the legs, primarily the trajectories of nodes 2 and 4. Interference between these nodes of the rear legs and either the front legs, the drive system or the vehicle frame will determine the minimum pitch value, but it may be increased to place the centroid in a desirable position. When walking, L_b will also be the pitch between foot positions at the front and rear of the machine. This pitch will remain constant, assuming all legs are identical and the crankshafts are coupled together in the correct phase and rotate synchronously.

6.2.1 Longitudinal stability with vertical loads

Figure 35 shown below is identical to Figure 33. It is reproduced here to ease development of the static analysis that follows.

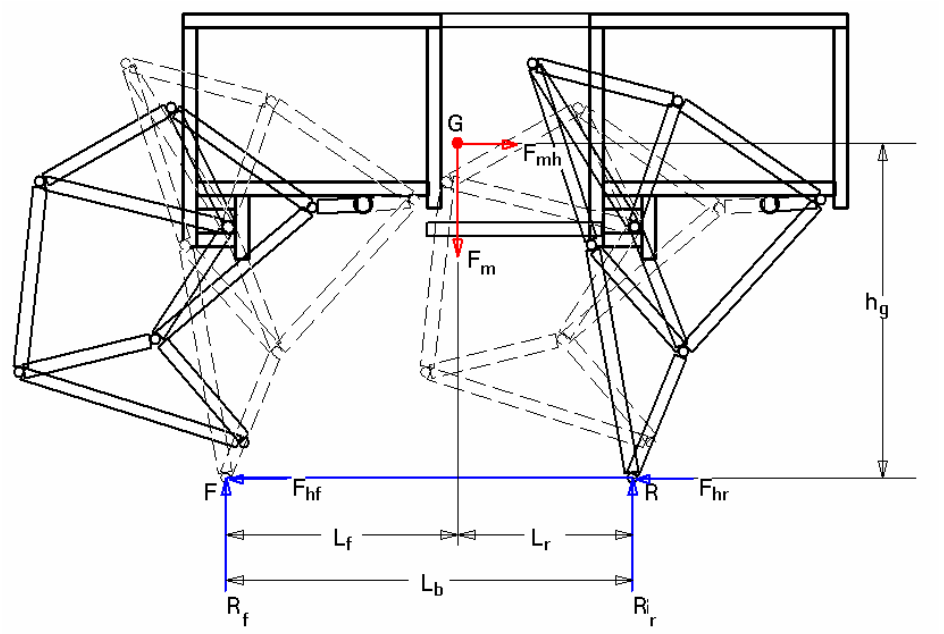

Figure 35. Longitudinal FBD of walker with Jansen legs.

With the walker in the position shown in Figure 35, R_r should be larger than R_f., as the centre of gravity is nearer to the rear foot position. As the crankshafts turn (anti-clockwise) and the walker walks (to the left), the line of action of F_m will move to the left in relation to the position of feet, which remain fixed. The rear reaction R_r will decrease and the front reaction R_f. will increase. The animations provided on the CD ROM in the "*Animations\Animations for mechanics chapter*" gives graphic demonstrations of this process.

Longitudinal stability requires that the projection of the line of action of F_m is always to the left of point R and to the right of point F. The animation called "*animation showing hg changing*" in the same directory of the CD shows how walking may move the centroid into an unstable position, as well as how the centroid height may change.

These relations can be expressed mathematically in the following manner. Considering vertical force equilibrium:

$$F_m = R_f + R_r \qquad \text{Equation (6.2.1)}$$

Taking moments about point R

$$F_m \times L_r = \left(R_f \times L_b\right) + \left(F_{mh} \times h_g\right) \qquad \text{Equation (6.2.2)}$$

To simplify equation (6.2.2), we assume that $F_{mh} \approx 0$, and ignore the second term on the right hand side of the equation. With this simplifying assumption, we have:

$$R_f = F_m \times \frac{L_r}{L_b}$$ Equation (6.2.3)

Substituting Equation (6.2.3) into Equation (6.2.1) gives

$$R_r = F_m - R_f = F_m \times \left(1 - \frac{L_r}{L_b}\right)$$ Equation (6.2.4)

where

F_m = Force due to mass of vehicle. $F_m = m \times (g + a_v)$

F_{mh} = Horizontal force on vehicle. $F_{mh} = m \times a_h$

M = Vehicle mass.

g = Acceleration due to gravity. 9.8 m/s^2

a_v = Vertical acceleration of body, due to leg kinematics.

a_h = Horizontal acceleration of body.

R_r ,R_f. = Vertical reaction at feet, as in Figure 33.

F_{hr} ,F_{hf} = Horizontal reaction at feet, as in Figure 33.

L_b = Leg-base, or longitudinal pitch between legs.. $L_b = L_f + L_r$

L_r = Longitudinal distance between F_m's line of action and rear foot reaction. A constraint is that $L_r > 0$ and $L_r < L_b$ at all times.

L_f = Longitudinal distance between F_m and front foot reaction. $L_f = L_b - L_r$.

h_g = Vertical height of the centre of gravity, G, above the walking level.

The parameter F_m is predominately the weight of the vehicle i.e. the quantity $m \times g$. However, if the vehicle body is moving vertically, as it may, depending on the leg kinematics, the body also experiences an acceleration, a_v. If the leg moves the body upwards, then a_v is positive, and increases the effective weight of the vehicle. If the body is instantaneously descending, then a_v will be negative, and the forces exerted on the ground would be reduced. It is precisely this a_v value that the foot trajectory optimization was attempting to minimize. However, for completeness, and because other leg configurations may not minimize the body's vertical acceleration, this term is included in the analysis and not ignored.

The mass of the vehicle could be determined by weighing it or by calculating it during CAD design. The variable values a_v and L_r can be determined from foot trajectory data and knowledge of the centroid position.. A sophisticated analysis could also allow for a_h, which is also available in this data.

6.2.2 Lateral stability with vertical loads

Lateral stability with vertical loads is now considered, for the case of the octopod walker. As the legs are not arranged symmetrically, we must consider two FBD's, one pertaining to the situation at the front legs, and the second showing forces at the rear legs. The orientation of the walking machine is as shown previously in Figure 34, with the machine moving off the page toward the left. Figure 36, the FBD at the front legs, is drawn as a front view of the vehicle, facing in the opposite direction that the vehicle is travelling in, so the left and right sides have been reversed on this FBD. The rear FBD is a rear view, looking in the same direction as walker motion, and so the left hand side of the vehicle is also the left of the FBD.

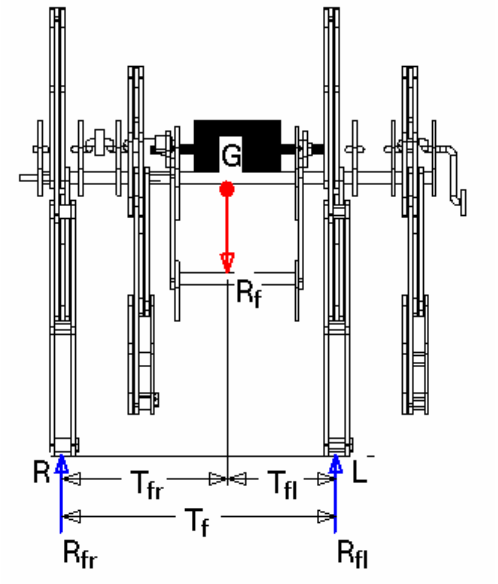

Figure 36. Lateral FBD at front legs.

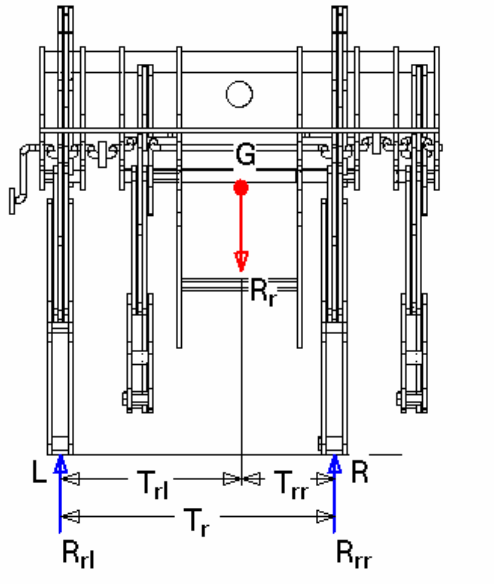

Figure 37. Lateral FBD at rear legs.

For the front legs, for vertical force equilibrium, we can write:

$$R_f = R_{fr} + R_{fl}$$ Equation (6.2.5)

Taking moments about point L, we have:

$$R_f \times T_{fl} = R_{fr} \times T_f \quad \Rightarrow$$

$$R_{fr} = R_f \times \frac{T_{fl}}{T_f}$$ Equation (6.2.6)

Substituting Equation (6.2.6) into Equation (6.2.5) gives

$$R_{fl} = R_f - R_{fr} = R_f \times \left(1 - \frac{T_{fl}}{T_f}\right)$$ Equation (6.2.7)

Similarly for the rear legs, we can write:

$$R_r = R_{rr} + R_{rl}$$ Equation (6.2.8)

$$R_r \times T_{rl} = R_{rr} \times T_r \quad \Rightarrow \quad R_{rr} = R_r \times \frac{T_{rl}}{T_r}$$ Equation (6.2.9)

$$R_{rl} = R_r - R_{rr} = R_r \times \left(1 - \frac{T_{rl}}{T_r}\right)$$ Equation (6.2.10)

For this design of octopod, we can distinguish between three track widths. T is the overall track width. T_i the distance of the inner legs from the centroid projection, and T_o is the half track to the outer legs. Note that $T = T_i + T_o$. We can then make use of the following simplifying equalities:

$$T_r = T_f = T$$ Equation (6.2.11)

$$T_{rl} = T_{fr} = T_o$$ Equation (6.2.12)

$$T_{rr} = T_{fl} = T_i = T - T_o$$ Equation (6.2.13)

After the crankshaft has turned half a revolution, the other legs at each corner will be taking the walking forces. At this crank position, the simplifications would be:

$$T_{rr} = T_{fl} = T_o$$ Equation (6.2.14)

$$T_{rl} = T_{fr} = T_i$$ Equation (6.2.15)

For brevity and convenience, we can define the following constant, K_T:

$$K_T = \frac{T_o}{T}$$ Equation (6.2.16)

Similarly, for the longitudinal dimensional factor, we may define a pseudo-constant, K_L, as:

$$K_L = \frac{L_r}{L_b}$$ Equation (6.2.17)

Note that the parameter K_L is not really constant, but will vary as a result of the foot trajectory. K_L will assume its minimum value as the feet touch the ground at the start of a cycle, increasing to a maximum value as the feet leave the ground at the end of the walking cycle.

If we now substitute the values for R_f and R_r from equations (6.2.3) and (6.2.4) back into equations (6.2.6), (6.2.7), (6.2.9) and (6.2.10), using all the above simplifications, we obtain the following four equations for the load on each of the four legs currently on the ground.

$$R_{fr} = F_m \times K_L \times K_T \qquad \text{Equation (6.2.18)}$$

$$R_{fl} = F_m \times K_L \times (1 - K_T) \qquad \text{Equation (6.2.19)}$$

$$R_{rr} = F_m \times (1 - K_L) \times (1 - K_T) \qquad \text{Equation (6.2.20)}$$

$$R_{rl} = F_m \times (1 - K_L) \times K_T \qquad \text{Equation (6.2.21)}$$

When the next set of legs is carrying the load, these equations become:

$$R_{fr} = F_m \times K_L \times (1 - K_T) \qquad \text{Equation (6.2.22)}$$

$$R_{fl} = F_m \times K_L \times K_T \qquad \text{Equation (6.2.23)}$$

$$R_{rr} = F_m \times (1 - K_L) \times K_T \qquad \text{Equation (6.2.24)}$$

$$R_{rl} = F_m \times (1 - K_L) \times (1 - K_T) \qquad \text{Equation (6.2.25)}$$

For the hexapod walker, the rear reaction force R_r will be taken jointly by the two legs at the rear, which are both in contact with the ground. The front reaction force R_f. will be taken entirely by the single front leg currently on the ground.

$$R_f = F_m \times K_L \qquad \text{Equation (6.2.26)}$$

$$R_{rr} = R_{rl} = F_m \times \frac{(1 - K_L)}{2} \qquad \text{Equation (6.2.27)}$$

When the two front legs plus the centre rear leg of the hexapod are load bearing, then

$$R_r = F_m \times (1 - K_L) \qquad \text{Equation (6.2.28)}$$

$$R_{fr} = R_{fl} = F_m \times \frac{K_L}{2} \qquad \text{Equation (6.2.29)}$$

As the parameter K_L is not constant, these equations (6.2.18) to (6.2.29) show that the load on the various legs varies continuously as the machine walks. This is in contrast to a wheeled vehicle on a flat surface, where the reactions at the wheels are dictated by their positions i.e. by the wheelbase and track. Once these are computed for a wheeled vehicle, they do not vary as the vehicle moves.

These continuously varying foot loads mean that fatigue and vibration, particularly in torsion, will be considerations in the detail design of the body, legs and drive-train of a walking machine. The frequency of any cyclical loading will depend on the rotational speed of the driving crankshaft. As we do not wish these frequencies or their harmonics to be felt, it means that the excitation frequency must be kept low, which in turn means a slow moving crankshaft. To keep excitation frequency below 5 Hz places an upper crank speed limit of 300 rpm.

A walking machine designed to travel at 60 km/hr (= 1 km/min) would need a stride length of 1000 / (2 $\times$ 300) = 1.667 metres, as there are two strides per revolution. The stride length for the best leg found, with a 100 mm crank radius, is 372 mm, from Figure 31. This implies a scale factor of (1667 / 372) = 4.48, so the crank radius would have to be about 450 mm. Such a walking machine would carry its crankshafts 2.5 metre off the ground and have a leg-base of around 4.2 metres if scaled from the prototype octopod walker.

The size of such a machine may restrict its practicality, so a focus of future detail design work must be to deal with vibration issues, to allow design of smaller machines that could move faster. In robotic or un-manned walkers, these speed restrictions could probably be much relaxed. But there will probably be an upper speed limit at which a walking machine may travel, limited by vibration considerations.

If the detail design of the walker has made the centre of gravity too far to the rear of the machine, then the centroid may be only slightly ahead of the point R (i.e. $L_r \approx 0$) at the start of the walking cycle. In this case, $K_L \approx 0$. For the hexapod walker, at this time in the walking cycle, nearly the entire weight of the vehicle is carried on the single central rear leg. As the foot position of this leg is also the apex of the triangular support polygon of the machine, it may make stability of such a walker extremely sensitive to minor irregularities in foot level, especially if they displace the leg laterally. This issue is much reduced in the ocotopod, due to the presence of two legs at the rear. For this reason, the hexapod layout will not be considered further in detail. All analysis subsequent to this deals primarily with the octopod layout.

This simple analysis also applies to other situations where there are front and rear legs, including animals. Considering the anatomy of mammalian quadrupeds such as horses and dogs, the hindquarters of these animals are considerably more heavily built and muscled than the forelegs. This is due to the above formulae, as the animal body's centre of gravity is nearer to the line of action of the rear legs than to the front legs, so the rear legs on these animals are much more heavily loaded than the front ones are. It also explains the torso

shape of these animals – clearly nature has attempted to move the centre of gravity as far forward as possible. Hence the body has a deep chest and a light rear section.

6.2.3 Longitudinal stability with horizontal loads

Although the major loads the legs of a walking machine needs to bear are due to the weight of the vehicle, the legs are also subject to longitudinal loads. These result partially from the horizontal speed variation present in the velocity profile of the foot trajectory. There may also be a component due to accelerating the vehicle up to speed or due to braking. The situation of horizontal loads is shown in Figure 38 below.

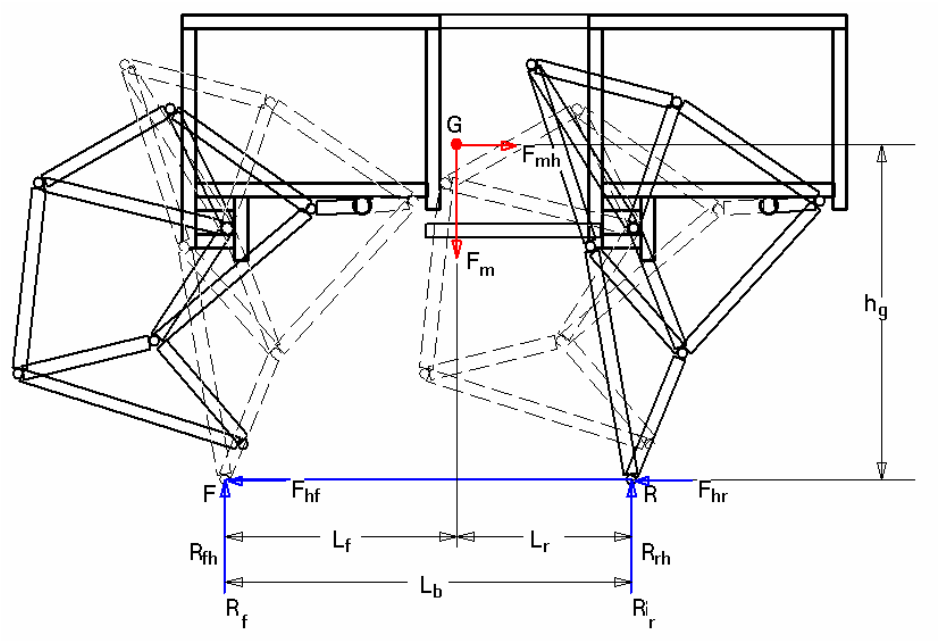

Figure 38. Horizontal FBD for walker on flat surface.

Considering horizontal force equilibrium:

$$F_{mh} = F_{hf} + F_{hr} \qquad \text{Equation (6.2.30)}$$

However when we come to take moments, so we may evaluate F_{hf} and F_{hr}, we find that none of the salient points of the FBD, points G, F or R, can be used. The forces applied by the feet are applied on the same line of action. The force that prevents the vehicle from overturning backwards is the reaction at the rear legs, R_r.

To assess stability, take moments about F.

$$\left(F_{mh} \times h_g\right) + \left(F_m \times L_f\right) = R_r \times L_b \qquad \text{Equation (6.2.31)}$$

From equation (6.2.4), and knowing that $L_f = L_b - L_r$, we get

$$\left(F_{mh} \times h_g\right) = \left(R_r \times L_b\right) - \left(F_m \times L_f\right) = \left(F_m \times \left(1 - \frac{L_r}{L_b}\right) \times L_b\right) - \left(F_m \times \left(L_b - L_r\right)\right) = 0$$

Equation (6.2.32)

As the assumption $a_h \approx 0$ was made earlier to simplify solution of equation (6.2.2), this result is consistent. To account for the fact that a walker would be stable even when the body is being decelerated as shown in Figure 38, we need to include a new factor to counter the tendency of the decelerating force to rotate the structure around point F in the FBD. To do this we introduce a new force, R_{rh}, which acts along the same line as R_r. and a similar force, R_{fh}, at the front legs, associated with R_f. Reconsidering moments about F, and ignoring F_m and R_r, we now have:

$$\left(F_{mh} \times h_g\right) = R_{rh} \times L_b \quad =>$$

$$R_{rh} = \frac{\left(F_{mh} \times h_g\right)}{L_b}$$

Equation (6.2.33)

To maintain vertical force equilibrium, R_{fh} = - R_{rh}. This negative reaction must be counteracted by R_f, the reaction at the front legs. If the body is accelerated too fast, or if the body is ascending a slope, then ($|R_{fh}| > R_f$) and the front legs may lift off the ground.

In the case of a decelerating vehicle, where the direction of F_{mh} is reversed, we take moments about R, and by similar logic:

$$R_{fh} = \frac{\left(F_{mh} \times h_g\right)}{L_b}$$

Equation (6.2.34)

R_{rh} = - R_{fh}. Equation (6.2.35)

Although we have now isolated additional forces that allow us to deal with horizontal stability of the vehicle body, we still have no method of calculating what proportion of horizontal thrust is provided by the front legs and how much stems from the action of the rear legs. In fact, in this simplified analysis, we do not have sufficient information to be able to tell what the situation would be in reality. We must assume that all legs contribute equally, so F_{hfl} = F_{hrl} = F_{hrl} = F_{hrr} = F_{mh} / 4.

As long as vertical stability is maintained, it matters little which legs provides the horizontal thrust. If some feet were placed in such conditions that they would slip on the ground, and therefore be unable to exert horizontal force on it, then the other legs would need to provide the horizontal forces. If all legs slipped simultaneously, then the body of the vehicle would not move forward, and leg kinematic motion would be absorbed in sliding the feet along the slippery surface. The vehicle would remain stationary, but stable, under these conditions.

6.3 Walking up a slope

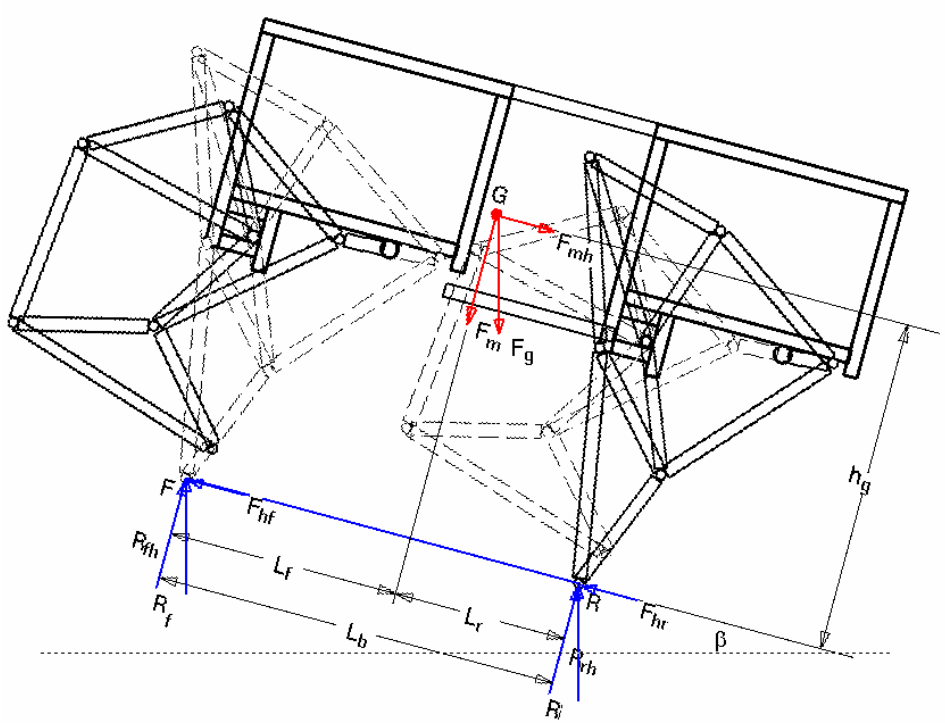

Figure 39. FBD of a walker walking up a slope.

Consider the walking machine shown in Figure 39 above, walking up a slope of β degrees. In this case, the weight of the machine, shown as F_g, continues to operate vertically downward. The simplest approach to solving these dynamics is to resolve this force into two components, one (F_{gv}) parallel to F_m and one (F_{gh}) parallel to F_{mh}. As the angle between the lines of action of F_m and F_g is also β, these components can be resolved as:

$$F_{gv} = m \times g \times \cos(\beta) \qquad \text{Equation (6.3.1)}$$

$$F_{gh} = m \times g \times \sin(\beta) \qquad \text{Equation (6.3.2)}$$

If the vehicle is also accelerating up the slope, at an acceleration of a_s, another force $F_a = m \times a_s$ must be acting along the plane of the slope, co-linear with F_{mh}.

One may now evaluate

$$F_m = F_{gv} + m \times a_v = m(g \cos\beta + a_v) \qquad \text{Equation (6.3.3)}$$

$$F_{mh} = F_{gh} + (m \times a_{h)} + (m \times a_s) = m(g \sin\beta + a_h + a_s) \qquad \text{Equation (6.3.4)}$$

We can now substitute equations (6.3.3) and (6.3.4) back into equations (6.2.3), (6.2.4) and (6.2.23) to give new reactions, R_{fi} and R_{ri}, with *i* subscript to denote “incline”, thus:

$$R_{fi} = R_f - R_{fh} = \left(F_m \times \frac{L_r}{L_b}\right) - \left(F_{mh} \times \frac{h_g}{L_b}\right)$$

$$R_{fi} = \frac{m}{L_b}\left(L_r\left(g\cos\beta + a_v\right) - h_g\left(g\sin\beta + a_h + a_s\right)\right)$$

Equation (6.3.5)

$$R_{ri} = R_r + R_{rh} = \left(F_m \times \left(1 - \frac{L_r}{L_b}\right)\right) + \left(F_{mh} \times \frac{h_g}{L_b}\right)$$

$$R_{ri} = \frac{m}{L_b}\left(\left(L_b - L_r\right)\left(g\cos\beta + a_v\right) + h_g\left(g\sin\beta + a_h + a_s\right)\right)$$

Equation (6.3.6)

Note that the slope is assumed to be level in the transverse direction. So the situation at the left and right legs at each end will be the same as described in the previous section 6.2.2 and equation (6.2.7), (6.2.8), (6.2.9) and (6.2.10) will apply.

Equation (6.3.5) can evaluate to zero, or even become negative, when the term in the outer brackets equates to or is less than zero. This will depend on the value of β, as all other terms on the right hand side are constant. This makes sense intuitively, as at a certain steepness the walker is likely to topple over backwards, or “wheelie” at least, see Figure 40.

Figure 40. Walker "rearing" while hill climbing.

Equating the terms in the brackets from equation (6.3.5) gives:

$$L_r\left(g\cos\beta + a_v\right) = h_g\left(g\sin\beta + a_h + a_s\right)$$

Equation (6.3.7)

$$L_r g\cos\beta - h_g g\sin\beta = h_g a_h + h_g a_s - L_r a_v$$

Equation (6.3.8)

If we ignore the terms in a_h, a_v, and a_s, as these are all likely to be small, this equates to:

$$\tan \beta = \frac{L_r}{h_g}$$

Equation (6.3.9)

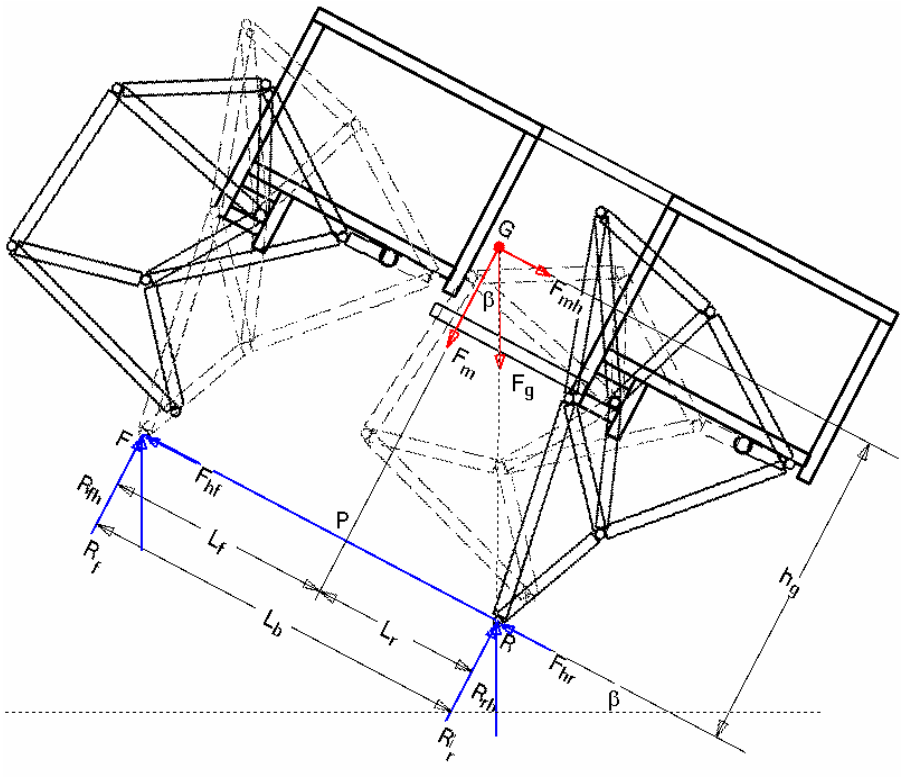

Figure 41. Climbing walker at the point of toppling over backwards.

A confirmation of this relation is available if one considers the physical situation when the machine is about to fall over backwards, as shown in Figure 41. At this inclination, the position of the centre of gravity, G, is vertically above the foot position at the rear legs, R. Considering triangle GPR, and knowing the angle PGR = β, then from elementary trigonometry, tan β = L_r / h_g, and equation (6.3.9) is correct. This is the limit of longitudinal stability, discussed in section 6.2.

This limiting angle of the slope will be a minimum when L_r is smallest i.e. when the rear feet first touch the ground at the start of a new stride. So, if the vehicle is going to "rear", it is going to do it at this point. As soon as the front legs lift off the ground, the dynamic situation changes substantially. This has not been analysed here, but practical experience indicates that a positive feedback loop arises, and once the vehicle has lifted its front legs, a backwards over-turning is inevitable.

Notice also that the larger L_r is, then the larger β will also be. Thus vehicles with a long leg-base or with the centre of gravity placed far forward will be able to climb steeper slopes before overturning backwards. Another way to improve hill climbing abilities is to minimize h_g, the vertical height of the centre of gravity. This makes intuitive sense and is confirmed by equation (6.3.9).

The forces that act in the plane of the slope at the feet still cannot be individually discriminated, so, as when walking on a transversely level surface, $F_{hfl} = F_{hrl} = F_{hrl} = F_{hrr} = F_{mh} / 4$. However in this case the value of F_{mh} is given by equation (6.2.30).

The ability of a particular foot to apply this horizontal force will depend on friction and on the reaction at that foot. The maximum horizontal force that can be transmitted is given by

$$F_{h\,(max)} = (\mu \times R) \qquad \text{Equation (6.3.10)}$$

where

μ = the coefficient of friction between the foot pad and ground materials

R = the vertical reaction force

If the horizontal force required to be transmitted by a particular leg is greater than this value, the foot will slip and will not be able to exert its contribution to the total in-plane force required to keep the walker moving up the incline. Once slip occurs at one foot, the horizontal force components on the other feet increase. The new load on the next most lightly vertically loaded foot is perhaps now made greater than this foot can transmit. This foot will then also slip, increasing the load further on the two remaining legs that are still held in place by friction. But the in-plane forces on these remaining legs are now double what they were initially, and it is possible that the vertical loads are insufficient to keep these feet in place. So all feet slip on the surface, and in fact the walker will slide down the hill, backwards, with the legs still operating, but not being able to gain purchase.

In this scenario, the leg most likely to slip first will be the outer front leg, as this will have the lowest vertical load. Using the information in equations (6.2.6), (6.2.29) and (6.2.30)

$$0.25 \times m \times (g \sin \beta + a_h + a_s) = \mu \times K_L \times (1 - K_T) \times m \times (g \times \cos \beta + a_v)$$

Equation (6.3.11)

Once again, ignoring terms in a_h, a_v, and a_s, we get

$$\tan \beta = 4 \times \mu \times K_L \times (1 - K_T) = \frac{\mu \times 4 \times L_r \times (T - T_o)}{L_b \times T} = \mu \times 4 \times K_{fra}$$

Equation (6.3.12)

$$K_{fra} = K_L \times (1 - K_T) = \frac{L_r \times T_i}{L_b \times T}$$

Equation (6.3.13)

If the value of this friction modification factor, K_{fra}, is less than 0.25, then it acts as a friction reduction factor. In this, the most likely case, the angle at which the first foot of the machine is likely to slip is less than the standard friction analysis would dictate. To actually ascertain what would happen when the first leg slipped, a further analysis of the case of three legs, then two legs, then a single leg providing the horizontal forces, would have to be done. This has not been done. It is sufficient to say that the maximum climb angle will be effectively reduced by this factor.

This factor will be a minimum when L_r is small i.e. at the beginning of the walk cycle. So, if initial contact can be maintained, then as L_r increases, so do the friction modification factor and the vertical reaction, and grip is assured.

The effect of this factor can be significant. For the Perspex octopod walker, $K_{L(min)} \approx 0.3$ and $(1-K_T) \approx 0.33$, so $K_{fra} \approx 0.1$. This means that the friction at the front outer foot is only 40% of what could be expected. To allow this prototype to climb steeper hills, the ground against foot friction was increased by equipping the feet with sandpaper shoes.

Although it is hard to imagine a machine design where $K_{fra} > 0.25$, if such a machine could be designed, it would have improved hill climbing abilities. Although T_i can never be greater than $T/2$, by definition, if it were near to this value, the modification factor would be maximised. If one could arrange a design such that $(L_{r(min)} / L_b) > 0.5$, then K_{fra} could be made to be greater than one quarter, thereby increasing effective friction. However, as will be seen in the following section, increasing this ratio will have a detrimental effect on hill descent.

6.4 Descending an incline

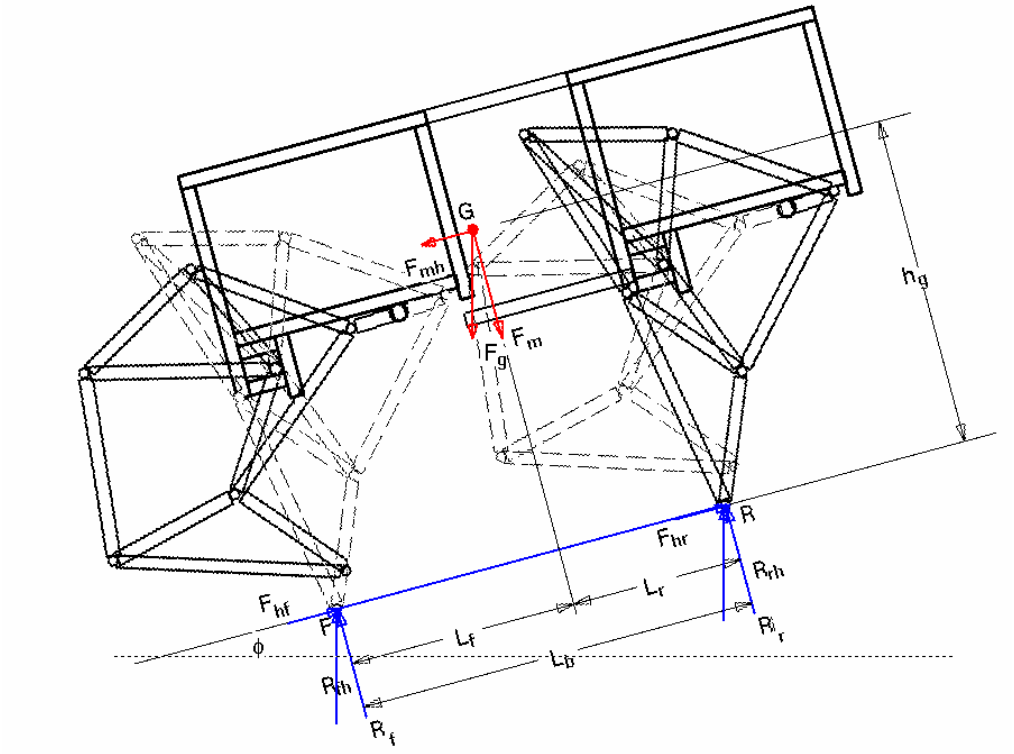

Figure 42. FBD of a walking machine walking downhill.

The case of the walker descending a slope of angle ϕ is similar to the case of ascending. The horizontal force F_{mh} now tends to accelerate the machine down the hill, and the front legs are more heavily loaded. Once again we may resolve the vehicle's weight into two components, parallel and perpendicular to the slope.

$$F_{gv} = m \times g \times \cos(\phi)$$ Equation (6.4.1)

$$F_{gh} = m \times g \times \sin(\phi)$$ Equation (6.4.2)

We can again substitute these equations back into equations (6.2.3), (6.2.4) and now (6.2.24) to give the reactions, R_{fi} and R_{ri}, for the case of moving downhill, thus:

$$R_{fi} = R_f + R_{fh} = \left(F_m \times \frac{L_r}{L_b}\right) + \left(F_{mh} \times \frac{h_g}{L_b}\right)$$ Equation (6.4.3)

$$R_{fi} = \frac{m}{L_b}\left(L_r\left(g\cos\phi + a_v\right) + h_g\left(g\sin\phi + a_h + a_s\right)\right)$$ Equation (6.4.4)

$$R_{ri} = R_r - R_{rh} = \left(F_m \times \left(1 - \frac{L_r}{L_b} \right) \right) - \left(F_{mh} \times \frac{h_g}{L_b} \right)$$

Equation (6.4.5)

$$R_{ri} = \frac{m}{L_b} \left((L_b - L_r)(g \cos\phi + a_v) - h_g (g \sin\phi + a_h + a_s) \right)$$

Equation (6.4.6)

In the case of a hill descent, the stability issue would be if the rear legs lifted off the ground, making the machine tumble over its front legs. Analogous to the case for hill climbing, this case occurs when the terms in the bracket in equation (6.2.33) are equal.

$$(L_b - L_r)(g \cos\phi + a_v) = h_g (g \sin\phi + a_h + a_s)$$

Equation (6.4.7)

If we make the substitution $L_f = L_b - L_r$, then equation (6.4.7) is exactly the same form as equation (6.3.6), and so

$$\tan\phi = \frac{L_f}{h_g}$$

Equation (6.4.8)

As $L_f = L_b - L_r$, this condition will occur at the end of the walking cycle, as the rear leg is being lifted. Given the deterministic kinematics of the leg, this means the next set of legs will be very nearly in place to make their footfall. The front legs in this position would prevent the walker from actually overturning forwards, and as soon as contact is made with the ground, the toppling angle re-evaluates with a smaller L_r thus greater L_f, and tumbling is averted.

In the case of sliding forwards down a hill, we would expect that a friction modification would be experienced at the rear feet. In a similar manner to the analysis given in the previous section, for the rear outer legs to loose grip we have

$$0.25 \times m \times (g \times \sin\phi + a_h + a_s) = \mu \times (1 - K_L) \times (1 - K_T) \times m \times (g \times \cos\phi + a_v)$$

Equation (6.4.9)

$$K_{frd} = (1 - K_L) \times (1 - K_T) = \frac{L_f \times T_i}{L_b \times T}$$

Equation (6.4.10)

In this case, as with tumbling forwards over the front legs, K_{frd} is least when L_f is smallest i.e. when L_r is largest, at the end of the cycle. Once again the deterministic foot trajectory will come to the rescue, and though the leg may start to slide, the imminent new footfall will have greater reaction and higher friction modification. This should be sufficient to halt the slide.

Sliding is a reduced risk in descent, as $K_{frd} = 1 - K_{fra}$, and so the modification factor is usually a friction amplification factor. For the Perspex octopod walker, with $K_{fra} = 0.1$, then $K_{frd} = 0.9$ and the total friction modification is $(4 \times 0.9) = 3.6$.

As mentioned prior, if $(L_{r(min)} / L_b) > 0.5$, then $L_{f(min)} < 0.5$, and K_{frd} will become a reduction factor. Therefore the best design compromise between good hill climbing and descent is to make $(L_{r(min)} / L_b) \approx 0.5$. This will mean that the centre of gravity of the overall machine must be kept fairly far forward. Varying the leg-base dimension can be used to achieve this result.

6.5 Walking transversely across a slope

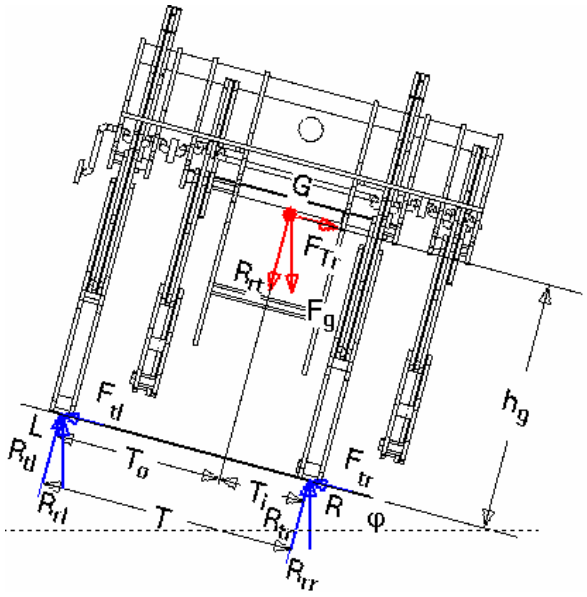

Figure 43. FBD of a walker walking transversely across a sloping surface.

The sketch in Figure 43 shows the situation when the walker travels across a sloping surface of angle φ, assumed to be level in the longitudinal direction. As when ascending or descending an incline, the effect of the slope is to make the weight of the vehicle exert a force parallel to the slope. In the transverse slope case, this force is felt at the centre of gravity, operating transverse to the longitudinal axis. This force is shown as F_{Tr} in the figure. Similarly to the cases of longitudinal slopes, the resulting force components normal (F_{Tv}) and parallel (F_{Th}) to the slope can be expressed as:

$$F_{Tv} = m \times g \times \cos(\varphi) \qquad \text{Equation (6.5.1)}$$

$$F_{Th} = m \times g \times \sin(\varphi) \qquad \text{Equation (6.5.2)}$$

As the slope is assumed level in the longitudinal direction, the front / rear force distribution on the legs will be the same as in the case of walking on a level surface. Equations (6.2.3) and (6.2.4) can be used to determine this distribution. At the rear legs,

$$R_{rT} = m \times g \times \cos(\varphi) \times \left(1 - \frac{L_r}{L_b}\right)$$ Equation (6.5.3)

$$F_{Tr} = m \times g \times \sin(\varphi) \times \left(1 - \frac{L_r}{L_b}\right)$$ Equation (6.5.4)

At the front legs:

$$R_{fT} = m \times g \times \cos(\varphi) \times \frac{L_r}{L_b}$$ Equation (6.5.5)

$$F_{Tf} = m \times g \times \sin(\varphi) \times \frac{L_r}{L_b}$$ Equation (6.5.6)

As Figure 43 shows the situation at the rear legs, we will analyze lateral forces at this position. The force resolution at the front legs will be analogous. In a similar fashion as encountered in the slope climbing case, the previously considered reactions at the left and right legs will not provide a correcting force to prevent the lateral forces at the centroid from overturning the machine. Once again we introduce supplementary reaction forces (R_{tl} and R_{tr}) to perform this duty.

$$R_{tr} = F_{Tr} \times \frac{h_g}{T} = m \times g \times \sin\varphi \times (1 - K_r) \times \frac{h_g}{T}$$ Equation (6.5.7)

$$R_{tl} = -R_{tr}$$ Equation (6.5.8)

As for the case of lateral stability on a level surface, we also need to ascertain the left / right distribution of the vertical ground reactions. We can use equations (6.2.9) and (6.2.10) to compute the force at the left and right feet, to yield R_{rl} and R_{rr}, thus:

$$R_{rr} = R_{rT} \times \frac{T_o}{T} = R_{rT} \times K_T$$ Equation (6.5.9)

$$R_{rl} = R_{rT} - R_{rr} = R_{rT} \times (1 - K_T)$$ Equation (6.5.10)

A lateral instability condition will occur when the negative reaction felt at the left leg balances the ground reaction at that leg. So equating equations (6.5.7) and (6.5.10) gives

$$m \times g \times \sin\varphi \times (1 - K_r) \times \frac{h_g}{T} = m \times g \times \cos(\varphi) \times (1 - K_r) \times \left(1 - \frac{T_o}{T}\right)$$

Equation (6.5.11)

$$\tan\varphi = \frac{T_i}{h_g}$$

Equation (6.5.12)

Inspection of Figure 43 shows that this is indeed the case at the rear legs, as the walker is nearly at the point of toppling in this sketch. At the front legs, the critical angle will be given by tan $\varphi = T_o / h_g$. As ($T_o > T_i$) by definition, then the critical angle at the front legs will be higher, and toppling over would start at the rear of the machine. When the other set of legs are weight bearing, the situation would reverse, and lateral toppling would commence at the forelegs.

As the lateral overturning condition is experienced at an “axle” of the vehicle, different conditions will be experienced at each end. For the legs in the position shown in Figure 43, we have shown that the rear of the vehicle will tend to topple first, but the front end of the vehicle would still be stable, as the left (inner) front leg would be nearer to the line of action of the reaction at the front, and so be safe from overturning. This would to tend to lift the left (outer) rear leg. This would twist the vehicle chassis, and to the extent that the twist is resisted, the vehicle should not actually overturn. It is likely that foot lifting would allow the in-plane forces to become unbalanced, and resulting in-plane moments would turn the vehicle so as to climb the slope more directly i.e. the back of the machine would slip down the slope, and the new heading would be a combination of ascent and walking across the slope.

If the other legs were doing duty i.e. half a walking cycle from the position shown, then the front of the machine would experience lateral instability first. The upper front leg would slip, and the resulting in-plane moment would turn the machine to walk downhill.

The forces at the feet acting parallel to the plane are nominated F_{tl} and F_{tr}. As for the previous case with inclines, the values of these in-plane forces cannot be individually discriminated and are all assumed equal to one quarter of the total force required. Once again friction will determine whether the foot can actually exert the required force. This ability would be least for the front leg which is higher up the plane, at the start of the new stride when this front foot is furthest from the vehicle centroid. However, due to the asymmetric layout of the legs, it will be worst when the upper front leg is also the outer leg i.e. when the

crankshaft has turned 180° from the position shown in Figure 43. In this condition the balancing condition becomes

$$0.25 \times m \times (g \times \sin\varphi) = \mu \times K_L \times (1 - K_T) \times m \times (g \times \cos\varphi) \quad \text{Equation (6.5.13)}$$

The friction modification factor for transverse slopes, K_{frt}, is given by:

$$K_{frt} = K_L \times (1 - K_T) = \frac{L_r \times T_i}{L_b \times T} \quad \text{Equation (6.5.14)}$$

Note that Equation (6.5.14) is identical to Equation (6.3.13), as it was also the outer front leg that would slip first when climbing hills. However this factor, K_{frt}, will modify friction on lateral slopes whereas the previous formula dealt with friction in longitudinal ascents.

If lateral slippage of the front upper foot occurs, the resulting imbalance between the in-plane forces at the rear and at the front would tend to turn the machine to face down the slope. This is due to the fact that the first slippage causes the lateral forces to re-distribute themselves equally between feet again, but this time at a value of one third the total required. Now two-thirds of the total force is applied at the rear two non-slipping feet and only one third at the remaining front foot. This difference causes a net moment which will push the rear of the machine up the slope and the front will then point downhill. The longitudinal axis is no longer level and the analysis given above must be modified.

In this new attitude, the walking machine would be subject to a new set of forces, which could be calculated by integrating the theory of this section with that in sections 6.3 and 6.4. This is discussed briefly in the next section.

6.6 Walking over rough terrain

The stability criteria described in the previous few sections will determine the overall type of terrain that any walking machine could operate in. If a designer required information on loadings in a particular terrain, then knowledge of the topography of the walking surface would be required. If a suitable support polygon can be mapped onto the terrain topographical model, then the surface can be resolved into longitudinal and transverse slope components. If these components are within the stability criteria, then the walker would be able to negotiate the terrain. The attitude of the body could be determined from the attitude of the support polygon and the forces could be calculated with the methods given in the previous sections.

In very rough conditions, it may not be possible to fit a suitable planar polygon to the terrain topography, particularly for quadrilateral polygons. It is always possible to find a plane that

connects three points in space, but no so for four points. For a hexapod walker, this would mean the machine's attitude would be determined by that of the support triangle. Stability would have to be assessed at this condition. For an octopod, with a trapezoidal support polygon, some terrain may not accommodate all corner points of the trapezium, and the support polygon would default to a triangle, with one leg not in contact with the ground. This is the "restaurant table" effect mentioned earlier.

This rocking in uneven conditions is a fundamental problem and only limited solutions are possible. If the legs had some compliance, this would extend the range of topographies that could carry a trapezoidal support polygon. Feet with ground sensing and extensible rams or pads could be used to ensure contact at all four feet. Given the prospective walking machine's stated design environment, such complication could probably be dispensed with. Simple springs and dampers on the feet may bestow sufficient compliance in the legs to make a serviceable walker.

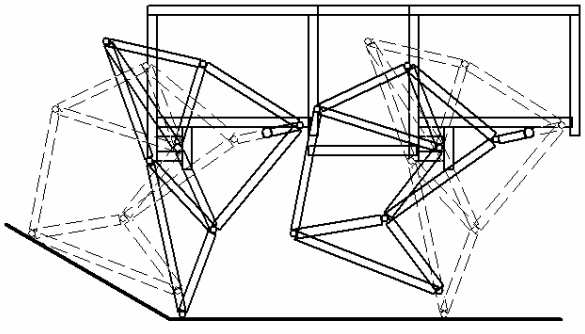

Figure 44. Approach angle

A very steep ascent slope could also lead to a situation where the links of the legs of the machine are not able to follow the trajectories determined by their proportions. If a walker with Jansen legs approaches a very sharp ascent, then the leading link of the mechanism (links 3 and 7 at node 4 or link 4) may strike the slope, as illustrated in Figure 44. If the rear legs still exert forward force, the front legs become trapped, and will stall. The machine is stopped and the front leg linkages may be damaged in the collision.

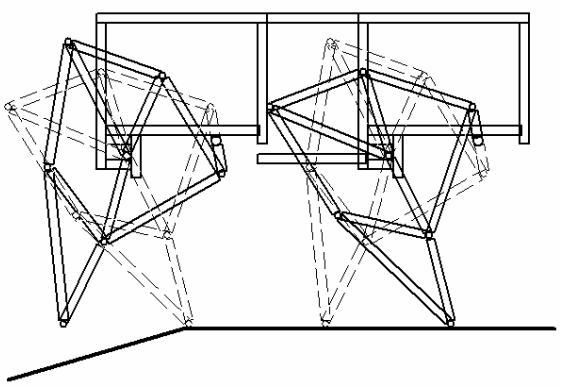

Figure 45. Walking onto a declining slope

On approaching a descending slope, the walker will continue walking off the end of the transition, with its front legs initially and momentarily in space above the slope, as shown in Figure 45. As the legs move and weight is transferred forwards, the front of the machine will descend, accelerated by gravity. The front legs on their return stroke would not lose contact with the ground, and would carry the forward weight of the machine. If the alternate set of front legs, those intended to be on service, have not yet contacted the ground before the returning pair reach the highest point in their trajectory, then the machine may stall. In any event, use of the return stroke for load bearing is problematic as the foot speed in return is much higher than when walking. This would lead to additional stress in both legs and body. The extent of this effect will depend on the specific foot positions in relation to the topography of the terrain.

Even a reasonably level unprepared walking surface will probably contain a range of minor surface imperfections –boulders, potholes, ruts, ant-hills etc. For obstacles to impede walking, the leg or foot of the machine must contact the obstacle. If the foot trajectory lifts the foot vertically at the end of the stride before commencing the return part of the trajectory, then any obstacles shorter than this lift will have no effect on foot motion. If the obstacle is taller than the maximum foot lift, then this is equivalent to a leg collision mentioned above, and the walker may stop. For obstacles of heights in between these two values, the effect of the obstacle depends on where in its path the foot or leg encounters the obstacle, and the geometry of the contact event. Hopefully, if the walker is big, with strong legs, and the obstacle is small, the leg will kick the object as it strikes it, and hopefully the boulder will remove itself and not interfere further. If the object does not move, it may stall the leg.

Another possibility is that the foot lands on top of a protrusion on an otherwise flat terrain. The machine would probably experience rocking at this point. A similar situation could arise if a foot landed in a shallow pot hole. Larger potholes, deep and wide enough to contain a large portion of the leg, would not be negotiable.

The design environment is outdoors and fortunately staircases are unlikely to be encountered. This is one type of hazard that would probably trip a walker with Jansen legs, especially if the rise of the staircase is only slightly less than the foot lift. In this case, the foot or link 4 would strike the stair while on the forward part of its return trajectory, and this would result in some impact. If the foot lift was substantially higher than the stair rise, then the walker may be able to negotiate the stairs. But the best trajectory found only lifts its feet 110 mm for a stride of 372 mm. Given most stair case are pitched at something like 200 mm rise for 300 mm tread width, a walker on this scale would certainly be defeated by a staircase. Larger walkers with higher lift would fare no better, as though they could lift above the immediate stair, they would not be able to lift high enough for the stair 3 ahead, which is where the foot trajectory's horizontal motion would want the foot to land.

This is not to say that a better foot trajectory for staircases could not be selected with a GA with other fitness criteria. However this type of indoor locomotion also usually requires other obstacle avoidance abilities, particularly manoeuvrability. Given also the width of any walker with reasonable stride, it is unlikely that walkers with Jansen legs would be suited to operate in an indoor environment.

6.7 Leg load paths

This simplified analysis has thus far said nothing about the load paths for the forces. Clearly the walking machine body will place its weight on the legs, but if the crank were not driven, the legs would be collapse into the position of lowest overall energy of the system. At this point, static structural methods could be used to resolve all forces in the leg, treating it as if it were a truss.

Conversely, if one wanted to maintain the mechanism at a particular position, this could be done by applying a suitable force at the crankshaft. In either case, solution of the forces at the crank and fixed pin can be resolved by structural analysis, specifically the method of joints [52]. This method need not be re-developed here, as it was developed in previous work [1]. Techniques developed there have been extended to also deal with horizontal force components.

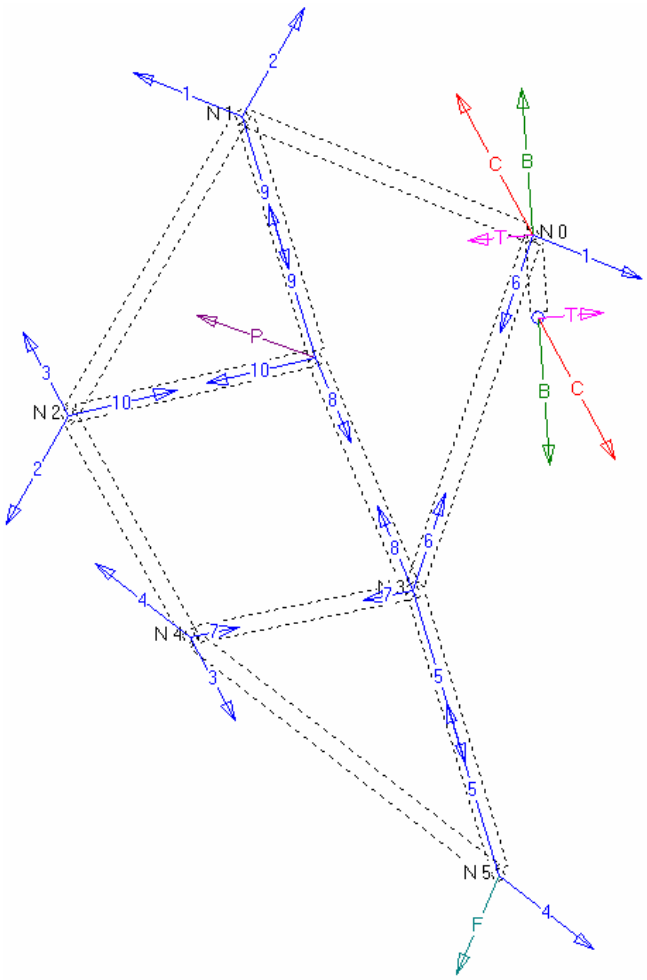

Figure 46. Resolution of forces in links by the method of joints.

The sketch in Figure 46 shows how the loads in links are resolved by calculating forces required for static equilibrium at each node. The reaction to the applied foot load is shown as $\vec{F}$ (in teal) at node 5. Blue vectors represent forces in the links, with the identity of the link printed on each vector. The outputs of the algorithm are the magnitude and direction of the forces exerted at the fixed pin (the purple vector, $\vec{P}$) and at the crankpin, node 0 (the red vector, $\vec{C}$). The crankshaft force $\vec{C}$ is resolved into a radial component, felt in the crankshaft bearings (the green vector, $\vec{B}$) and a tangential one, which equates to a torque ($\vec{T}$, in fuchsia). The forces experienced at the crankshaft main bearing are also shown, acting at the crank centre, equal and opposite to those at node 0.

One may solve the force distribution in the linkage and the driving torque required at each crank position, knowing the magnitude and direction of the applied force. Note that at the position shown, the leg is driving the crankshaft anti-clockwise – the applied torque is negative. The situation may reverse at another crank position.

To allow easier visualization of the loads in links a series of animations are provided on the CD-ROM, in the "*Animations\Animations for mechanics chapter*". These show the forces changing in the legs as the machine walks on level ground, or climbs or descends a fifteen degree slope.

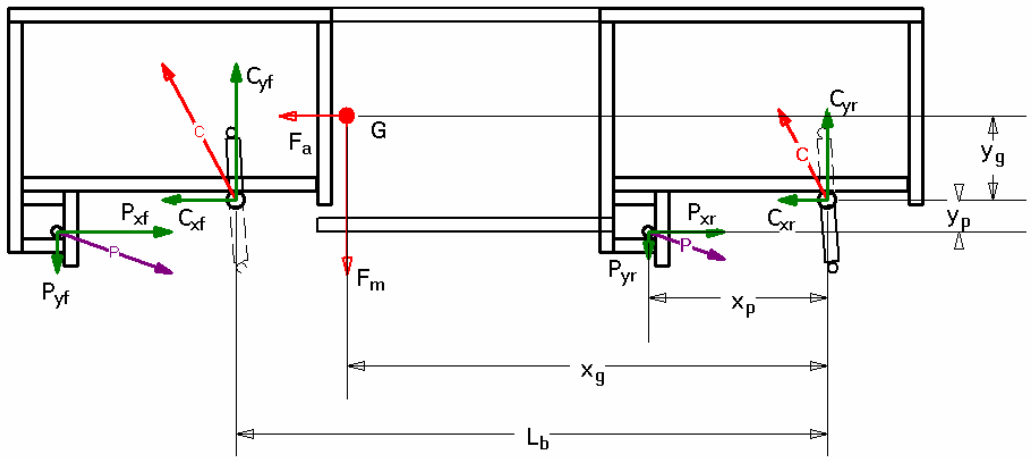

Figure 47. FBD of the chassis of a walking machine

Considering the FBD of the vehicle chassis with legs removed (Figure 47), reaction forces from the legs into the chassis should balance the forces experienced at the centre of gravity. Notice that these reactions are different at the front and rear legs.

As these forces can all be calculated, this fact acts as a check. If forces have been miscalculated either in the vector solutions or in the force distribution between legs, they would not balance. Static equilibrium will not be experienced by the chassis, and theoretically it should move off, driven by the remainder force left over after forces are resolved.

For horizontal and vertical force equilibrium:

$$P_{xf} + C_{xf} + P_{xr} + C_{xr} = F_a \qquad \text{Equation (6.7.1)}$$

$$P_{yf} + C_{yf} + P_{yr} + C_{yr} = F_m \qquad \text{Equation (6.7.2)}$$

These equations can be applied to all solutions to verify correctness or at least mathematical consistency of these solutions.

6.8 Power requirements

The method outlined in the previous section can evaluate the torque required at the crankshaft to impart particular forces at the feet. The forces required at each foot depends on which leg is being considered, what slopes the machine is negotiating and the mass and layout of the vehicle, as discussed in previous sections. The values of $L_{r,}$, a_v and a_h all change, so the instantaneous force applied at each leg will also change. To distinguish these various contributing forces, we can define the total force required as:

$$F_{tot} = \pm F_m \pm F_h \pm F_v \pm F_{ls} \pm F_{ts} + F_{losses} \qquad \text{Equation (6.8.1)}$$

where

F_{tot} = Total force experienced at a particular foot

F_m = Force due to the mass, normal to walking surface

F_h = Horizontal force, due to longitudinal acceleration in foot trajectory

F_v = Vertical force, due to vertical acceleration in foot trajectory

F_{ls} = Force adjustment due to longitudinal slope

F_{ts} = Force adjustment for walking transversely on a slope

F_{losses} = Force required overcome losses in linkage e.g. link inertia, friction etc

The values of these constituent forces can be evaluated for each crank position, knowing the leg's location and the vehicle's layout and attitude. Once the magnitude and direction of the applied force have been determined, the torque required to turn each leg can be calculated using the method of joints. The total torque required to move the machine will be the sum of the torques applied to each leg. Although the returning legs will require some torque to move them, this will be much less than that required to power the legs that carry weight.

If the two sets of weight bearing legs are numbered set 1 and set 2, then the total torque required to turn all the cranks in the machine when leg set 1 is in service, will be:

$$T_1 = T_{fl1} + T_{fr1} + T_{rl1} + T_{rr1} + T_{ml1} \qquad \text{Equation (6.8.2)}$$

where

T_1 = Total torque required to drive all legs in set 1

T_{f11} = Torque required for front left leg of set 1

T_{fr1} = Torque required for front right leg of set 1

T_{r11} = Torque required for rear left leg of set 1

T_{rr1} = Torque required for rear right leg of set 1

T_{ml1} = Torque required for machine losses in leg set 1, including torque to return leg set 2

If these torque values calculated at each crank position are plotted against crank position, the graph will show a distinct pattern. Figure 48 shows such a torque contribution graph for the prototype octopod walker with the crank turning at 20 rpm.

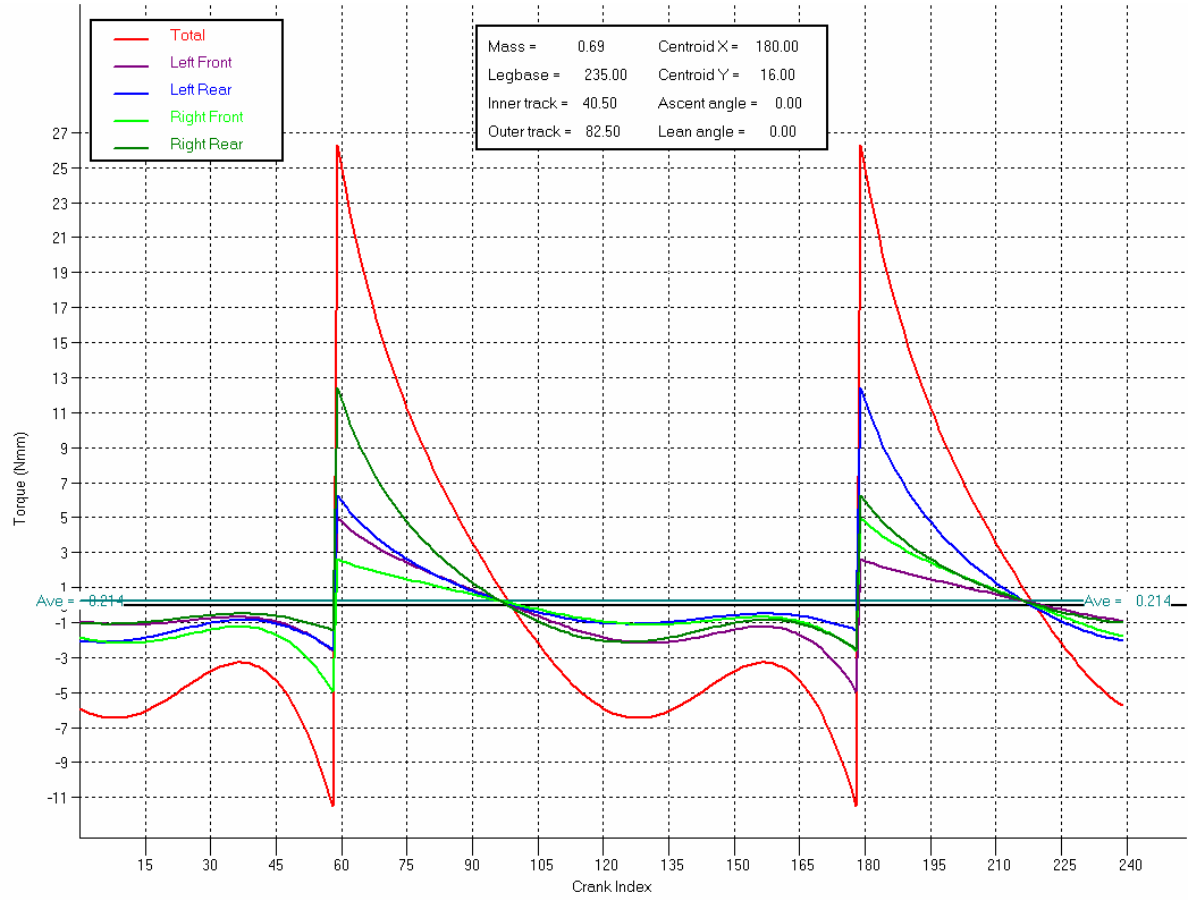

Figure 48. Graph showing torque required to drive legs

In a similar fashion, when the other set of legs, set 2, is on duty, the following expression applies:

$$T_2 = T_{fl2} + T_{fr2} + T_{rl2} + T_{rr2} + T_{ml2} \qquad \text{Equation (6.8.3)}$$

The instantaneous values of T_1 and T_2 will be the same for corresponding crank angles, as the mechanics of the overall machine will be the same. The sets of legs occupy different lateral positions in the body of the machine and so $T_{fl1} \neq T_{fl2}$, $T_{fr1} \neq T_{fr2}$, $T_{rl1} \neq T_{rl2}$ and $T_{rr1} \neq T_{rr2}$ at any instant. This affords a simple way to check whether the above theory is correct. Doing the calculation with a hypothetical vehicle yields curves which exhibit the properties described, demonstrated in Figure 48.

If the inner and outer transverse leg position (the track) and centre of gravity position changes, then a new torque distribution is evident, shown in Figure 49. The total torque required to drive the machine remains the same as for the previous configuration.

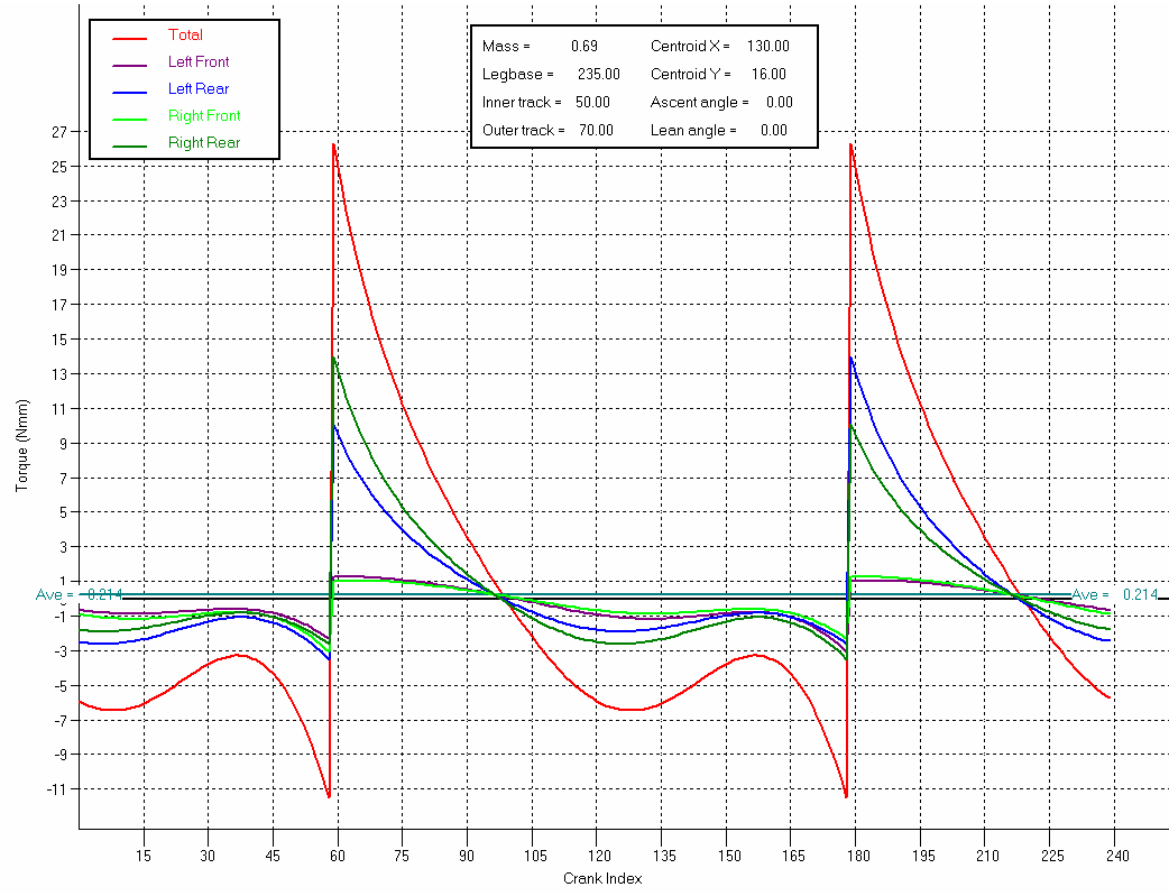

Figure 49. Torque distribution for walker with different track and centroid position

The above curves ignore losses, as no method for calculating friction in the linkage has been implemented. For experimental purposes, losses can be assessed by driving the machine without foot loads i.e. on a stand so that its feet cannot touch the ground. If losses remain constant, then the shape of the curve will remain unaltered, but will be displaced vertically.

We can now evaluate the power required to drive an actual walking machine, as we know from classical mechanics, as shown in [53], that rotational power is given by:

$$P = T \times \omega \qquad \text{Equation (6.8.4)}$$

Where

P = Power in watts

T = Shaft torque in Newton metres

ω = Shaft rotational speed in radians / sec

The graphs in Figure 48 and Figure 49 both demonstrate the low power requirements of walking machine's that use Jansen legs. The average torque required is 0.214 Nmm, which for a machine with cranks turning at 20 rpm (2.04 radians per second) -the actual speed of the slow turning ocotopod prototype - equates to a power consumption of 0.448 milliWatts.

These graphs also show the wide fluctuation in torque requirements. At the start of the cycle, the torque required is at its highest positive value, that is, the motor of the machine is doing work. At around crank index 102, the sense of the torque required changes to a negative value i.e. the motor is now being driven by the leg. This situation continues until the leg reaches the end of its stride, with the leg applying larger torque on the motor toward the end of this period. If it were possible to find a configuration where the total area of positive torque is balanced by this negative torque, then the net torque to drive the machine would be zero. This limiting value is the same as the torque required to drive a wheeled vehicle with no longitudinal acceleration and the absence of friction.

This seemingly counter intuitive aspect of the Jansen mechanism is best understood with the help of the animations of machines walking provided on the CD Rom in the "*Animations\Animations for mechanics chapter*" directory. These demonstrate that the linkage forces applied at the crank resolve with large radial components and relatively small tangential forces. As the bearings at the crank are assumed frictionless, the applied torque is remarkably small.

In reality, several of the assumptions on which these calculations are based will break down. Friction will act to increase the magnitude of all forces. The torque fluctuations will result in the machine being unable to maintain a constant crankshaft rotational speed. The effect of the moment of inertia of the cranks / connecting rod assembly will reduce fluctuations, but in reality the crankshaft rotational speed is likely to vary.

In spite of these limitations, this provides an opportunity to verify this theory. We can measure the power input required to drive a machine. Comparing these measured values to those computed by this method may demonstrate the validity of the model. This subject is dealt with at length in section 8.3 below.

This concludes the theoretical section of this thesis. As design is a merging of theory and practise, it is appropriate to discuss now the various attempts that have been made to convert these theories into practical walking machine.

Chapter 7 Prototypes

7.1 Introduction

The construction of prototypes has been an active part of this research. Their function has been to act both as a verifying but also modifying factor. As the goal of this research is to enumerate theoretical principles of this new type of machine, the prototypes constructed have been extremely useful in pointing out the limitations of existing theories and also in indicating what specific aspects are in need of more development or even a new approach. The theory / prototype interaction is another example of an evolutionary process that is an essential part of the development of any new concept.

The first prototype was constructed in October 2000, soon after the first analytical attempt and shortly after the Jansen leg had been encountered for the first time in June 2000. The first models built were of solitary legs and were used to visually confirm that the computer model was correctly describing the motion of the links. Subsequently a set of these legs were assembled to create the first prototype. This was done in a largely ignorant context and much was learned from this machine. However, this first prototype can in no way be considered a practical walking machine.

The second prototype was constructed in 2002. Although much had been learnt about the Jansen linkage, including most of what was described in the previous dissertation [1], there were still considerable areas where it was too difficult to develop further models without developing visualizations aids that would allow the problems to be understood. Specifically these related to the geometry of turning such a machine and also the packaging of the various subsystems in a practical machine. Although this second prototype had a greater aspiration to being a practical walking machine, it was primarily constructed to facilitate an understanding of how a useful machine may be assembled, what it would look like and how it would operate. Many of the design principles applied in arriving at the final prototype were confirmed by its construction and will be incorporated into future prototypes and also practical machines if these are ever built.

Both of these attempts were made before the academic pursuit of the Jansen mechanism was started in 2004. It was perhaps the failure of these early attempts that lead to a decision to pursue a formal academic analysis of the problem. Some progress has been made in understanding the problem of walking on Jansen legs and it was decided that it would be useful to once more test the accumulated understanding by constructing a new machine. Hopefully, the problem was by now sufficiently understood that it would be possible to build a machine that would actually walk under its own power.

The decision to construct this new prototype was arrived at in a roundabout way. Initially it had been intended to construct an experimental rig consisting of a pair of legs that could run on a treadmill. The experimental rig would have been instrumented and used to experimentally confirm the kinematic and kinetic models developed. One of the more difficult aspects of the experimental design was to develop a method of measuring the torque applied to a rotating shaft without the use of slip rings. These could not be fitted into the confined space of the standard bicycle crankshaft that was to be used to drive the Jansen mechanism. It was decided to use commercially available radio transmitters integrated into process control microprocessors to transmit signals from the rotating shaft to a stationary receiver. Due to the author's lack of skill in constructing electronic hardware the services of a former colleague was solicited to assist in this task. However, this colleague would not accept payment for the work done. The Perspex prototype was originally conceived as a gift that could be given in lieu of compensation, a kind of executive toy.

The technology that had been researched to allow construction of the experimental rig i.e. laser cutting of plane links from sheet material, was adopted to allow the construction of several similar machines. One of these machines could be given away, others used for demonstration. A range of variants could be constructed to explore different aspects of the problem. However it was also likely that these new prototypes would provide additional information.

The following sections provide more detail on the prototypes constructed. They also enumerate the contributions each prototype has made to the theoretical understanding of this new type of walking machine.

7.2 Drinking straw walker

The first models of Jansen linkages were made to demonstrate the operation of the mechanism in an early attempt to validate that the mechanism described superficially in the New Scientist article [29] really would work.

Plastic drinking straws were used as a construction material as they are cheap, have relatively good strength to weight ratio and can withstand loads in both compression and tension. The straws were covered with a paper template that allowed the length of each link to be achieved accurately. These templates were printed out with a laser printer, allowing a theoretical accuracy of 1/600 of an inch for the 600 dpi printer. Initially the base of the machine was a match box, as shown in Figure 50. A handle was provided to allow the crank wheel to be rotated. The node connections were household sewing pins.

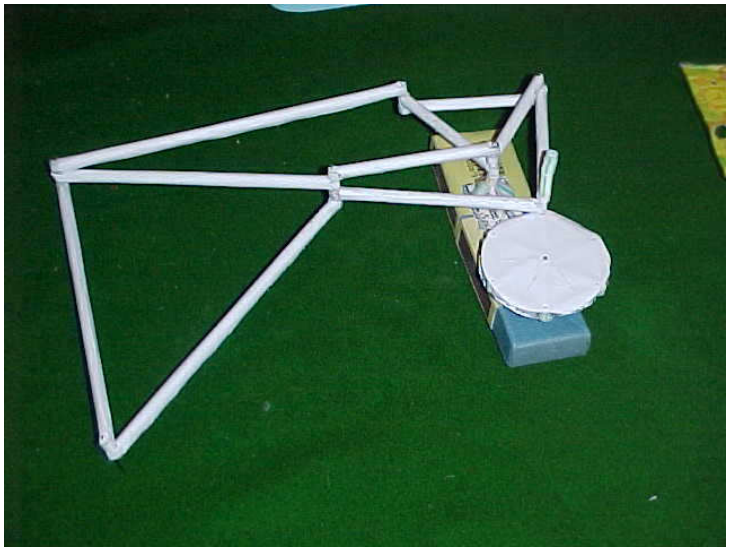

Figure 50. Original prototype of a single leg

Several of these simple prototypes were constructed with various link length configurations. All the configurations tried did provide motion that appeared consistent with the simple animations that were then available in the first software model. The success of these simple straw demonstration models meant that an actual walking machine could be constructed using similar technology. At the time the author had no experience with synthetic walking, and the data available about the details of the Jansen strandbeeste was scant. So the first attempt was to demonstrate that the linkage could be used to power an actual walking machine.

The proportions for the mechanism were not well understood. Although some searching was done, as described in section 4.4 above, no legs that worked better than the Jansen design then available was found. These proportions were obtained by scaling the drawing provided with the original New Scientist article. Although these proportions were presumed to be different from Jansen's actual proportions, the simulation software demonstrated that they could provide a reasonable foot trajectory. Hence the machine was built with the leg proportions shown in the following table.

Link	Dim.
Crank	20
c2p	54
Angle	10°
1	74
2	82
3	60
4	93
5	71
6	89
7	54
8	60
9	60
10	60

Sketch

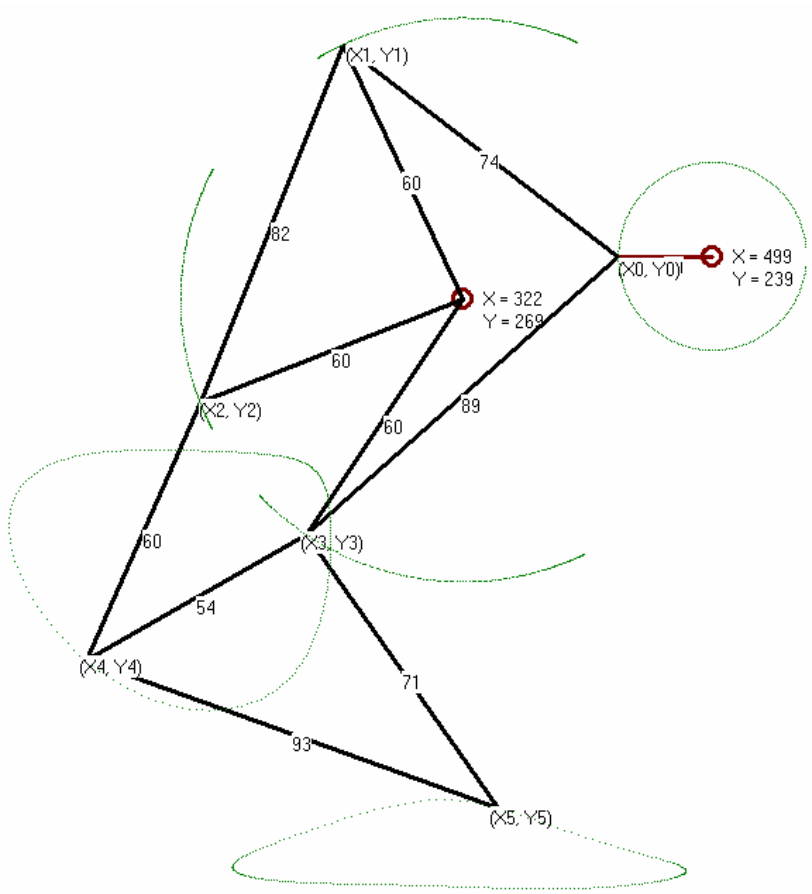

Figure 51. Link lengths and node trajectories for the drinking straw leg

The overall dimensions and specifications for the machine and its legs are shown in the table below.

Mass	0.25	kg
Overall length	600	mm
Width	230	mm
Height	200	mm
Stride length	90.5	mm
Foot lift	18.55	mm
Mechanical advantage	1.44	

The mechanical advantage metric is a simple way of comparing the stride to a wheel of the same size as the crankshaft. Mathematically, this is given by

$$MA = \frac{S_L}{\pi \times r} \qquad \text{Equation (7.2.1)}$$

where

MA = mechanical advantage

S_L = stride length

r = crank radius

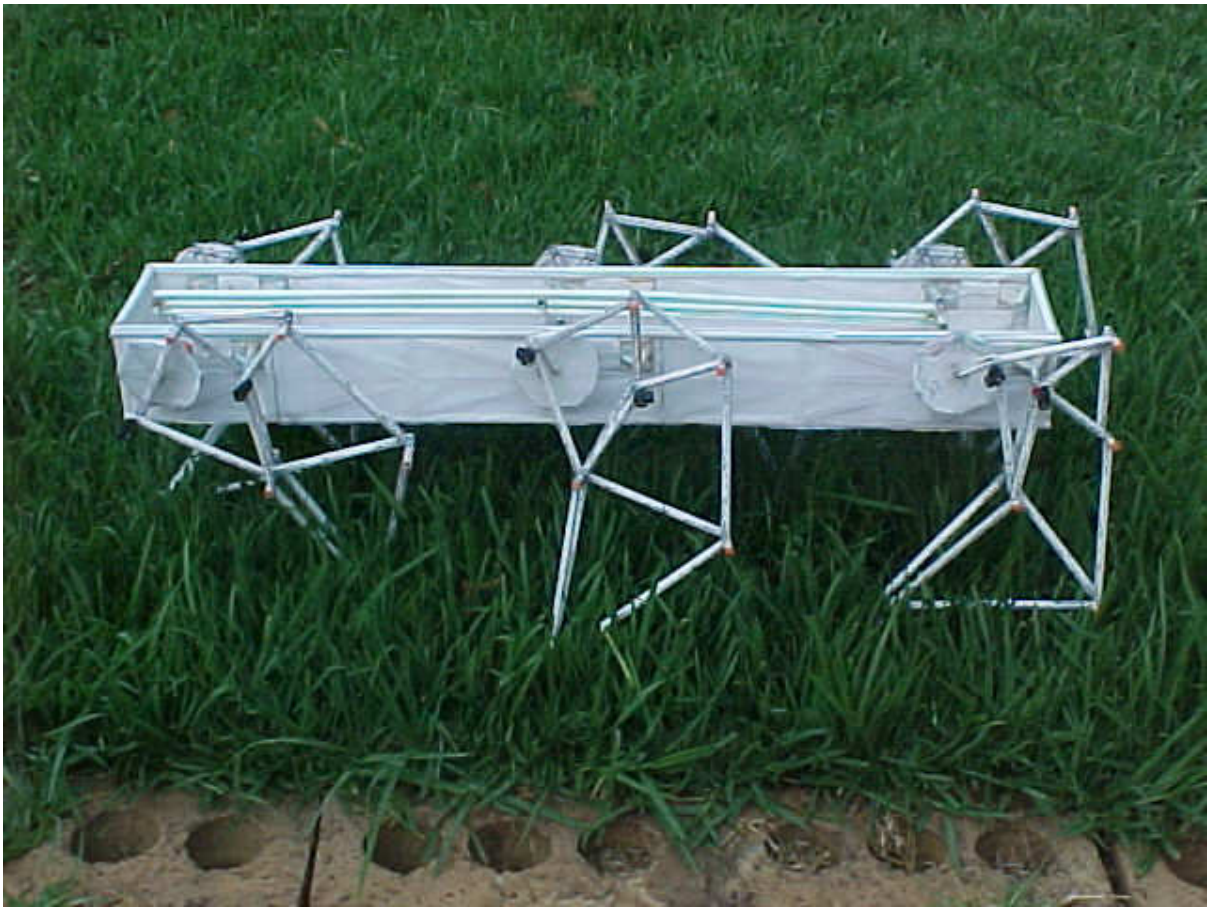

Figure 52. Walker made from drinking straws.

The machine that resulted from this early attempt is shown in Figure 52 above. It was already realised that stability would require at least six legs. Due to the cantilever design of the mechanism used, the legs needed to be mounted on the side of the body. This requirement led to the layout shown, with three legs down each side.

The first version of this walking machine used legs identical to those shown in Figure 50. Although these worked as planar unloaded models, the practical requirements of real legs had not been considered. As this design has essentially zero lateral stiffness, when the newly constructed machine was first placed on its legs, they all collapsed, and the machine fell to the ground like a newly born antelope foal. The first modification required was a redesign of the legs to provide lateral stiffness. This was achieved by doubling the width of the thigh link, link 8, and creating a laterally triangulated lower leg, link 5. This is the configuration shown in the photograph.

Simultaneous drive to the crankshafts was achieved by use of connecting links that connected an additional set of cranks carried in the central tube of the machine. Two of these

connecting links were provided, operating 180 degrees out of phase. This arrangement was not ideal, and suffered from locked regions as the connecting links moved through the horizontal position. No drive mechanism was provided for the machine, and motion was achieved by turning the rear crankshafts by hand. A later attempt to use a suspended weight to provide drive via a planetary gearbox from a redundant dot matrix printer failed, as inadequate gear reduction and insufficient selection of sprockets for the toothed belt final drive prevented the cranks from being turned.

The question of gaits had not been considered at that time, nor had planar stability of the body or the velocity variation of the foot in its stride. In this prototype, the legs were arranged to operate 60 degrees out of phase with each other. The three legs down one side were spaced at 120 degree intervals around the crank circle, as can be seen in the photograph. Those on the other side were also spaced at 120 degree intervals, but 180 degrees out of phase.

This arrangement led to a gait where four legs were usually carrying weight at any time. However, which grouping was active would vary continuously. As the feet were all moving at different speeds, the links were subject to substantial loads as they tried to move the entire body at their own velocity, resisted by other legs attempting to move the vehicle at their speed. The result was that the leg linkages would fail by ripping the pins at joints out of the link termination and the machine was not very durable.

But it walked. Although no records were taken of the achievement, this walking machine was capable of walking on a level flat surface supporting its own weight. It displayed a fair degree of body motion, both longitudinal and transverse. It walked quite slowly and was dependent on the power provided by manually turning the drive system. It could not turn, and would not even walk in a straight line, as the gait arrangement led to a slow weaving from side to side as it moved.

But this confidence that walking could be achieved relatively simply motivated the next attempt. A new machine designed shortly after this drinking straw walker, but not built until two years after that. This inactive reflective period led to several realizations. The second prototype built was an attempt to implement these insights.

7.3 Steel walker

The prospect of designing a machine that could be large and strong enough to carry a human passenger was a major factor motivating the work. It was realized that the geometry of the Jansen mechanism could be scaled to any desired size while retaining proportionate movements.

Limitations that had appeared in the simple drinking straw walker would need to be addressed before a practical person carrier could be contemplated. These included drive arrangement, gait, speed and manoeuvrability. The layout shown schematically in Figure 32 previously was arrived at. In this arrangement, the legs are arranged transversely across the machine. Instead of the out of phase leg movements which had caused stress in the drinking straw walker's links, this new layout had two sets of legs moving in unison, which would eliminate these stresses. Each leg set would provide a triangular support polygon.

This arrangement also reduced the number of crankshafts required to two. These could be driven together using chains and sprockets, which would be easily available for a machine of this scale. Motive power could be provided by a small internal combustion engine, with initial thoughts of using a lawn-mower engine, but later modified to use a motorcycle engine and gearbox unit. The length of the vehicle would also be reduced by use of only two crankshafts.

Informal experimentation with simulations of the mechanism showed that for a specific mechanism, variation in the stride length and foot lift height could be obtained by varying the distance between the crankshaft centre and the fixed pin. It was realized that this would allow a simple way of steering the vehicle, as the inner legs could be arranged to walk a shorter stride than the outer legs. The resultant distorted support polygon was hoped to provide a curved walking path, although this was assumed at that time.

The advantage of this method of stride variation is that it does not require the various leg mechanisms to be driven at different speeds, and so complicated braking and differential drive systems can be avoided. Leg synchronization issues are also eliminated.

The mechanism's variable stride length was used in this design. The crank to pin dimension was designed to vary from approximately 200 to 235 mm. This translates to the stride varying from 805 to 910 mm. The pin movement was achieved by carrying the pin in a secondary linkage that could slide the pin horizontally in a slot in the vehicle's body. The links in the steering system are painted white in Figure 54. It was hoped that the prototype could verify this method of control.

To improve performance in terms of speed of travel, a new leg mechanism proportion was selected, as described previously in section 4.4. The leg proportions were as shown in the table below. As can be seen in Figure 53, this leg design provides a very much longer stride than the previously used mechanism. The trajectory during the walking phase is curved, but this was managed to be no more than 5% of the stride length. This was deemed a reasonable compromise between speed and comfort.

Link	Dim.
Crank	100
c2p	200 - 235
Angle	1.2
1	280
2	200
3	460
4	820
5	750
6	350
7	380
8	270
9	200
10	200

Sketch

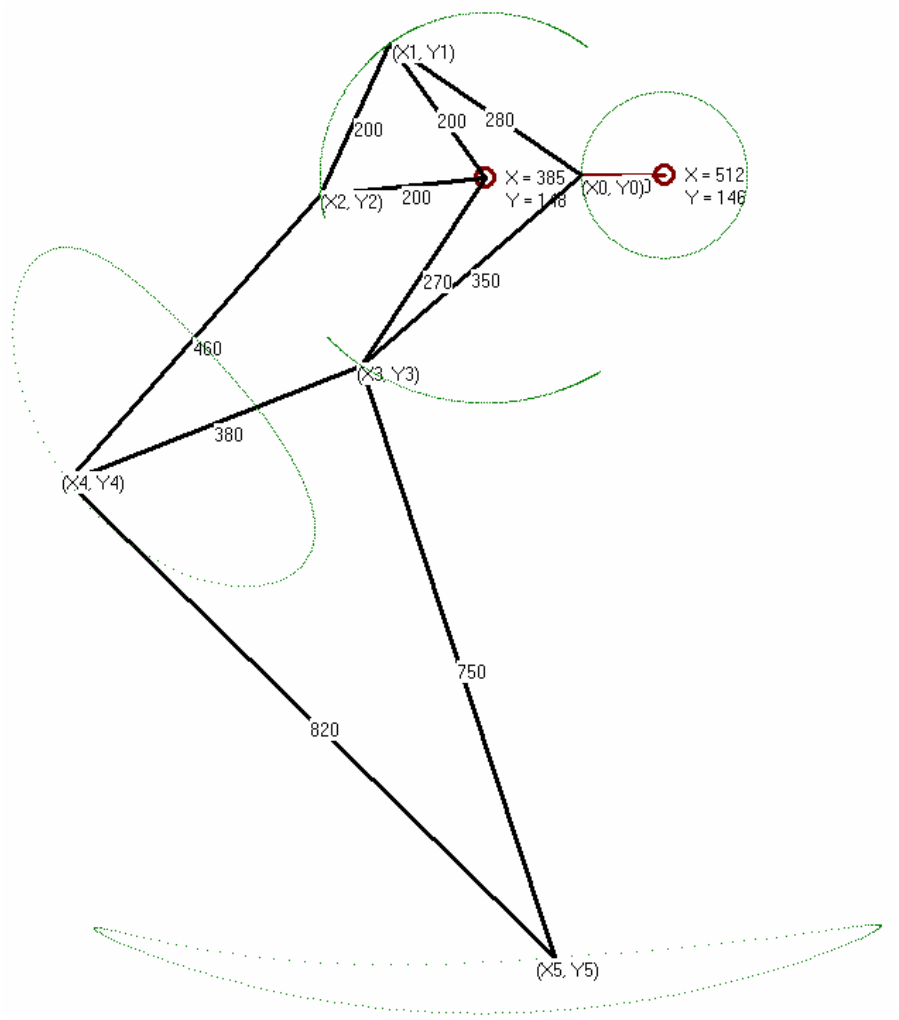

Figure 53. Link lengths and node trajectories for the steel walker's legs.

The vital statistics of the steel prototype are shown in the table below.

Mass	±300	Kg
Length	1800	Mm
Width	700	Mm
Height	1400	Mm
Stride length	805 - 910	Mm
Foot lift	63 - 118	Mm
Mechanical advantage	2.57 – 2.77	

Figure 54. Steel walker prototype

The final steel prototype is shown above. A popular account of the construction and design of this machine is available in [54]. Additional photographs are included on the CD ROM in the "*Photographs\Steel hexapod walker*" directory.

The machine had the following notable features:

1. The crankshafts are chain driven from a layshaft mounted above and behind the engine. Three chains were used, one from the engine to the layshaft, and one to each of the two crankshafts. Chain tension was individually adjustable for each chain, by expanding and contracting the central frame and moving the layshaft and the engine position relative to the rest of the frame.
2. The prime mover is a Kawasaki 200cc motorcycle engine gearbox unit. Both electric and kick starters were retained. The standard motorcycle exhaust was used.
3. Braking was provided by a disc brake, mounted on the layshaft, with a mechanically actuated calliper.
4. Steering was achieved by varying the fixed pin position. The handlebar controls were attached to a reversing linkage that drives the pins in the appropriate direction for turning.
5. The feet incorporate Hooke's joints and vertical springs. The foot pad could rotate relative to the leg. The pad surface was covered with a thin rubber layer for increased grip and to prevent the steel feet from damaging the walking surface.
6. The node pivot pins were made from ¼ inch steel pipe. The crankshaft main shafts and the layshaft were made from ½ inch steel pressure piping; both schedule 40 and schedule 80 pipe were used. The frame and links were made from 25 x 25 square steel tubing, with 1.6 mm wall thickness for most of the construction, but 1.2 mm wall thickness used for the lower part of the legs, to save weight. All links were assembled and welded in jigs to ensure consistency in size.
7. The bearings in the links were made from polyacetate bushes, pressed into the link ends. These bushes were commercially purchased. A grease lubrication system using the hollow pins was provided, with grease nipples in the pivot pins. Pins were drilled radially to ensure grease was supplied to the appropriate place. The node pins were prevented from rotating by grub screws that clamped the pins on one side of the hinge joint
8. The crankshafts were built up, with couplings between throws. The main bearings were also polyacetate bushes pushed in to holes provided in the frame. This construction method was a definite shortfall, and several versions of the crankshafts were constructed, but the final version also proved inadequate. Failure of the rear and imminent failure of the front crankshafts were the problems that prevented the machine from walking under engine power.
9. Construction and assembly took approximately 4 months. Simple tools were used, with a small lathe being the most sophisticated equipment used. Cost of the machine was approximately R10 000, including the scrap motorcycle that donated many parts.

The machine was assembled and could be test run on the stand shown. It was fully operational, and ran several times under engine power in the stand. The mechanism could also be turned manually using a spanner on the engine countershaft sprocket. This was useful to allow both walking of the machine and testing to check for non-collision of moving parts.

The machine was never walked under the engine's power. During testing, one of the feet jammed and locked the position of one of the rear outer legs. The first of the couplings on the rear crankshaft coupling sheared off. The machine was remounted on its stand to repair the damage. During inspection, the other outer rear leg was prevented from moving by the support frame and the other coupling between the throws on the rear crankshaft failed.

In spite of this inability to walk, this prototype was a useful learning experience. Primarily it demonstrated that walking machines with Jansen legs are simple enough to be constructed by single individuals with limited tools. Although Theo Jansen himself had already demonstrated this property of the class, this knowledge clearly had much more personal significance after this construction.

It also highlighted additional pitfalls that would need to be overcome before a further attempt to construct a machine on this scale could be undertaken. Primary of these is crankshaft construction.

In mechanical engineering, crankshaft construction presents a specific set of contradictory requirements. One needs to attach bearings to journals where the bearing cannot be moved along the shaft into place. Thus either the bearings must split, or the crankshaft itself must be disassembled to allow the bearing to be fitted to the various shafts. Either solution is problematic. Split bearings are generally hydrodynamic bearings that require pressurized lubrication. Where the bearing system can be enclosed, as in current internal combustion engine technology, this is a viable solution. One piece crankshafts can be retained for strength, and split bearing provided at the main journals and the crank pin. Over lubrication is contained inside the engine block.

However, this arrangement is unsuitable for a walker with Jansen legs, as the crank must communicate with the rest of the mechanism through the connecting links, link 1 and 6. The motion of these links makes it difficult to conceive of a suitable sealed housing that would contain the lubricant from the bearing while allowing unimpeded link movement. Furthermore, the Jansen mechanism has many other revolute joints that need bearings, and pressurized hydrodynamic lubrication is clearly unsuitable at remote nodes.

The obvious solution would be to use ball or roller bearings at all nodes, including the crank main and eccentric shafts. As standard ball bearings do not split, the joints must be exposed to allow the bearing to be fitted over shafts. Although this prototype used plastic bushes, these were one piece, and so the same principle applied to that machine's crankshafts. Although an attempt was made to construct these parts robustly enough, clearly the design requirements for built up crankshafts had not been fully understood, and the parts failed. Given the space limitations, bearing geometry etc, it does not seem possible to create a stronger part that could be retrofitted.

A second lesson was that the legs were moving too fast. The total final gear ratio was largely dictated by the gearing of the standard Kawasaki engine / gearbox unit. According to the owner's manual [55], the speed range of the crankshafts can be calculated as follows:

Kawasaki Z200 gearing

Reduction stage	***Pinion teeth***	***Gear teeth***	***Ratio***	
Primary	21	69	3.286	
1st gear	11	29	2.636	
5th gear	19	21	1.105	
Countershaft to layshaft	15	40	2.667	
Layshaft to crank	17	38	2.235	
	1st gear	Min total gear ratio	51.634	
Idle revs	Min	1150	22.272	rpm
	Max	1350	26.145	rpm
	5th gear	Max total gear ratio	21.647	
Max revs		8000	369.565	rpm

So although the minimum crankshaft speed was approximately 25 rpm, this was subjectively too fast. The vehicle could not be made to start off from a standing start under its own power. Future prototypes would need even greater gear reduction than that provided for this machine.

The third lesson was stability. In the simple walking that was done, under the power of the manually turned spanner on the countershaft sprocket, it was clear that the machine was somewhat unstable, and that surface imperfections could easily cause it to stumble. The flexible feet also contributed to this feeling, as friction in the foot pivot joints meant that they would not easily return to a horizontal position. Springs were later added to control the foot orientation, but this was not completely successful.

The fourth lesson was the degree of lift of the vehicle body as the machine walked. Although this had been considered at the design stage, it had not been realized what a large factor this would be in a physical machine. The additional torque required to lift the machine at the start of the walking cycle was made tangible in this prototype. It was evident that a flatter body trajectory would be desirable in future machines.

Although one of the primary goals of the construction of this prototype had been to establish whether the machine could be steered by varying the stride length, this could not really be established due to the machine's failure to walk. Preliminary results from turning the machine over by hand with the pivot points moved showed that the machine would change course, but also that the legs were subject to considerable lateral force when moving in this state.

The final lesson from this prototype was that insufficient was known about the forces and stresses involved in walking. The machine had been constructed with a hobbyist approach, the primary goal being to build it. The fact that it was then not suitable for use was a humbling experience, which motivated the more academic approach that has been adopted subsequently.

7.4 Perspex walker

Both of the prototypes described above were hexapods. In these earlier designs the desire for simplicity had dictated that the minimum number of legs be used, that is, six. At the time that these machines were designed, walking dynamics had not been considered in any more than an intuitive way. Although the dynamics issues had still not been formally analysed by the time of the design of this new Perspex octopod, it was already clear that, in spite of apparent complexity (by virtue of the additional two legs), the additional stability afforded by these extra legs was desirable.

The steel walker had also demonstrated that the considerable effort required to make full scale machines was largely wasted. Development was evidently insufficiently advanced for it to be likely that a successful large machine could be constructed yet. Hence it was decided to build a small machine, similar in size to the straw walker.

The new walker was designed using a commercial three dimensional solid modelling package - SolidWorks. Drawings for the previous two prototypes had been produced by extending the analysis software. The use of modelling software enabled the construction method for the new prototype as it could produce industry standard CAD exchange files (DXF files). These files could be sent to commercial laser or water jet cutting companies who could then produce parts. It was decided that a plastic material should be used, as this was deemed strong enough while being lightweight and relatively cheap. After initially investigating ABS plastic, Perspex material was chosen, largely because it was readily available in the thickness required.

The proportions for the new machine's leg had been selected by the genetic algorithm, as discussed in section 5.4. The dimensions of the leg and of the overall machine are shown in the following two tables.

Link	Dim.
Crank	25
c2p	69
Angle	11.6
1	91
2	79
3	92
4	115
5	67
6	103
7	79
8	66
9	65
10	97

Sketch

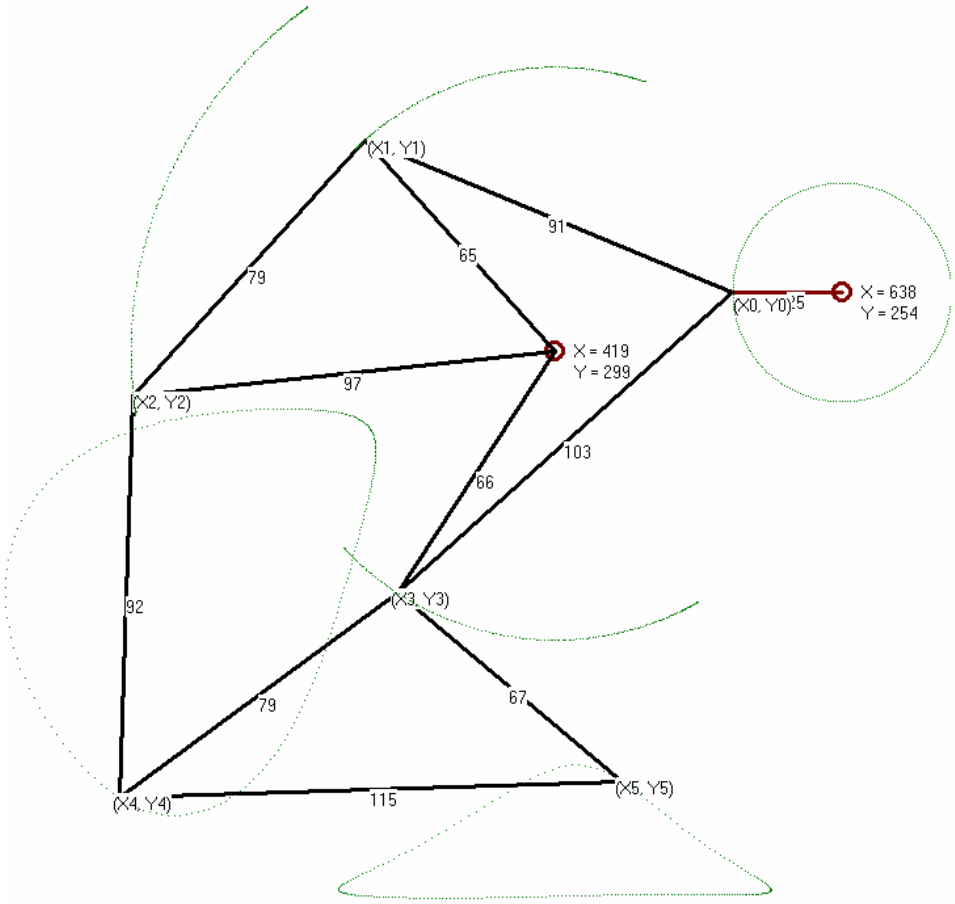

Figure 55. Linkage proportions for perspex octopod walker

The vital statistics of this prototype are shown in the table below.

Mass	0.7	Kg
Length	500	mm
Width	250	mm
Height	220	mm
Stride length	92	mm
Foot lift	30.35	mm
Mechanical advantage	1.17	

The first design attempt is shown in Figure 56. The concept was to use a series of identical frame plates that would be held parallel to each other with a series of through bolts with spacers. It has eight legs, with a gait based on the hexapod's gait, with the inner two legs operating together, and the outer sets operating as a set.

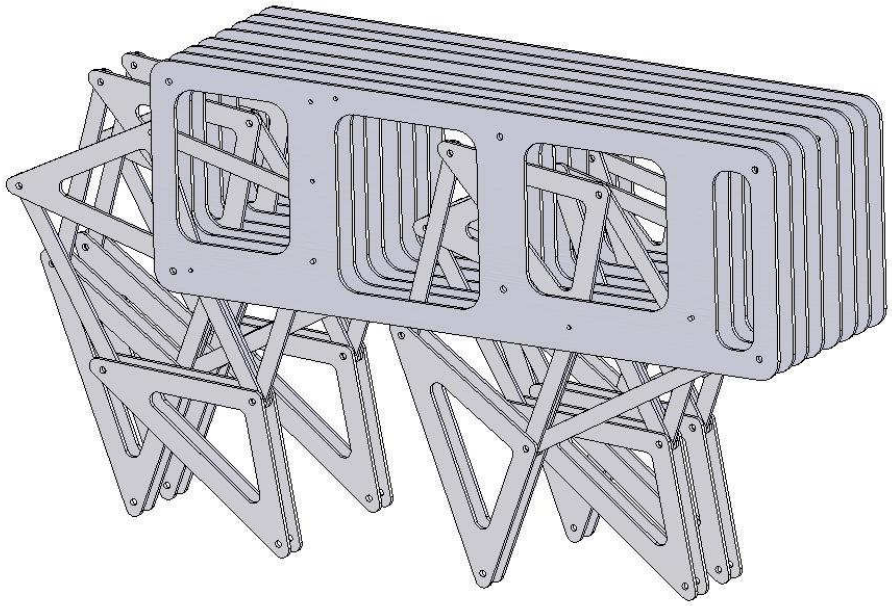

Figure 56. Initial concept for plastic prototype

This concept was deemed impractical. There was no space to fit a drive system and it would have been heavy. The crankshaft details were not finalised, but in the layout shown, a built up crankshaft would have been required. Previous experience on the steel hexapod made this feature unattractive. Aesthetically it resembled a group of cylinder head gaskets, which was also considered unattractive. The triangular ternary links were also undesirable as they contribute a significant portion of the material used for the legs, much of which is in the central “hole” and is cut out and discarded. It was thought possible to create a link design that would use less material.

The concept of using a series of parallel frame plates was considered a good one. This type of machine construction has been used in mechanical clocks for centuries and has many advantages. The frame plates are flat and can be cheaply cut from sheet material. They are all identical, which ensures lateral co-linearity of shaft centre holes and also makes the design cheaper to implement. Tubular spacers with a central through bolt makes for a sturdy, simple chassis that could be disassembled.

The second design attempt is shown in Figure 57. This evolution of the design incorporates one piece crank shafts. These were bent from 3mm diameter steel wire. The frame plates have slots into which the crankshaft fits. The shaft is retained in the slot with an “L” shaped retainer which is glued into the frame plate on assembly. The links that attach to the crankshaft have a removable central portion, allowing them to be threaded onto the crank. Once in place, the central link portion is inserted and retained in position with adhesive.

The front and rear crankshafts are coupled with connecting links, as used in the drinking straw walker. Although problems with the connecting links becoming locked had been anticipated, it was considered too difficult to bend the wire crankshafts in a three dimensional form so that orthogonal connecting links could be arranged. It was hoped that the combination of rotational inertia and the longitudinal inertia of walking would be sufficient to carry the connecting links through their locked angles. The first prototype assembled had only two connecting links, as shown in the figure, but this did suffer from locking. Subsequent machines had extension fitted to the crankshafts that carried additional connecting links, arranged 90° out of phase with the existing connecting links. The front view of the left hand walker in Figure 58 shows this arrangement clearly. This arrangement eliminated locking, and the two crankshafts rotate synchronously, though this connecting mechanism has introduced additional friction into the mechanism.

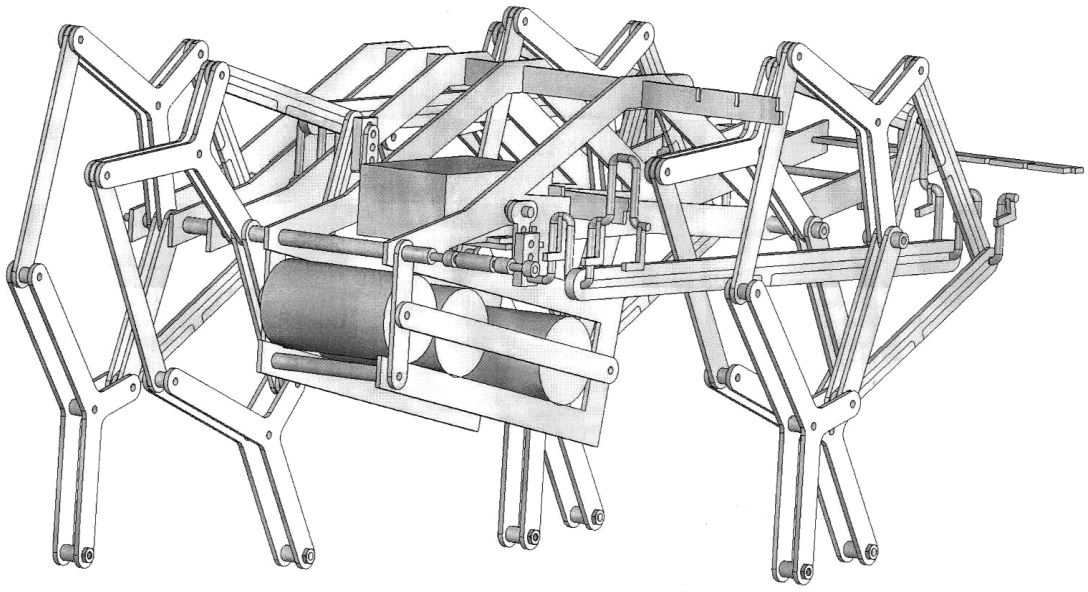

Figure 57. Final design with frame plates removed to show the one piece crankshafts.

Crankshaft construction proved difficult. The first hand made jig proved inadequate. Subsequently a jig plate with removable jig blocks was laser cut. This solved the crankshaft bending problem, and twelve crankshafts have been bent. The wire is bent hot, and making crankshafts is one of the most difficult aspects of building new prototypes. However, no problems have been experienced with the crankshafts in these Perspex walkers, so this design feature of one piece crankshafts should be retained in future walkers.

The gait used by this machine is different from any used previously. The legs on each crankshaft are arranged to move in pairs, with leg 1 and 3 moving together and legs 2 and 4 in phase. The second crankshaft has the same general arrangement, but 180° out of phase

with the first, so that when leg 1 of crank 1 is lifted, leg 1 of crank 2 is in walking mode. This arrangement provides a support quadrilateral for the machine which is trapezoidal in shape. The reason this gait was selected was intuitive and the same basic machine could be assembled to use different gaits, if a suitable crankshaft is provided. Although all three of the machines built so far use this gait, it is unlikely that the two future ones will. This is discussed further in the next section.

Lateral position of the frame plates is maintained at three points – at the front by a through bolt and spacer arrangement, which also serves as the fixed pin for the front legs. Above the motor, and at the rear of the machine, the frame plates are held with connecting strips that have slots that mate with corresponding slots in the frame plates. The frame plates themselves have been much reduced in size. The triangular ternary links have been replaced with “Y” shaped pieces.

The pins at the joints were M3 machine screws with nuts. M3 flat washers were inserted to space the links laterally. Where necessary, links were doubled, to ensure correct pin support at each node. Lateral stability of the entire leg is ensured by the doubling up of the “thigh” and “calf” links.

The drive system is a Tamiya “6-speed gearbox”, which was purchased from a hobby shop. This motor /gearbox unit can be assembled with differing gear ratios. The design of the walker allowed the motor to be used in two different gearing configurations, which would yield a slow walker, geared to turn at 19 rpm, and a fast walker, where the cranks turn at 54 rpm. Tamiya also produce a “twin motor gearbox”, which has two independent motors with gearing. The design was adaptable, allowing for the different width of this drive unit. The resultant lateral displacement of the frame plates was accommodated with a new motor mounting plate and new connector strips.

Initially the motor’s electric requirements were not known, so provision was made for the vehicle to carry four batteries, three of which are shown in Figure 57, slung below the motor. These could supply up to 6 Volts DC. Subsequently it was discovered that the motor only required 3 V DC, and power was supplied using a wire to a remote battery container with switch, an adapted torch. The original idea of placing a switch on the machine was discarded; this would mean that controls for the machine would move with it, which was considered impractical and un-ergonomic.

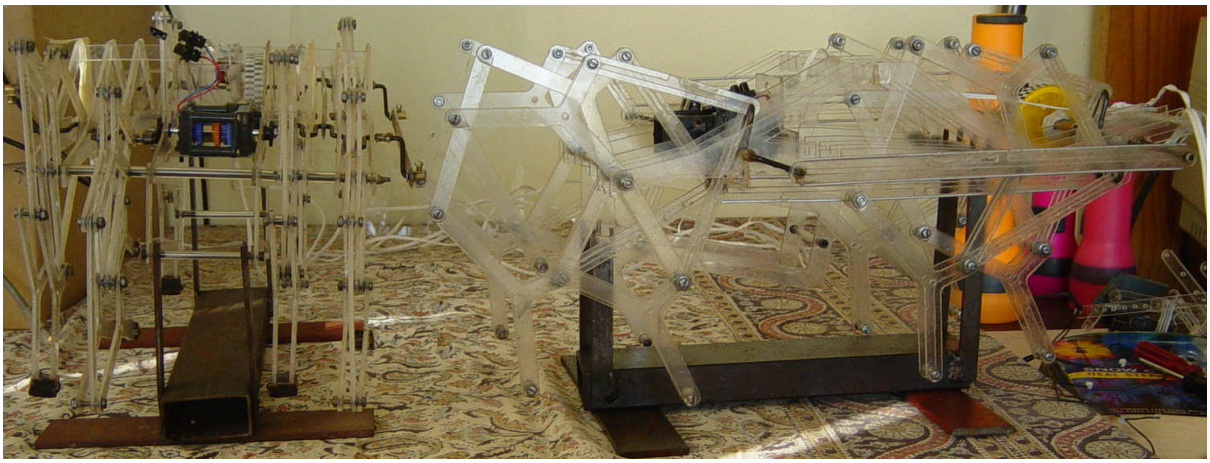

Figure 58. Two perspex octopod walker prototypes

With the design finalised, sufficient parts for an initial group of four machines were laser cut from 2mm thick Perspex sheet. Three machines have been assembled. Walker 1, a slow walker, suffers from connecting link locking. An ad-hoc addition of a single additional orthogonal connecting link enables the machine to walk, but the mechanism is rough in operation. The second machine, also a slow walker, has two additional orthogonal connecting links, and the mechanism operates much more smoothly. It does feel “tight” when turned by hand, and this is probably due to the four connecting links running slightly out of phase. The third prototype, assembled with a faster turning drive, is the best assembled of the machines built thus far. It turns very smoothly, and presents the lowest friction, as is demonstrated in section 8.3 later. Additional care was taken in the attachment of the crank extensions, with a special jig built for assembly of this machine’s cranks, and the result is evident in the machine’s performance.

One unanticipated problem is that the laser cut parts have distorted due to the heat of the laser cutting. None of the “flat” parts are plane, and all exhibit a curvature, presumably having bent away from the cutting table on cooling. Although intelligent assembly was attempted to select mating parts with opposing curvature, this was not always possible. One of the main effects has been that the rear legs do not all run true in the bays between frame plates. Some legs are so distorted that the joint at nodes 2 and 3 actually fouled on the adjacent frame plate.

The replacement of the machine screws with countersunk machine screws allows the node joint to be laterally much flatter, and this solution, along with judicious placement of masking tape, prevents the link from jamming. One unnoticed link to frame jamming event lead to shearing off of the plastic motor to crank connector pieces, and these had to be replaced. Although the machines are glued together, some disassembly is possible, fortunately.

Parts for a single machine, subsequently ordered separately, were cut with water jets, cold. These parts do not suffer from distortion, and although the machine has not yet been assembled, the problems with distorted parts are not expected in this machine.

All three machine walk successfully on level surfaces such as floors or boards. A selection of video clips of the various machines walking in various circumstances is available on the CD ROM in the "*Photographs\Perspex octopod walker\movies*" directory. All three machines have proved durable, and the two later machines have been used for much of the experimental work described in Chapter 8.

A fair amount of informal testing has taken place. The fast machine has been equipped with sandpaper "shoes" on its feet, to enhance friction, and can successfully climb slopes up to 33°. The machines walk over grass reasonably well, although the grass plants and the gaps between them are relatively large on the scale of the machine. One definite problem is the approach angle of these machines, which limits their off road capability. The forward "knee" at node 4 follows a trajectory that brings it far forward while low to the ground, and this knee impacts on approaching steep inclines. Minor impediments, lower than the foot lift height, such as a thin book or a stack or papers placed in the machines path, are usually negotiated without problems. A larger scale machine promises to have very good off road performance.

7.5 Future prototypes

Sufficient parts have been made to allow five Perspex prototypes to be constructed. Only three have so far been built. As part of ongoing research, these two additional machines will be assembled in different configurations.

The first new configuration planned is a steerable machine. This will incorporate a twin motor gearbox. A suitable variable speed control has been sourced to allow the machine to drive the legs on the left side at a different speed from the right hand legs. It is hoped that this speed differential will allow the machine to be steered. Although preliminary work has been done on steering of these walkers, this is not sufficiently complete to be included in this thesis. It will need to become part of post doctoral research. Particular issues concerning lateral loads on the legs and the vehicle chassis and leg synchronization need to be addressed before this machine can be constructed. Current thinking is that it may be advantageous to incorporate designed lateral flexibility into some links, to enable steering. These innovations would also be included in the prospective steerable walker.

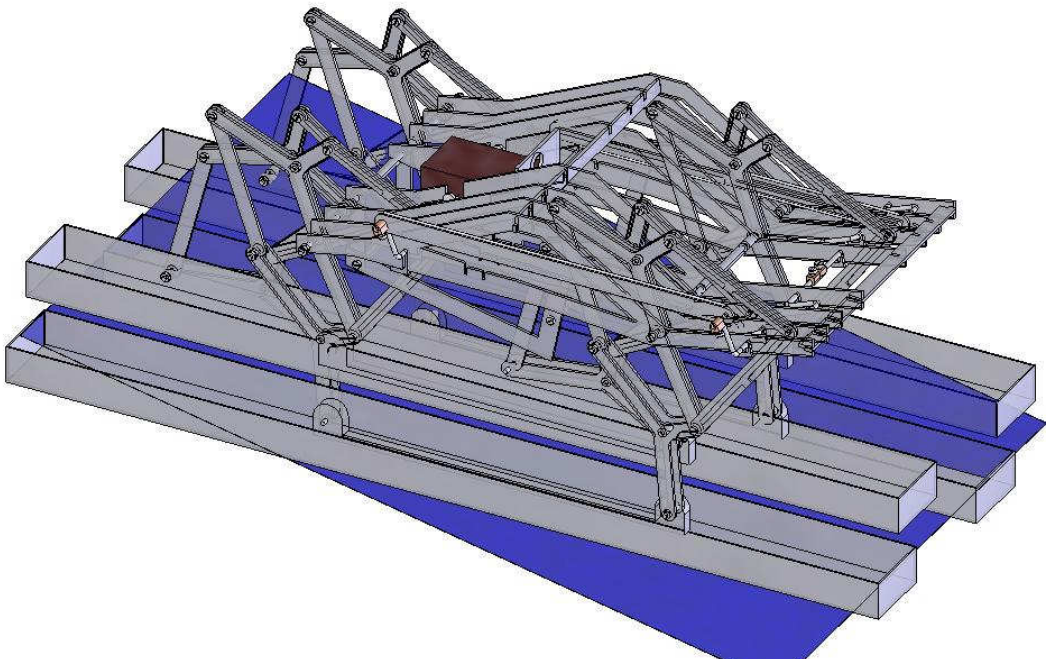

Figure 59. Perspex prototype with floats for amphibious operation.

The second new prototype will walk on floats, as shown in Figure 59. As mentioned previously, it is possible that walking machines may be able to walk on the surface of water. This rare phenomenon is achieved by some lizard and insect species, although these

animals use surface tension and not Archimedes principle to support their weight when walking on water.

No record can be found of any previous machine that can successfully walk on water. Previous walking machines would be far too heavy and dense to achieve this. The simplicity of the Jansen linkage, and consequent light weight, makes this possible for the first time.

Considering this Perspex prototype, it weighs approximately 700 grams. A float to support it would need to displace 700 cc of water, by Archimedes principle. The floats shown in Figure 59 are approximately 60 cm long by 7 cm wide, giving an area of 420 cm^2. The two floats that support the vehicle at all times give a total area of 840 cm^2, which means these floats would sink to an average depth of 700 /820 = 0.85 cm = 8.5 mm when supporting the machines weight. If the floats themselves can be made to weigh less than 120 grams in total, then the sinking could be limited to 10 mm. Given that mechanism lifts its foot up to a maximum height of 30 mm, and the lift is greater than 10 mm for a large portion of the return cycle, this machine should be able to lift the returning set of floats clear of the water's surface. Hence locomotion by walking on water could be achieved.

The intended final walking machine will be much larger than these prototypes. It is also intended to build at least one additional larger prototype, able to carry perhaps two passengers. This machine would need to provide the intended functionality of the steel prototype, but do it successfully. It is anticipated that such a machine may not be constructed for some time.

Chapter 8 Validation of analytic models

8.1 Introduction.

The final aspect of the work completed for this thesis is the validation of the models developed in previous sections and also in the previous dissertation [1]. Initially it was intended to construct a purpose built laboratory test rig, as illustrated in Figure 60 and Figure 61. This rig would walk on a treadmill and would be suitably instrumented so various parameters could be measured. Displacement information was to be captured with variable resistance devices, while torque was to be measured on the rig's crankshaft. As previously mentioned, this torque measurement presented something of a problem.

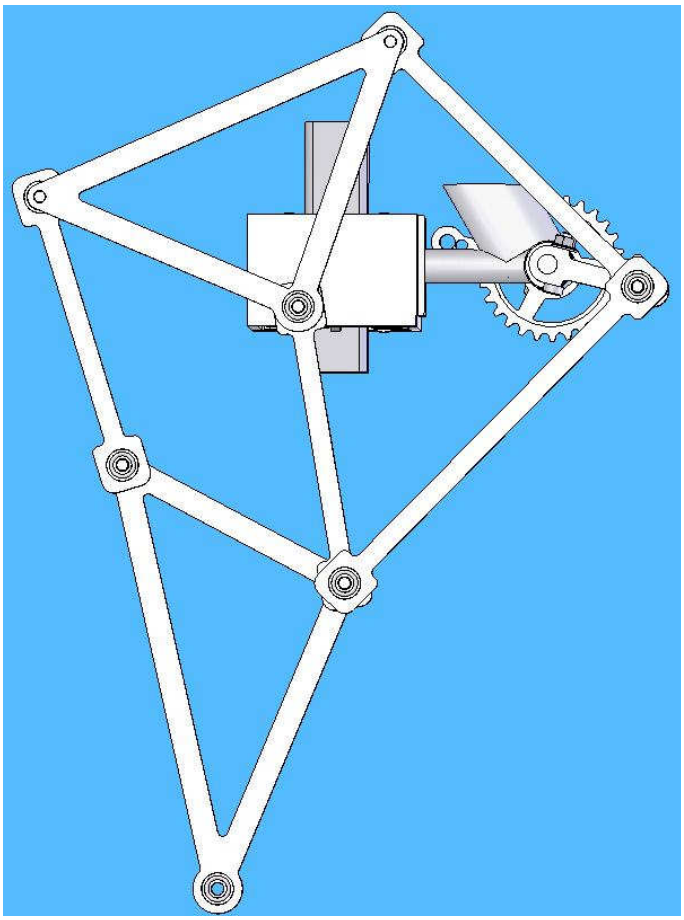

Figure 60. Side view of experimental test rig.

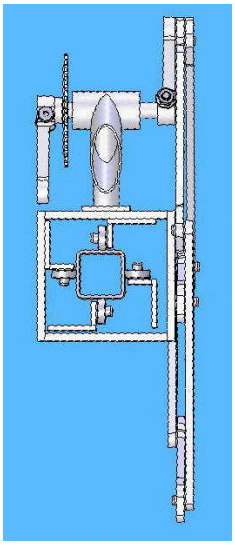

Figure 61. Top view of experimental rig

In the process of developing this rig, it was decided to proceed with a simple plastic prototype, as discussed prior in section 7.1. Although the construction of these prototypes took some time, the development of the electronics required for the test rig appeared to be taken even longer. The availability of the new prototype and the machine's evident ability to

walk initiated an alternative approach to validating the models. Thus work on the experimental test rig was abandoned, and the Perspex octopod prototype walkers were then equipped with simple instrumentation. This strategy proved fruitful, as discussed in the following sections.

8.2 Validation of kinematic analysis

8.2.1 Method

To demonstrate the validity of the kinematic model, it was necessary to establish the relationship between the crankshafts angular position and the horizontal or vertical movement of the walker body. Although some ways of determining the vertical movement of the body were considered, such as by using accelerometers, it was realized that this would be difficult. The mechanism had been specifically selected to have limited vertical movement and so small dimensions would have to be resolved, requiring greater accuracy in instrumentation. Furthermore, if the horizontal velocity of the machine could be confirmed, the vertical motion would also be confirmed. Effectively this meant determining the horizontal velocity of the machine and the rotational speed of the crankshaft.

A PC web camera was used as a type of stroboscope. The camera could film a calibrated degree wheel attached to the crank and the different angular positions recorded in each frame could be resolved to an angular velocity, if the video frame rate was known. Similarly, if the camera recorded the distance walked, the same logic could be used to calculate the walking speed of the walking machine.

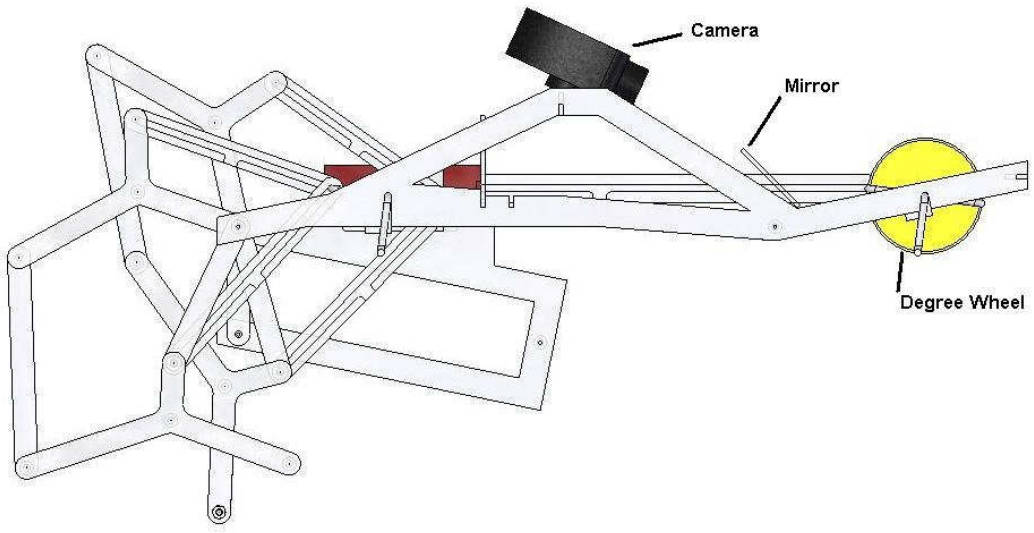

Figure 62. Experimental setup for kinematic validation

Figure 62 shows how a camera, a mirror and a degree wheel were attached to the machine. The mirror was placed so that the ground below the machine appeared in each frame. When a tape measure was placed on the ground, the camera gave an image such as those shown in Figure 63 and Figure 64. As can be seen, each subsequent frame of the video captures the machine's state at that time.

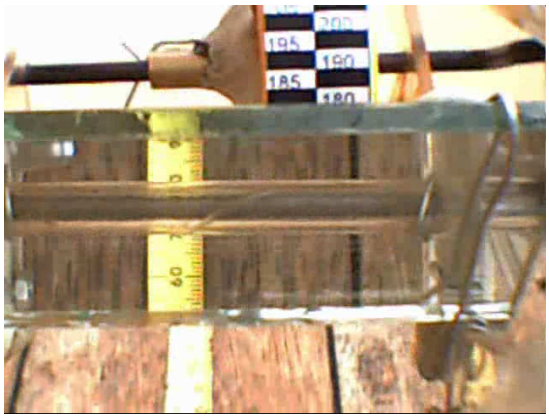

Figure 63. A still picture from a video of walking on a tape measure.

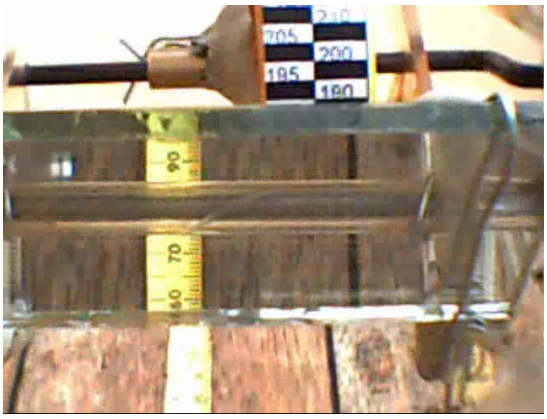

Figure 64. The frame after the one on the left.

To use this technique to directly measure rates of change, the frame rate of the video needs to be determined. Although the low cost web camera specification lists the frame rate as 15 frames per second at the resolution used (640 x 480 pixels), it was known from previous experience that his would be a nominal figure. It would be necessary to calibrate the frame rate of the camera against some reference before the videos could be confidently interpreted.

To calibrate the camera, a video was taken of a computer screen which was running a timer program. The timer program would display the computer time, and the camera would film the display. As the computer was displaying a new time every 10 milliseconds, it was possible to record the times of subsequent frames, which would be captured approximately every 67 milliseconds. The details of these calibrations are available on the CD ROM in the "*Experiments\Web cam Calibration*" directory.

The result of this calibration was that it was established that although the camera would shoot on average 15 frames in every second, it was not certain that the time between frames would be a constant 67 milliseconds. The actual time difference between frames was unpredictable, and appeared to depend on the available processor time slice available on the PC to which the camera was connected. So the plan to use the camera as a stroboscope would have limited ability to read velocities directly.

The camera timing was considered reliable enough to measure the rotational speed of the crankshaft. This would give an overall sense of the mechanism's operation. From the initial videos taken, it was clear that the angular speed of the crankshaft was more or less constant. This confirmation is available in the spreadsheets in the "*Experiments\kinematics\crankshaft rotational speed*" directory on the CD ROM.

It was realised that once the constant speed of the crankshaft had been confirmed, the time dimension could be dispensed with, and the horizontal movement of the machine could be correlated with the change in angular position between two frames. As the crank angle rotated through is constant for each time slice of the computer model, the calculated horizontal movement per degree of crank rotation could be plotted against the crank angle as shown in Figure 65. As this curve has a distinct profile for each leg proportion, if this profile was also found in the experimental data, the model would be confirmed.

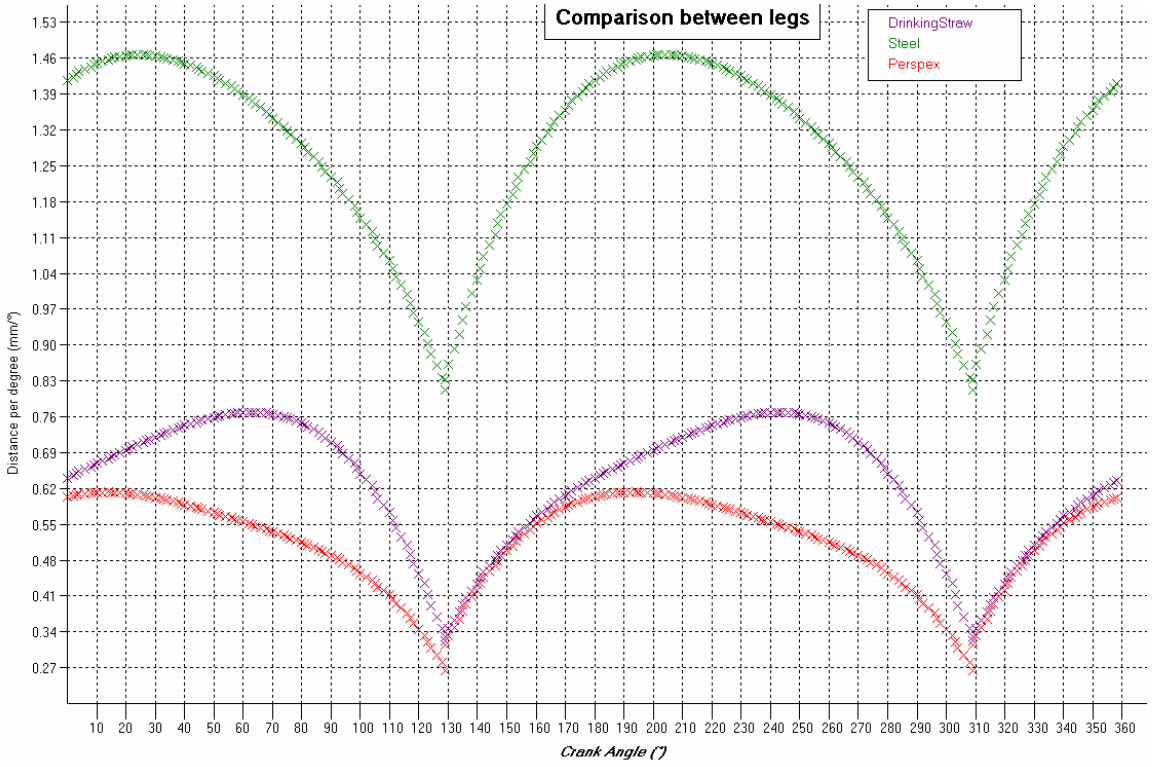

Figure 65. Graph showing characteristic velocity profiles of different leg proportions.

The interpretation of the videos resulted in a data set consisting of a horizontal (tape) position, X_i, and an angular (degree wheel) measurement, θ_i. For each frame subsequent to the first frame, the distance walked (δX) and angle turned ($\delta\theta$) was computed thus:

$$\delta X = X_i - X_{i-1} \qquad \text{Equation (8.2.1)}$$

$$\delta\theta = \theta_i - \theta_{i-1} \qquad \text{Equation (8.2.2)}$$

The two parameters are combined to give the distance walked per degree of crank rotation (*dW*). This is the ordinate plotted against the angular position in the graphs shown later. Mathematically, *dW* is given by:

$$dW = \frac{\delta X}{\delta\theta} = \frac{X_i - X_{i-1}}{\theta_i - \theta_{i-1}} \qquad \text{Equation (8.2.3)}$$

This parameter is unaffected by time, and the graphs shown in Figure 65 are independent of rotational speed of the mechanism's crankshaft. Measurements from both the slow and the fast versions of the Perspex prototype should produce plots of exactly the same form, as they have the same link geometry, and in spite of the fact that they move at different speeds.

The accumulation of data was done by stepping through the videos, one frame at a time. This process was laborious, tedious and also suffered from limited accuracy. As each frame had to be interpreted visually, it was only possible to resolve measurements of approximately 1 degree for the degree wheel, and 2 mm on the tape measure. As the video clips were of approximately 20 seconds duration, each experiment involved the interpretation of at least 300 images. This process could take eight hours of manual processing.

All three of the Perspex walker prototypes were equipped with cameras, mirrors and degree wheels so that this experiment could be run using all of them. The first two experiments were run using machine 1 and the fast machine. These videos were interpreted by manually single stepping through each frame and visually extracting the data directly to a spreadsheet. Although the data captured appeared to confirm the theory, wide variance in results was noted. It was felt that this variance may be reduced by increasing the precision of measurements.

To increase precision of readings, it was decided to write software that would interpret the video frames. This would have the additional benefits of reducing the time required to interpret movies and relieving the tedium of visually interpreting results. This software is described in more detail in the "*Image**Software**image Reader*" directory on the CD ROM.

The software worked by attempting to match portions of the bitmaps of each frame, thus attempting to find a correspondence between contiguous frames. It also maintained the reference position in the frame from which measurements were taken. Being able to resolve detail to a single pixel meant that this software was capable of interpreting videos to a precision of 0.25 degrees of rotation and 0.25 mm of horizontal movement, approximately 4 times finer than could be achieved visually. The reliability of interpretation could also be expected to increase with use of machine interpretation.

In later experiments, an attempt was made to establish the time of each frame. This was achieved by including a stopwatch in the field of view of the camera, as shown in Figure 66. A series of experimental walks were conducted with the stopwatch running. However this was of limited success, providing no more accuracy than that inherent in the use of a video camera. This was due to the slow update time of LCD display of the digital stopwatch. Although changes of 0.1 second could be seen, it was not usually possible to resolve the value of the 0.01 second display digit. Images from the video would capture the segmental display in transition; with all segments either in the process of being switched on or off, and the actual state of segments could not be determined.

Figure 66. Stopwatch added to instrumentation.

Figure 67. Still frame with stopwatch in field of view.

Figure 67 shows a display from the image processing software. The lines added near the tape and the degree scales are inserted by the software. This particular frame shows the machine's horizontal position to be 1135.75 mm at a crank angle of 353.50 degrees. These measurements are taken relative to a constant position in each frame. These results were found by the software itself, and demonstrate the additional precision made possible by the interpretation software.

Note that the degree wheel is shown on the left of the camera in Figure 66, but appears on the right hand side of Figure 67. Notice also that the stopwatch display in Figure 67 is laterally inverted. The reason for this is that the web camera image capture software has laterally inverted the captured image. This was necessary to ensure that the image of the tape measure, which is viewed through the mirror, and thus inverted by it, would be readable when doing manual interpretation. The calibration for the degree wheel was printed on a laser printer, and this scale was printed laterally inverted. Figure 67 results when the video capture software inverts the image. Both the tape calibration and the degree wheel are normally readable, but the watch display is now inverted.

Figure 68. Image processed by video interpretation software.

Figure 68 shows more of the display of the image interpretation software when processing the same frame as in Figure 67 previously. The above figure shows how the reading from the stopwatch has been laterally inverted by the software. The lower portion of the display shows how the current frame is linked to the previous frame. For both the tape and degree readings, the software attempts to match markings on the scales from the previous frame with those on the current frame. Using a combination of this match and scanning for horizontal colour changes, the calibrations and values on each scale could be determined.

The stopwatch reading mechanism differed slightly. To decipher the time value in each frame, the inverted segmental display was compared to a mask which attempted to determine which of the segments were on and which were off. Once the segment pattern was determined, a lookup function would yield the numeric value of each digit, if the pattern could be recognized.

The figure illustrates the problem with reading the least significant digit of the stopwatch display, the “9” on the right. When viewed in the context of the previous and subsequent frames, the time for this frame could not be 27.29, and is in fact taken as 27.23. The camera has captured the LCD display in the process of updating. In this image, the display is either changing from 3 to 4 or from 4 to 5, and it is not possible to distinguish which. Any interpreting software would read this digit as a 9.

The net result was that the use of a clock in the display was of limited value, and forced a reversion to a situation where each video had to be manually interpreted, frame by frame. For videos without clock display, about 75% of frames could be interpreted by the software unaided, and a typical video of 400 frames could be interpreted in less than an hour. Interpretation was still somewhat interactive, as minor adjustments were necessary as the degree wheel did not run entirely true on its shaft. Although the tests were conducted with the machine walking between guide rails on a track, it would never walk entirely straight, and the tape measure would wander in the video images. Adjustments to the software were necessary to allow for these minor differences between frames.

The final stage of experimentation was accumulation of data and graphing. Manually interpreted software had captured the data into spreadsheet files. The interpretation software created a comma separated text file containing its values. These raw data could be plotted on a graph. This showed a large amount of scatter of data points. To make sense of the data, it was averaged, with readings in a band of angular positions being accumulated and averaged. Outlying points were discarded if they differed from the expected value by more than 100%, but a low percentage of outliers were affected in this way. Custom software was developed to do these accumulations and plot the results. The output of this software and its implications are discussed in the next section.

8.2.2 Results

Although all three available prototypes were used in the experiment, the results from the fast walker are discussed in detail. Plotted results for the other machines are available on the CD ROM in the "*Experiments\kinematics\walking*" directory. The results from the other prototypes generally confirm the conclusions drawn from the case of the fast walker.

Figure 69 shows the result of plotting the data obtained from videos of the fast Perspex prototype walking along a tape measure. As can be seen, there is an obvious pattern to the data points, but there is also a large amount of scatter in the data.

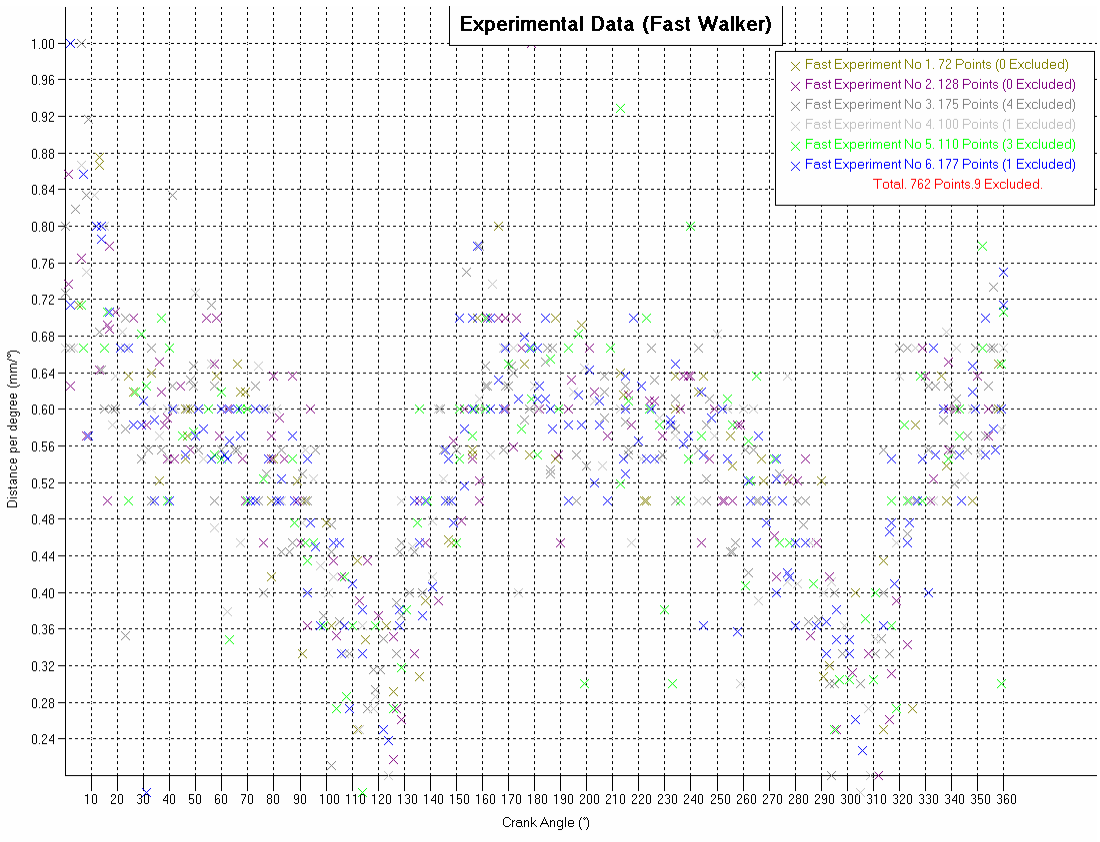

Figure 69. Graph of horizontal movement against crank position for the fast prototype.

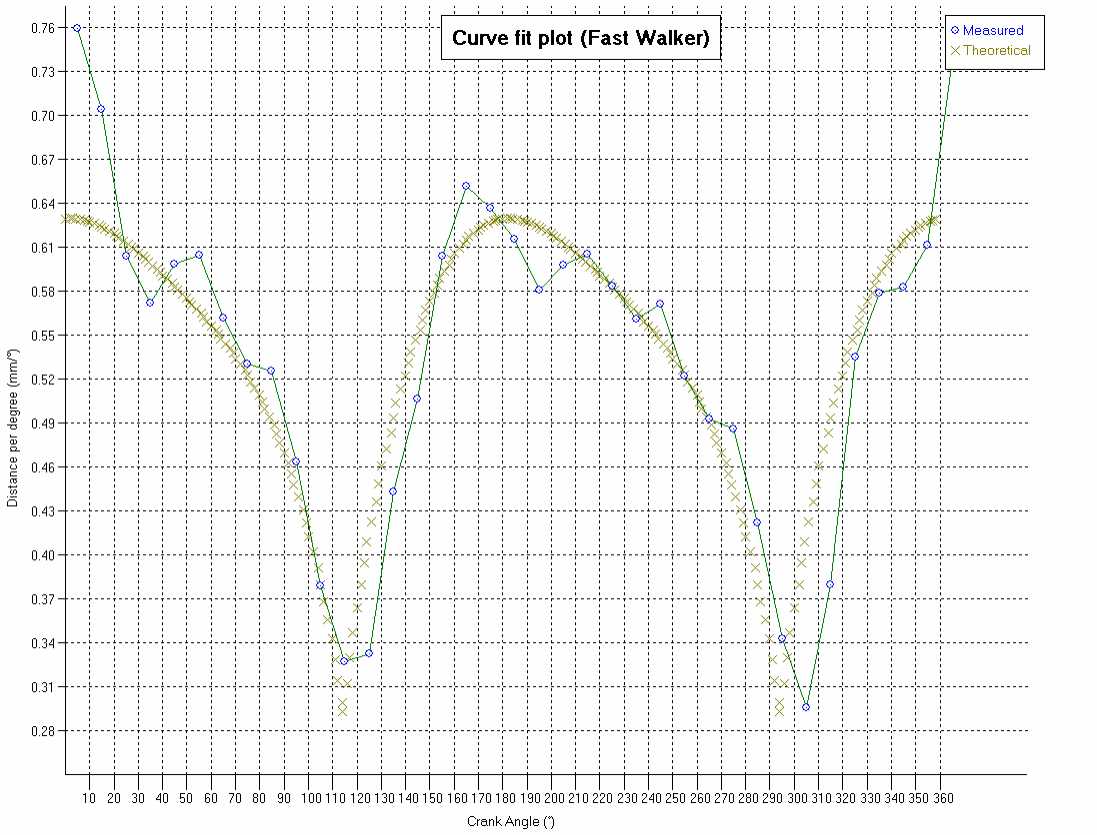

Figure 70. Experimental walking speed plotted against theoretical values.

To make the pattern in the data more discernible, the data points were accumulated and averaged. In Figure 70, the experimental data has been grouped every 10 degrees of crank rotation, so each point on this graph represents the average of approximately 20 discrete data points.

Once this averaged curve was calculated, it was necessary to plot the theoretical values on the same axes. A remaining unknown was the relative crank positions or phase difference between the prototype and the theoretical model. As the crankshafts themselves do not appear in the video frames, it was not possible to directly read this phase difference. An estimate could be made by viewing the video camera output while manipulating the crankshaft. This reading was taken for each machine. However, the most reliable way of establishing this phase difference is to fit the theoretical curve horizontally to the data. To achieve this, a sum of squared deviations was calculated between the experimental data curve and the theoretical curve for a range of phase shift angles. The phase shift angle that yielded the lowest sum of the squares of deviations was taken as the actual phase difference. The theoretical curve in Figure 70 is shifted along the horizontal axis so as to minimize the sum of squares of deviations between itself and the experimental data curve.

Once the relationship between the reference points for the experimental reading and the theoretical model had been established, the deviations in the measurements were assessed. The variances were calculated for each measured data point by subtracting the theoretical values from the measured values. The variances were then plotted, as shown in Figure 71. The variance distribution was also assessed, and this is shown in Figure 72.

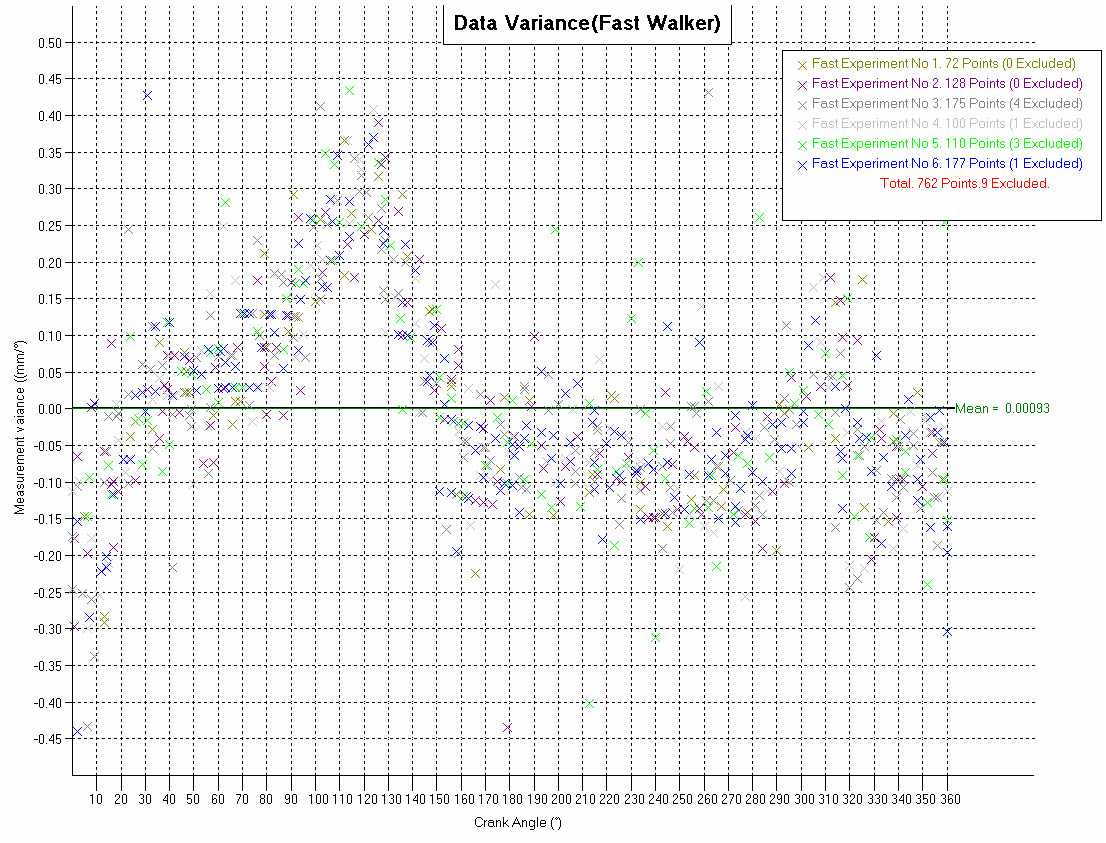

Figure 71. Graph of data variance against crank angle for the fast walker

As can be seen from the graph the mean variance is approximately zero. The variances are distributed relatively randomly. The largest positive variances occur at indices of around 120 degrees and 300 degrees. These positions correspond to the change over of leg sets when walking, when the vehicle body movement is slowest. These peaks in variance result from the inertia of the vehicle, both longitudinal and rotational. This inertia will tend to smooth out the velocity curve, speeding it up at slow points, and slowing it down at fast points. This slowing down at fast points is evident in the generally negative variances that occur between indices 160 and 290 and again between 320 and 30 degrees, which correspond to fast period of the walking cycle.

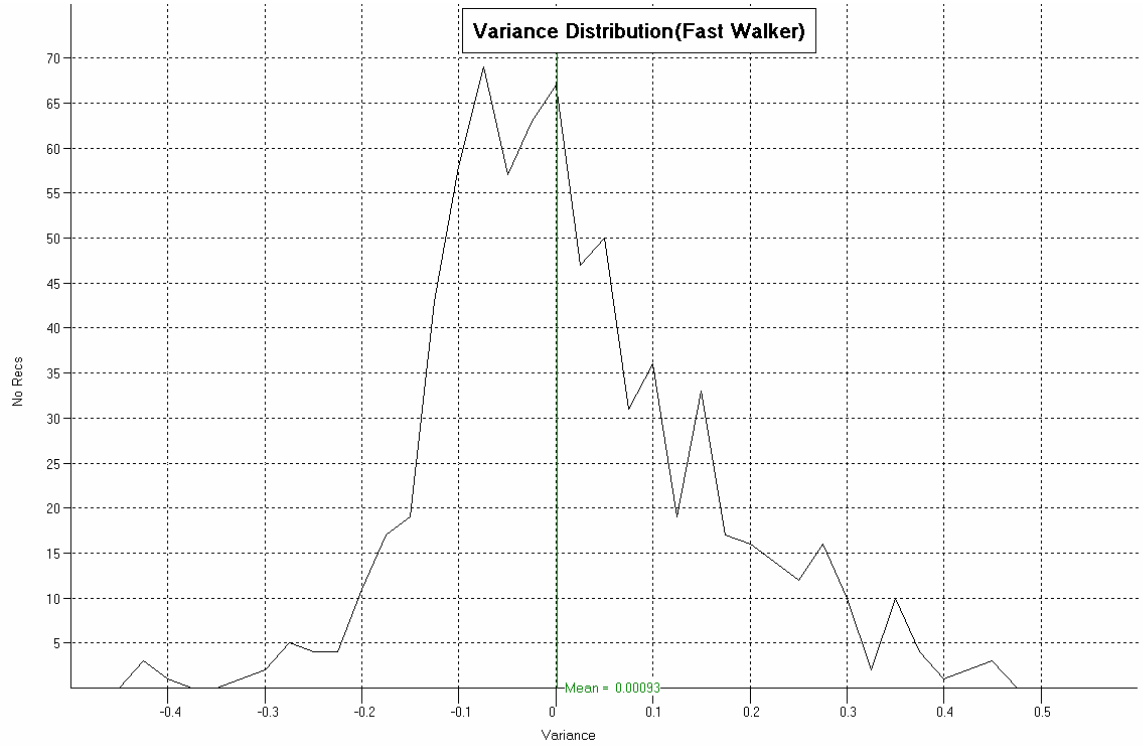

Figure 72. Variance distribution for the fast walker.

The distribution of the variances found is shown in the graph above. These data were obtained by sorting the variance data into containers 0.025 units wide, and counting the number of variances in each range. As can be seen, the resulting graph bears a strong resemblance to the bell shaped curve of a Gaussian distribution. The implication of this resemblance is that the deviations measured generally result from noise and there appears to be no experimental bias.

Consultation with an experienced statistician [56] provided no definitive way of quantifying the fit between the measured and experimental data. Given the explicable pattern in variance and their Gaussian distribution, it is unlikely that the measurements taken occurred due to some mechanism other than the one tested. Hence the kinematic model of the Jansen linkage can be considered confirmed, subject to the limitations stated in the following section.

8.2.3 Discussion

The deviations between the measured velocity profile and the theoretical one can be explained by the following factors.

Firstly, the theoretical model represents the performance of a single leg, while the measured values represent the average performance of the four legs that are in service at any time. Individual variations in dimensions of parts will add variance. The phase angle between legs of a group may not be exactly zero, due to inaccuracies in assembly. This will also create a wider distribution of data points.

Secondly, the model ignores inertia, both the rotational inertia, or flywheel effect, of the rotating parts of the mechanism and also the spatial inertia of the entire construction. As mentioned prior, the inertia will have the effect of smoothing the velocity distribution curves, and can explain the pattern in deviations that was actually recorded.

The third factor is that the theoretical model assumes a smooth, constant rotation of the crankshaft. Although the rotational speed measured is broadly constant, there is variation in speed, due primarily the highly non-linear and uneven torque requirements of the mechanism, as described in section 6.8. The other source of crank speed variation is the connecting linkages that couple the front and rear crankshafts on the prototype models. Imperfections in these linkages, particularly resulting from inaccurate attachment of the crank extension pieces in the first two (slow) walkers assembled. These two machines exhibit distinct jumps in their graphs, especially the first machine constructed. This large systematic variation can be seen at around crank index 235 in Figure 73 below. The physical cause of this deviance is that the single orthogonal connecting link is inaccurately coupled and at the index mentioned the third connecting link is flexed and acts as a kind of rotational spring where rotational energy is stored in the bending of the link. At a later point in the rotation, this energy is released, adding a momentary impulse to the crankshaft speed.

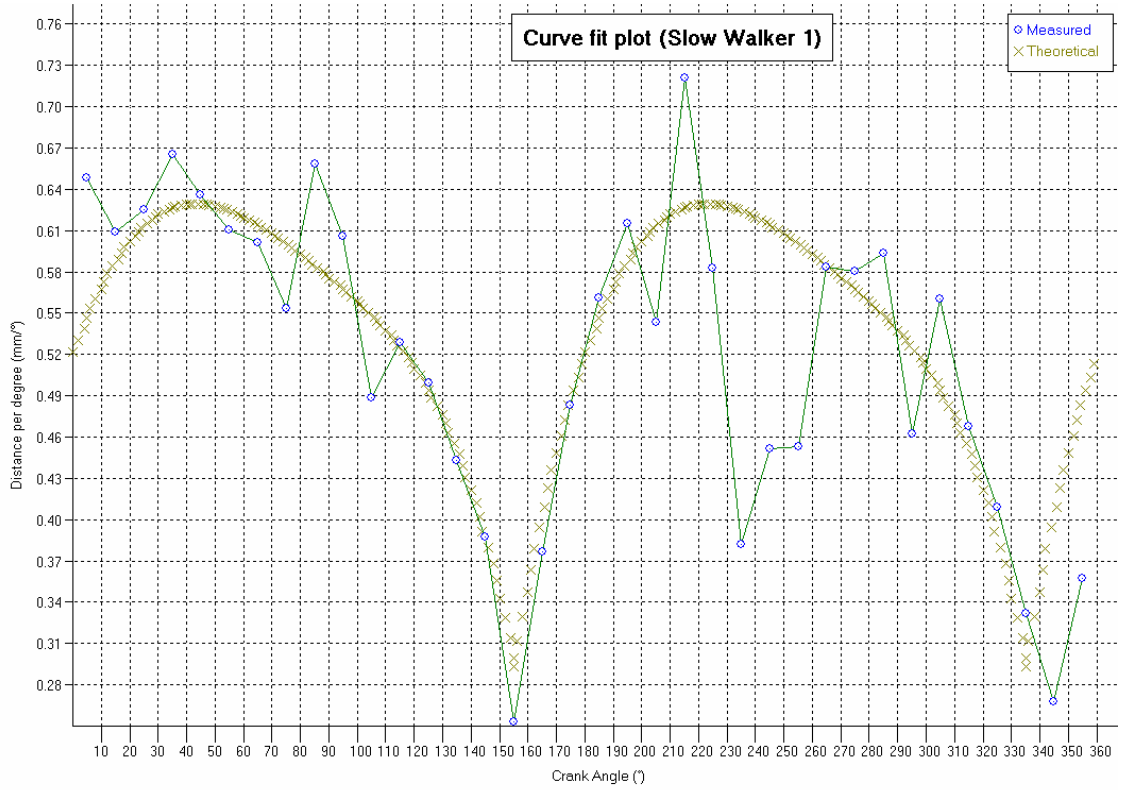

Figure 73. Velocity profile for the first slow walker.

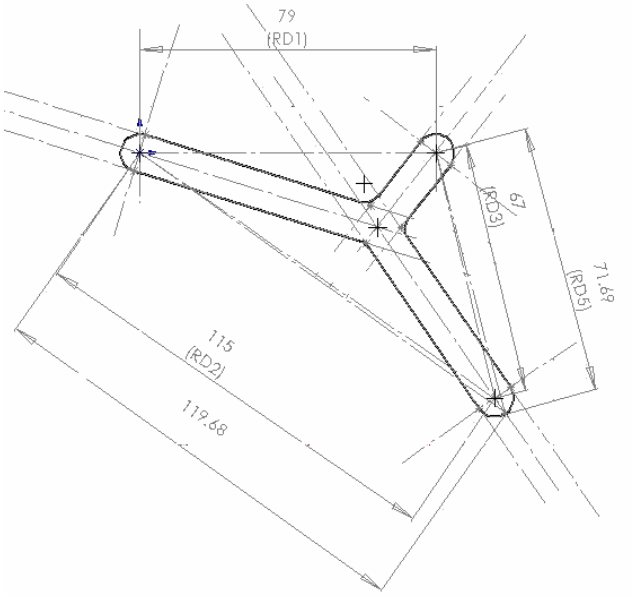

Figure 74. Actual versus designed walking point of contact position.

Finally, there is a difference between the theoretical leg proportions and those actually used by the prototype. The actual machine walks on the end of the link, and so the effective lengths of links 4 and 5 should be measured to the end of the link, and not to the centre of the hole provided for foot attachment. This means that the lengths of both link 4 and 5 will be

increased. This is shown in Figure 74. This results in a longer effective leg length, which in turn changes the velocity profile of the mechanism, as shown in Figure 75. Inspection of this graph and the corresponding ones for the other experiments indicates that the measured results do indeed correspond more closely to this curve than to the nominal curve.

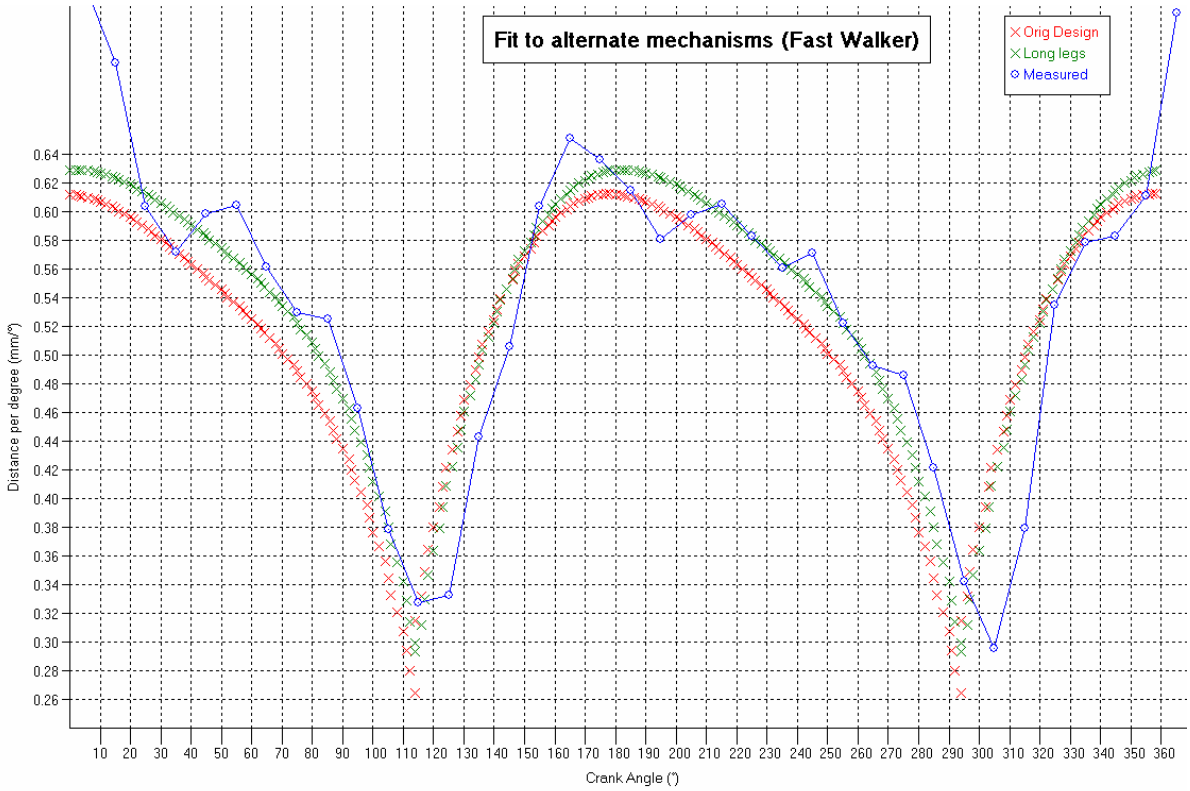

Figure 75. Variation in velocity distribution between nominal and actual leg design.

The actual point of contact will not remain stationary at the location at the end point of the link that is shown in the sketch. The point of contact will move along the curve at the end of the link. Its actual location will depend on the tangency point for the particular orientation angle of the longitudinal axis of the leg member. As the foot touches the ground, this tangency point will be located behind the nominal end point. As the machine walks, the contact point will move forward along the radiused end and will be forward of the nominal point by the end of the cycle. This change in position will continuously change the effective leg length, and will be a definite source of experimental deviance.

The conclusion to this series of experiments is that the model developed to describe the leg kinematics is confirmed and validated by these experiments.

8.3 Validation of kinetic model

8.3.1 Method

The energy required to turn the mechanism when walking under a variety of conditions has been derived in section 6.8. To validate this theory, it is necessary to measure the torque required to turn the prototype machine. The direct measurement of torque is usually achieved by measuring torsional strain using strain gauges. This requires that the strain gauges be mounted on a rotating shaft. Some means must be provided to read the resistance changes in the gauges. This can be achieved using slip rings and contacts on the shaft. It could also be achieved by using commercially available microprocessors that incorporate low power radio transmitters and receivers. It is also possible to measure torque indirectly by measuring the power supplied to an electric motor. This was the method used to validate the model chosen in this case.

The electrical power supplied to a motor can be determined by measuring the voltage across the motor and the current the motor draws. With DC motors, there is no phase difference between these and so these two parameters alone will give the power used by the motor. If we can also measure the rotational speed of the motor, then we can determine the torque experienced at the shaft. Mathematically this can be expressed as:

$$P_e = V \times I \qquad \text{Equation (8.3.1)}$$

$$T = \frac{P_e}{\omega} \qquad \text{Equation (8.3.2)}$$

where

P_e	=	Electric power on motor, in Watts
V	=	Voltage across motor in Volts
I	=	Current drawn by motor in Amperes
ω	=	Angular velocity of motor shaft in radians / sec
T	=	Torque at motor shaft in Nm

To determine these parameters, the circuit shown in Figure 76 was used. In this sketch, V_1 represents the voltage across the motor. V_2 is the voltage drop across the high precision 0.1 ohm shunt resistor placed in one leg of the circuit. This current flowing through the resistor can be found by Ohm's law.

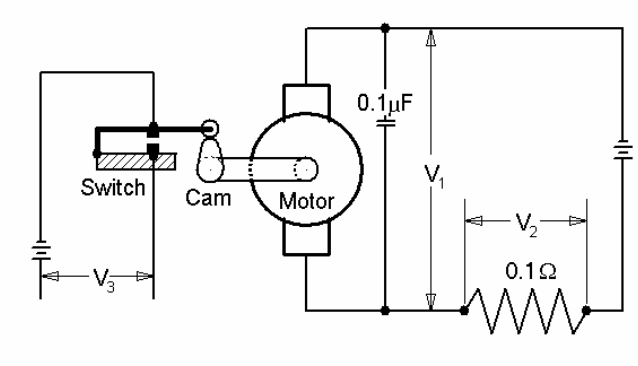

Figure 76. Schematic circuit diagram for measuring motor electrical power consumption.

The motor speed is determined by creating a pulse that indicates a particular shaft position has been passed. For simplicity, this was achieved by attaching a cam and switch to the motor output shaft. This device will generate a square wave pattern when a voltage is applied. When the circuit is set up, measurements can be taken using the transient recording function of an oscilloscope. The oscilloscope screen shown in Figure 77 below shows the voltage traces of the three voltages measured. The green trace represents the motor voltage (V_1), the light blue trace is the voltage drop across the shunt resistor (V_2) and the brown square wave trace is the voltage measured across the switch (V_3).

Although scaling in this screen shot makes it difficult to discern the signal, the software used could not present images at any other scale. Fortunately data interpretation could be done from the text file created by the software to contain the numerical values at each measurement point.

For these experiments, the cam and switch were attached to the machine's crankshaft, and not to the motor shaft itself. An oscilloscope is used to measure the time between rising (or falling) steps in the square wave trace representing V_3, the voltage across the switch. Knowledge of these times is used to determine the crankshaft speed, as the cam will close (or open) the switch at the same angular positions each revolution. This method assumes that the crank rotating speed is constant, but this has already been demonstrated in the previous section. As the rotating speed is constant, the instantaneous torque at each measurement point is taken as the instantaneous power measured divided by the average speed.

The signals measured for the voltages across the motor are noisy. This is primarily due to the commutator in the motor. A 0.1 μF capacitor was connected across the motor terminals, to form a simple low pass filter, in an attempt to clean up the electrical signals measured. However there was still a large amount of scatter in the measured data. The technique of re-

aligning data so that all data points are related to their angular position and then averaging the results was used to manage the data scatter, as had been done in the kinematics experiment.

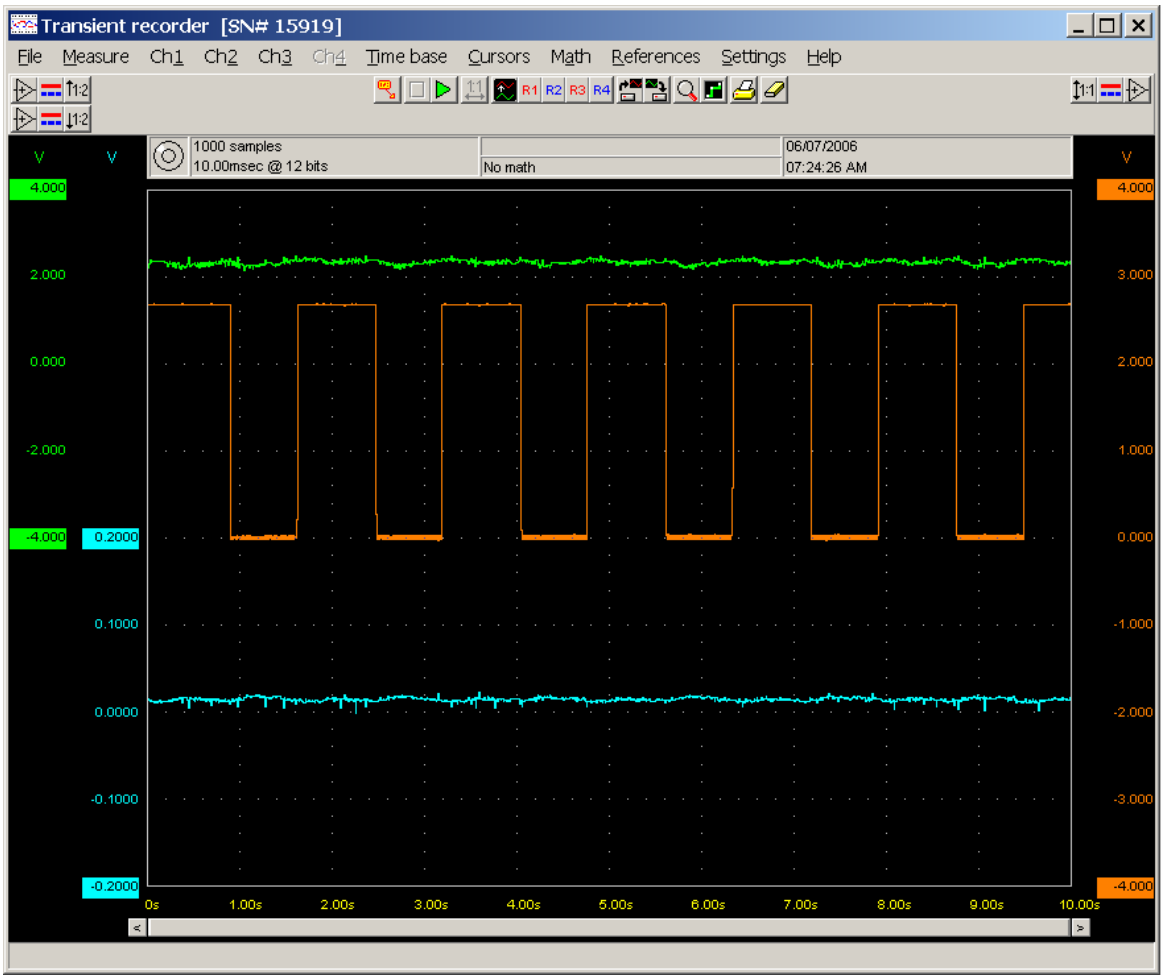

Figure 77. Oscilloscope screen when measuring motor power

The power consumed by the machine was measured with the machine mounted in a stand that holds the machine in the same orientation it would have when walking. This ensures that no walking forces are applied and that the forces due to gravity will have the same directions. The power measured was taken to represent the power required to overcome losses in the machine. The individual sources of loss were not separated, but losses would arise from friction in the gearbox, the revolute joints, the crankshaft main bearings and the connecting linkages and also the work expended overcoming weight and inertia of the links.

The results of these measurements of losses are shown in Figure 78 for both the fast and slow walkers. Note the large difference in the average frictional torque between the machines. Note also that these curves have not been aligned horizontally.

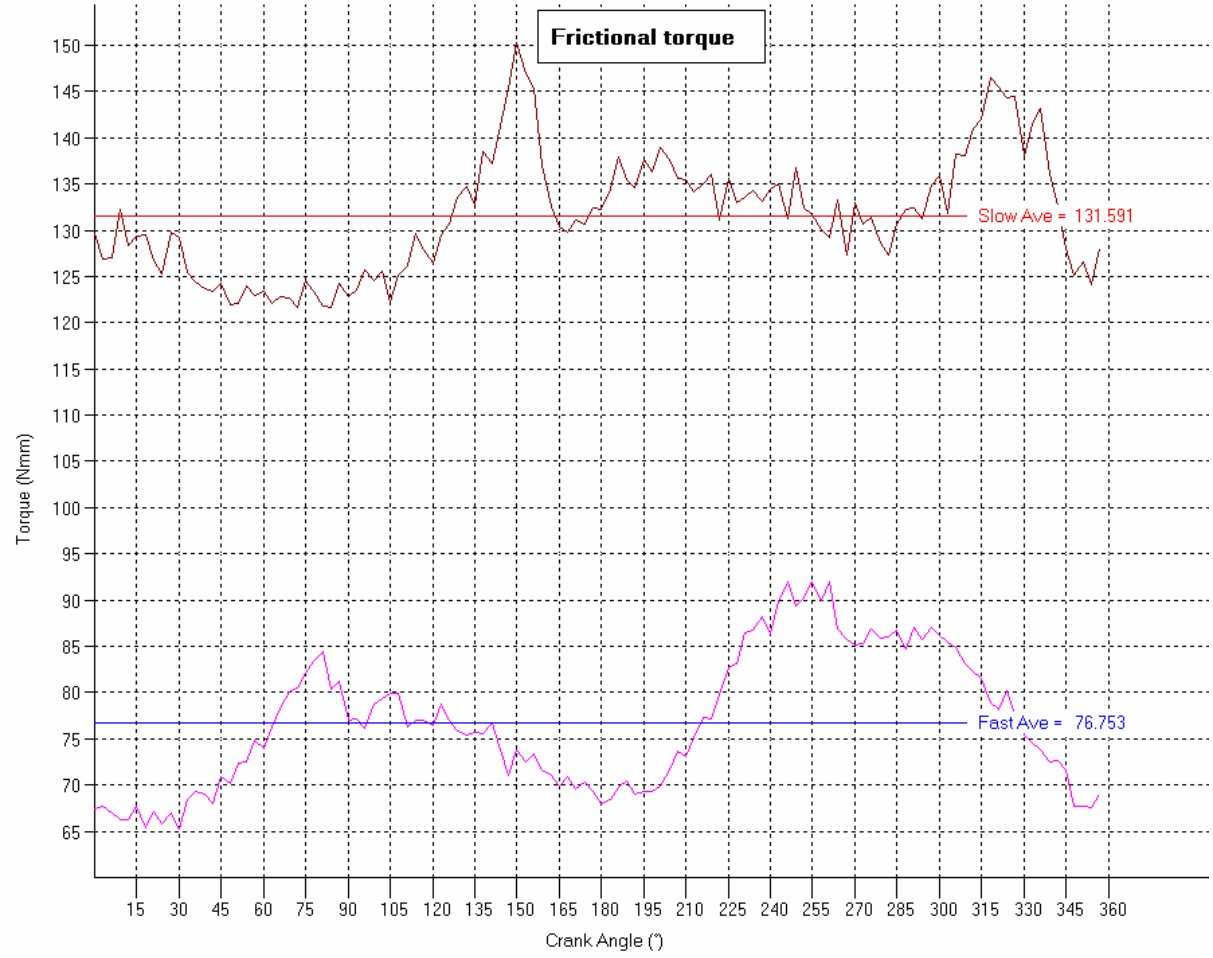

Figure 78. Torque required to overcome losses in experimental walkers.

To calculate the torque required to actually walk the machine, a series of test walks on both ascending and descending slopes of differing angles was conducted. The power measured for each test walk was recorded, and the corresponding frictional torque value, from the above curves, was subtracted. The remainder was taken to represent the torque required for walking.

There would be additional losses, not due to walking, but also not experienced by the machine running in the stand. These additional losses arise from rolling resistance of the foot radius on the ground and more seriously, the friction introduced by the sides of the outer feet sliding on the vertical surfaces of the guides placed along the edges of the test track. These guides were provided to ensure that machine would stay on the track. It was necessary to extend the through bolts at the feet, to ensure the feet are held inward from the guide, as the machines had a tendency to foul on the guide by lifting their knees at node 4 onto the top of the guide bar.

8.3.2 Results

The final result of the various test walks is shown in Figure 79, which shows the results for both the walkers tested. Positive angles represent ascending slopes while a negative value indicates a descending slope. The difference in crank rotational speed has some slight impact on the theoretical values used, but at the slow speeds used this difference can be safely ignored, and so the same theoretical curve is used as a reference for both machines.

As can be seen from the graph, the measured torque is in reasonably close accordance with the theoretical model, especially for the fast walker. The differences could probably be explained by the factors mentioned in the previous section, that is, the friction between the feet and the guide rails and the foot rolling resistance.

Note the very low values of torque required for walking. Even at maximum torque (50 Nmm) and speed (45 rpm) the power consumed in walking this 700g prototype up a 13 °slope was 0.235 W. Walking on a level surface consumes 0.047 W for the fast walker.

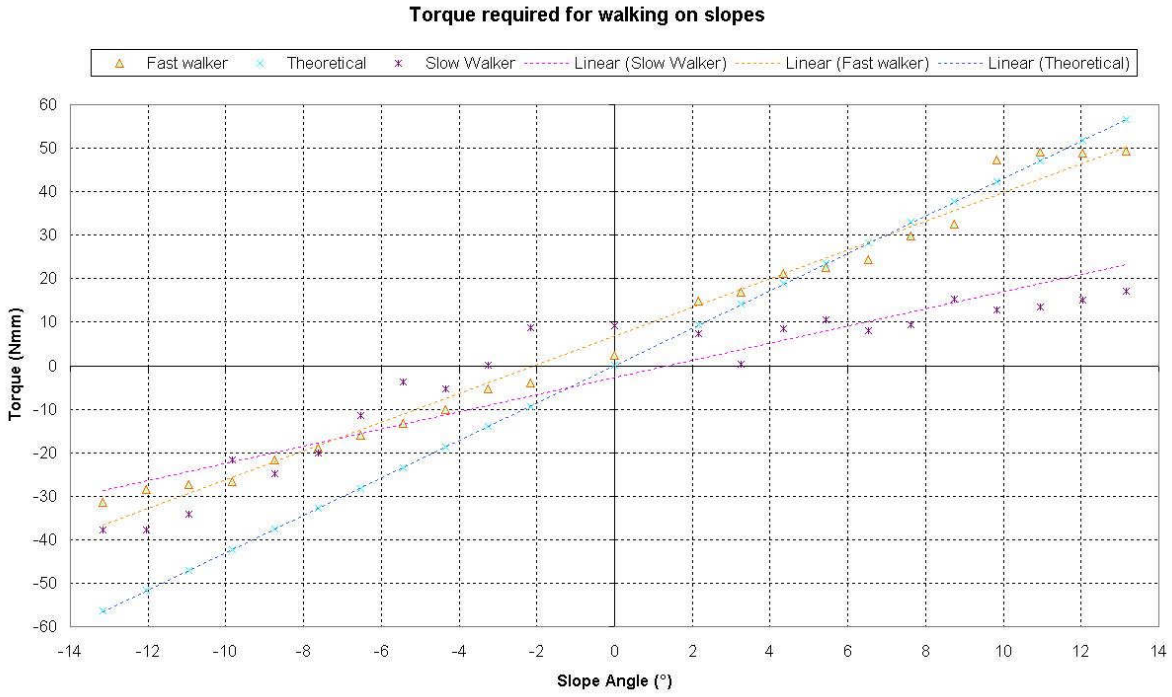

Figure 79. Torque required for walking on slopes.

The data recorded can also be presented as a direct comparison between the instantaneous torques required at various crank angles to walk on a particular slope. The measured data should assume a pattern similar to that shown previously in Figure 48. Such a plot is shown in Figure 80.

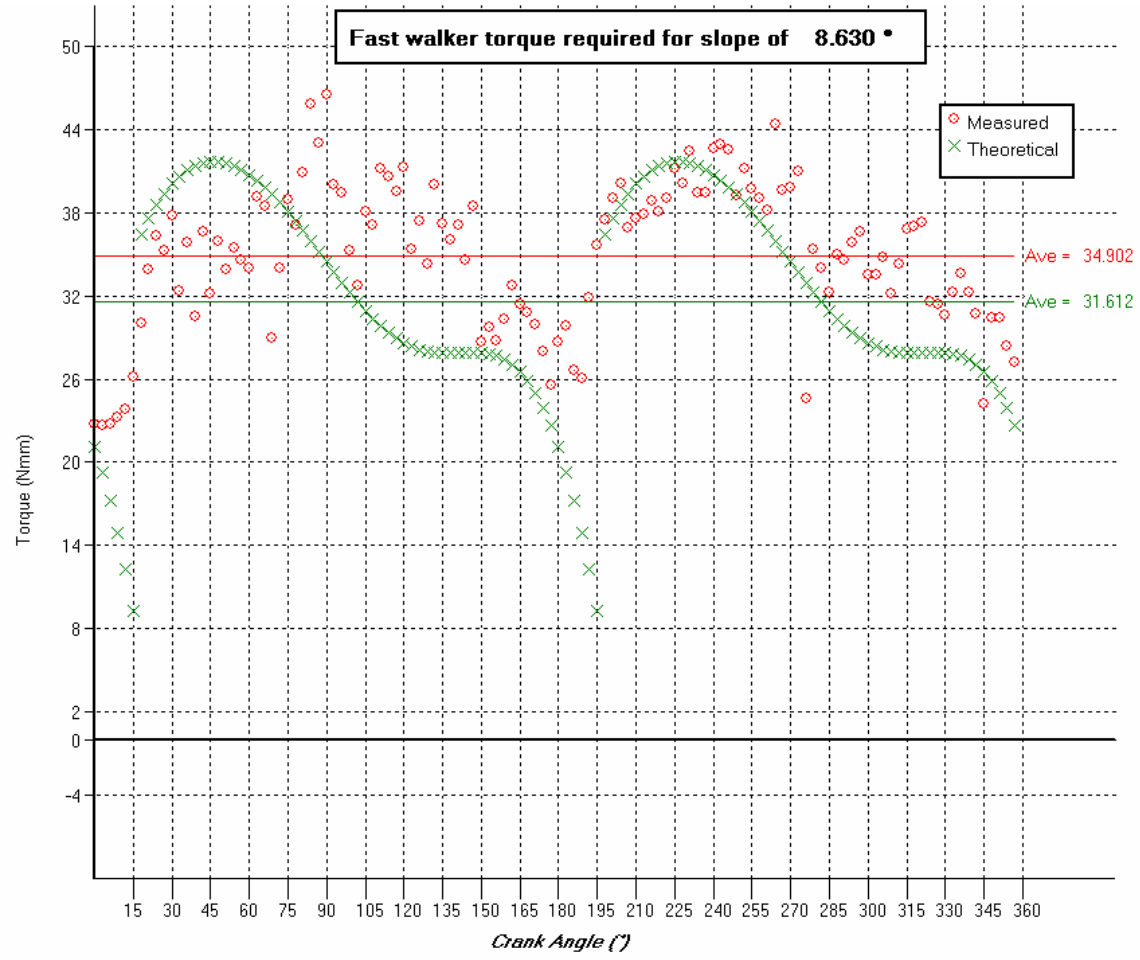

Figure 80. Instantaneous torque versus crank angle when climbing a slope of 8.6°.

Although it is not very clear, the measured torque distribution is similar to the theoretical one. There are several issues that may affect the conformity of the measured values to theory. The foremost of these is inertia, particularly rotational inertia.

The rotating parts of the machine will have some moment of inertia, which will tend to act as a flywheel. When torques is applied to the system, the rotating parts will resist any speed increase. If the torque demand is high, the combined moment of inertia will prevent the rotational speed from falling instantaneously. So the net result is that the torque distribution curve will be smoothed out, with the peaks lopped off and the valleys filled in.

On the basis of the conservation of rotational energy, it was decided that the best approach would be to average the power measured for a single revolution. The average theoretical power was also calculated, and these are the data plotted previously in Figure 79.

The second important issue is aligning the reference angle of the experimental data with the reference angle used in the computer model. This same problem was experienced with the kinematic experiments, but with these kinetic experiments, they present more of a problem. Firstly, it was not possible to get any accurate physical measure of the angle at which the cam driven switch would change state. Due to hysteresis in the switch, the exact switching position was difficult to establish. Secondly, as the data produced in these experiments was even noisier than that produced when validating kinematics, fitting a curve by least squares methods proved ineffective. Finally the horizontal shift of the theoretical curve was determined visually by trial and error. The offset that gave the best looking fit for all slope angles was the one used.

To confirm the validity of the experimental data, a simple analysis of variance was carried out, as was done in the prior kinematic experiments. The variances were plotted against crank angle, to demonstrate any systematic error positions. The variances were also counted and plotted to ensure that they were normally distributed. The graphical results of these various analyses and torque curves are all available on the accompanying CD ROM in the "*Experiments\Kinetics*" directory.

The result of this simple analysis of variance is less definite than for the kinematics experiments. The mean variances are small, but most differ significantly from zero. The variance distribution plots also indicate some skewing in the experimental data. Due to these patterns in the data variances, the certainty with which the measured results confirm the theory is significantly reduced.

8.3.3 Discussion

One of the main problems with the Perspex prototype walkers is friction. Perspex material was selected for its low cost and ease of manufacture, but the disadvantage is that the coefficient of friction between Perspex and steel is quite high. No reference-able source was found for this data, but an informal search of the World Wide Web yielded a static friction value (μ) of 0.5. Sliding friction, which would be the type experienced here, would be expected to be lower, but to what extent is not known as no value could be established. But regardless of the actual value, the friction would be much higher than would be possible with a larger machine which used rolling contact bearings at joints.

The result is that the power consumed to overcome friction is considerably more than the power required for walking. This is especially true when walking on level or nearly level surfaces. The parameter of interest is a small part of the total measured. Variance in frictional forces will have a major impact on the ability to detect small changes in power consumed for walking.

In conclusion, these experiments have established that the power consumed is at least of the same order of magnitude as that calculated. To obtain a higher quality of correlation, it would be advantageous to construct a larger prototype, where the frictional component of power consumption would be a smaller portion of the total power consumed.

Chapter 9 Conclusion

This thesis has succeeded in its goal of providing a theoretical framework to facilitate the design of this new class of walking machine. It describes in broad terms the competing devices and outlines the limitations of current attempts to walk using a machine. A simplification of existing machines is required and the thesis demonstrates how the Jansen mechanism meets the simplifying criteria better than any other mechanism considered here.

The details of the mechanism are exposed and the previously developed method is re-introduced, along with extensions to allow it to search for good designs. Requirements that a good design should fulfil are given and the use of the model to pursue an exhaustive search is described. The ineffectiveness of this means of searching is discussed.

The thesis then introduces optimization theories and assesses possible methods that could be used to find solutions. The method selected, optimization by genetic algorithm, is discussed. The details of the particular implementation used are given. The results of the search for good legs are discussed and a catalogue of mechanisms so far discovered in the class is presented. The best suited mechanism found in the search is described.

The thesis then turns its attention to the physics of walking using Jansen linkages for legs. A model of a hypothetical machine is developed by considering the forces the vehicle will be subjected to, under a variety of conditions. The operation of the machine in each of these circumstances is explored and the likely performance in real world conditions is discussed. The loading on various components of the machine are determined and a method for calculating power requirements is developed.

As this research has encompassed practical construction of prototype machines, a section about these prototypes is included. The details of the various models are given and the lessons learnt from each attempt are enumerated. Preliminary details of planned machines are given to indicate the types of issues that still remain to be resolved in researching this topic further.

Finally, this thesis details a series of experiments that were conducted to validate the various models developed. The kinematic model, developed primarily in previous work, was convincingly proven to be correct. The aspect of the model which deals with the kinetic or energy dimension was also partially validated.

This thesis has been successful in advancing knowledge on the subject of walking with Jansen linkages for legs. The initial hope that the mechanism could be used for locomotion has been justified by the construction of working prototypes that perform as designed. The discovery that the power consumed in walking is extremely low vindicates the decision to pursue this research.

The work described here should be considered a preliminary step in the envisaged design and development of a practical transport walking machine. A very significant aspect of the performance of any useable machine, namely manoeuvrability, has only been touched on in this work. Clearly this problem requires a solution before any practical machine can be considered. Until this problem is solved, the Jansen legged walker will remain a curiosity.

An aspect that requires additional work is the detail design of large scale machines that can successfully carry significant cargo. The ability to safely carry passengers is also a necessity as a ride in a machine of this type will be an important aid in convincing the general public that walking machines may be a viable transport option.

References

1 A.J.Ingram. *Numerical kinematic and kinetic analysis of a new class of twelve bar linkage for walking machines.* Master's Dissertation. University of Johannesburg. 2004.

2 WWW Reference –*Sinorama Magazine - The Wooden Ox Makes a Comeback (Page 1)* available at http://www.sinorama.com.tw/8511/511032e1.html

3 WWW Reference – *Romance of the three kingdoms. Chapter 102* available at http://www.threekingdoms.com/

4 S. Inwood. *The man who knew too much. The strange & inventive life of Robert Hooke.* McMillan. 2002

5 J. Uglow. *The Lunar Men. The friends who made the future. Faber and Faber.* 2002

6 WWW Reference – *MIT Leg Lab - Milestones in the Development of Legged Robots* available at http://www.ai.mit.edu/projects/leglab/background/milestones.html

7 R. Reeve. *Generating walking behaviours in legged robots.* Ph.D. Thesis. University of Edinburgh. 1999

8 WWW Reference – *Oricom Technologies 4-Legged Musings* available at http://www.oricomtech.com/projects/legs.htm

9 WWW Reference – *The Walking Machines Catalogue* available at http://www.walking-machines.org/

10 WWW Reference – *From ideas to first walking machines* available at http://www.fzi.de/divisions/ipt/WMC/preface/node14.html

11 WWW Reference – *HISTORY OF WALKING ROBOTS* available at http://www.bath.ac.uk/~en1tji/history.htm

12 WWW Reference – *History of the Study of Locomotion* available at http://guardian.curtin.edu.au/cga/history/enlightenment.html

13 WWW Reference - http://www.automation.hut.fi/

14 Song, S & Waldron K.J. *Machines that walk: the adaptive suspension vehicle.* MIT Press. Cambridge 1990

15 WWW Reference - http://www.plustech.fi/

16 WWW Reference - http://132.248.59.55/basilisc/basilisc.html

17 P.Ball. *Walk this way.* New Scientist. No 2537 4 February 2006.

18 WWW Reference - http://www.honda.co.jp/home/hpr/e_news/robot/index.html

19 WWW Reference - http://www.c-lab.de/vis/centaurob.html

20 WWW Reference - http://www.Siemens.com/ {NB Check URL !!!}

21 WWW Reference - http://robotics.stanford.edu/users/mark/polypod.html

22 WWW Reference - http://www.robotics.com/robomenu/stic.html

23 WWW Reference - http://maas-neotek.arc.nasa.gov/dante

24 WWW Reference - http://www.springwalker.com/

25 WWW Reference - http://agrosy.informatik.uni-kl.de/wmc/overview.php?id=171

26 K.J. Waldron, G.L. Kinzel. *Kinematics, dynamics, and design of machinery.* J. Wiley. Hoboken, N.J. 2004.

27 W.-B. Shieh, U L.-W. Tsai & S. Azarm. *Design and Optimization of a One-Degree-of-Freedom Six-Bar Leg Mechanism for a Walking Machine.* Journal of Robotic Systems Vol 14 No 12 , Pp 871 – 880. 1997

28 WWW Reference – *Planar motion hexapod walking machines: a new configuration* by G. Genta and N. Amati, Politecnico di Torino, Dipartimento di Meccanica available at http:/www.giancarlogenta.it/clawar.pdf

29 D. MacKenzie. *Shore Things.* New Scientist. No 2249. 29 July 2000. Pp 44-45.

30 WWW Reference – http://www.strandbeest.com/

31 H.J.A. Hofland and T. Jansen. *Strandbeeste van Theo Jansen.* Kunsthal. Rotterdam. 2001

32 Personal correspondence with Theo Jansen, by Email. August 2003.

33 Hewlett Packard. *HP-19C/HP-29C Applications Book.* 1977

34 C.A.C. Coello, D.A. van Veldhuizen, B.B Lalmont. *Evolutionary algorithms for solving multi-objective problems.* Kluiwer Academic / Plenum Publishers. New York. 2002.

35 J. Andersson. *A survey of multiobjective optimization in engineering design.* Technical Report: LiTH-IKP-R-1097. Department of Mechanical Engineering, Linköping University, 581 83 Linköping, Sweden.

36 Y. Sakakibara, K. Kan, Y Hosoda, M Hattori and M. Fjie. *Low Impact foot trajectory for a quadruped walking machine.* Advanced Robotics. Vol 7 No 4. Pp 343-360. 1993.

37 E. Garcia and P. Gonzalez-de-Santos. *Using soft computing techniques for improving foot trajectories in walking machines.* Journal of Robotic systems. Vol 18 No 7 Pp 343-356. 2001.

38 G.N. Sandor and A.G.Erdman. *Advanced mechanism design. Analysis and Synthesis.* Prentice Hall. New Jersey. 1984.

39 R. Hartenberg and J. Denavit. *Kinematic synthesis of linkages.* McGraw Hill. New York. 1964.

40 F. Freudenstein. *An analytical approach to design of four link mechanisms.* Transactions of the ASME 76. Pp 483-492. 1954.

41 C. Darwin. *The origin of species.* Mentor Edition. New American Library. New York. 1958. First published 1859.

42 J.H. Holland. *Adaptation in natural and artificial systems.* The Unversity of Michigan Press. Ann Arbor. 1975.

43 D.E.Goldberg. *Genetic Algorithms in search, optimization, and machine learning.* Addison Wesley Publishing. 1989

44 Z. Michalewicz. *Genetic algorithms + Data structures = Evolution programs.* 2nd Edition . Springer Verlag. Berlin. 1992

45 M. Mitchell. *An Introduction to Genetic Algorithms.* MIT Press. 1996.

46 T. Bäck. *Evolutionary algorithms in theory and practice.* Oxford University Press. 1996

47 A. Kanarachos, D. Koulocheris and H. Vrazopoulos. *Evolutionary algorithms with deterministic mutation operators used for the optimization of the trajectory of a four bar mechanism.* Mathematics and computers in simulation. No 63. Pp 483-492. 2003.

48 J.A.Cabrera, A.Simon, M. Prado. *Optimal synthesis of mechanisms with genetic algorithms.* Mechanism and machine theory. N0 37. Pp 1165-1177. 2002.

49 G. Renner and A. Ekart. *Genetic algorithms in computer aided design.* Computer aided design. No 35. Pp 709-726. 2003

50 F. Hardarson. *Stability analysis and synthesis of statically balanced walking for quadruped robots.* Doctoral Thesis. Royal Institute of Technology. Stockholm, Sweden. 2002

51 J.Y. Wong. *Theory of Ground Vehicles*. 3rd Edition. John Wiley & Sons. 2001

52 S.P. Timoshenko and D.H. Young. *Theory of structures*. McGraw Hill. 1965.

53 J. Hannah and R.C. Stephens. *Mechanics of Machines. Advanced theory and examples.* 2nd Edition. Edward Arnold. 1972.

54 B. Ingram. *Walk tall, break a leg.* Popular Mechanics. South African Edition. November 2003.

55 Kawasaki Heavy Industries. Motorcycle division. *Z200 motorcycle owners manual.* 1980

56 Personnel communication with Mr M Greyling of the Psychology Department, University of the Witwatersrand, Johannesburg. April 2006.